MASTER COPY - FOR REPRODUCTION PURPOSES

AD-A222 890

DTIC ELECTE JUN 15 1990

REPORT DOCUMENTATION PAGE

1b. RESTRICTIVE MARKINGS	
2b. DECLASSIFICATION / DOWNGRADING SCHEDULE	3. DISTRIBUTION / AVAILABILITY OF REPORT: Approved for public release; distribution unlimited.
4. PERFORMING ORGANIZATION REPORT NUMBER(S)	5. MONITORING ORGANIZATION REPORT NUMBER(S): ARO 23906.4-EL
6a. NAME OF PERFORMING ORGANIZATION: University of So. California	6b. OFFICE SYMBOL (If applicable)
7a. NAME OF MONITORING ORGANIZATION: U. S. Army Research Office	
6c. ADDRESS (City, State, and ZIP Code): University of Southern California, Vivian Hall of Engineering, Room 610, Los Angeles, CA 90089-0241	7b. ADDRESS (City, State, and ZIP Code): P. O. Box 12211, Research Triangle Park, NC 27709-2211
8a. NAME OF FUNDING / SPONSORING ORGANIZATION: U. S. Army Research Office	8b. OFFICE SYMBOL (If applicable)
9. PROCUREMENT INSTRUMENT IDENTIFICATION NUMBER: DAAL03-86-K-0155	
8c. ADDRESS (City, State, and ZIP Code): P. O. Box 12211, Research Triangle Park, NC 27709-2211	10. SOURCE OF FUNDING NUMBERS: PROGRAM ELEMENT NO. / PROJECT NO. / TASK NO. / WORK UNIT ACCESSION NO.

11. TITLE (Include Security Classification)

Measurement of Deep Levels at InGaAs(P)InP Heterojunctions (unclassified)

12. PERSONAL AUTHOR(S)

S.R. Forrest

13a. TYPE OF REPORT	13b. TIME COVERED	14. DATE OF REPORT (Year, Month, Day)	15. PAGE COUNT
Final	FROM 9/1/86 TO 12/1/90	4/01/90	

16. SUPPLEMENTARY NOTATION

The view, opinions and/or findings contained in this report are those of the author(s) and should not be construed as an official Department of the Army position, policy, or decision, unless so designated by other documentation.

17. COSATI CODES		
FIELD	GROUP	SUB-GROUP

18. SUBJECT TERMS (Continue on reverse if necessary and identify by block number)

heterojunctions, InGaAs(P), InP, Capacitance.

19. ABSTRACT (Continue on reverse if necessary and identify by block number)

We have studied the properties of semiconductor heterojunctions using several novel analytical and experimental techniques. A new, and highly accurate means for measuring the properties of heterojunctions has been demonstrated, where the measurements of the band offset energies can be made even in the presence of high densities of interface charge. The techniques developed have been applied to study both InGaAs/InP as well as HgCdTe/CdTe heterojunctions, affording the most accurate measurements obtained to date for the band offset energies of these materials systems. These measurements were made possible via the use of novel test structures consisting of organic-on-inorganic semiconductor contact barrier diodes. Furthermore, we have grown InGaAs/InP heterojunctions with the lowest defect densities yet reported, and obtained the surprising result that the defect charge density is independent of the degree of lattice mismatch. We observe that the defect density is strongly related to the purity of the source metals used in the semiconductor growth. Finally, we have employed our low defect density heterojunctions

20. DISTRIBUTION / AVAILABILITY OF ABSTRACT	21. ABSTRACT SECURITY CLASSIFICATION
☐ UNCLASSIFIED/UNLIMITED ☐ SAME AS RPT. ☐ DTIC USERS	Unclassified
22a. NAME OF RESPONSIBLE INDIVIDUAL	22b. TELEPHONE (Include Area Code) / 22c. OFFICE SYMBOL

DD FORM 1473, 84 MAR — 83 APR edition may be used until exhausted. All other editions are obsolete.

SECURITY CLASSIFICATION OF THIS PAGE
UNCLASSIFIED

9006 14 177

FILE COPY

19. continued...

in novel, high sensitivity heterojunction bipolar phototransistors.

TABLE OF CONTENTS

		Page
I.	Introduction	2
II.	Summary	4
	i) Heterojunction Offset Theory	4
	ii) InGaAs/InP Heterojunctions With Very Low Interface State Densities	5
	iii) HgCdTe/CdTe Heterojunctions	7
	iv) High Sensitivity Heterojunction Bipolar Phototransistors	8
III.	Conclusions	9
IV.	Acknowledgements	10
V.	References	10
VI.	Figure Captions	11
VII.	Appendix 1	25
VIII.	Appendix 2	52

Measurement of Deep Levels at InGaAs(P)/InP Heterojunctions

Final Report Submitted by:
Prof. Stephen R. Forrest
Departments of Electrical Engineering/Electrophysics and Materials Science
University of Southern California

Program Information:
Program supported by ARO Contract No.: DAAL03-86-K-0155
Contract Officer: Michael Stroscio
Duration: September 1, 1986 - December 31, 1989
Personnel Supported Under This Contract:
P.I.: S. R. Forrest
Graduate Research Assistants: L. Y. Leu, C. D. Lee
Degrees Granted: None

I. Introduction

In this report, we discuss the principle achievements of a three year program whose purpose was to investigate the sources of deep levels universally observed at InGaAs(P)/InP heterojunctions. Due to the utility of these heterojunctions for long wavelength optical communications systems, it is extremely important that we understand fully those properties of the materials which influence optoelectronic device operation. Indeed, the quality of the heterojunction plays a major role in device characteristics, and hence our interest in this subject. To study the heterojunctions, several unique tools were conceived in our laboratory. These tools involved the use of organic-on-inorganic (OI) semiconductor contacts, and have broad applicability to other materials systems, such as HgCdTe/CdTe, which was also explored in this research.

Details of some of the technical aspects of this program have appeared in four full technical journal articles (Appendix 1), a fifth paper which is currently

under review at Applied Physics Letters (Appendix 2), and one paper still in preparation to be submitted to the Journal of Applied Physics. Additionally, we have given two oral presentations (one at the First International Conference on InP and Related Compounds, and one at SPIE), and one patent application which is presently under review by the U.S. Patent Office.

Practical aspects of this work are also now being employed by at least two companies (Epitaxx, Inc. and Santa Barbara Focalplane) to assist in product commercialization. A third company (Santa Barbara Research Center) has taken sufficient interest in our results such that they are co-authors of the patent application. We note that this program has been critical to understanding and improving III-V semiconductor materials for use in optoelectronic circuits.

The major accomplishments of this three year program are highlighted below:

1) A theory for the measurement of heterojunction offsets *in the presence of interface defects* was developed for the first time. This theory is a significant extension of the method of Kroemer [1,2] for measuring band offset energies via C-V methods. In fact, the simple application of our theory to measurement provides for the ability to separate out the effects of interface defects from the actual offset energy. To our knowledge, this is the most accurate method available for measuring heterojunction band offset energies, surpassing other "conventional" techniques such as multiple quantum well luminescence and absorption, XPS, and current transport methods. It is simple to apply, and is relatively free of the need to employ numerous parameters of which the investigator has only a vague knowledge.

2) The validity of the theory was tested experimentally on both VPE and LPE grown InGaAs/InP heterojunctions. The VPE samples were obtained in a collaborative effort with Epitaxx, Inc., whereas we grew the LPE samples in our laboratory. During the course of this experimental work, we demonstrated the first InGaAs/InP heterojunctions which do not show evidence for a high defect density at the heterointerface. Indeed, using ultra high purity In source metals, we have achieved the lowest interface defect densities (by one order of

magnitude, or more) ever reported for InGaAs/InP heterojunctions. Furthermore, we have found that the defect density is unrelated to lattice mismatch, suggesting the source of defects is due to impurities in the source metals and gases used during growth.

3) The methods of using organic contacts in conjunction with our energy offset theory was applied to make the first measurements of HgCdTe/CdTe valence band offsets using C-V techniques. We obtained the surprising result that the HJ offset is of the Type II (rather than Type I) variety, contradicting conventional wisdom. Although there is some previous, weak data from other groups which infer a Type I junction, we are aware of at least one very recent report confirming the Type II geometry. Clearly more work needs to be done here to totally eliminate sample and growth-induced peculiarities. However, the organic method of C-V analysis on narrow band-gap materials is an important step in expanding our knowledge of these useful semiconductors. Furthermore, our results suggest many room temperature device possibilities for IR detectors using the organic/inorganic semiconductor approach.

4) Work on localized defects at heterojunctions was extended to the understanding of InGaAs/InP bipolar phototransistors (HPTs). Our modelling indicates that placement of low-doped layers within the base or emitter regions can result in a significant increase in the photocurrent gain at low input power intensities. This finding has already resulted in a marked improvement in HPT sensitivity at low input optical powers, thereby making these devices excellent candidates for integration in bipolar optical receivers (an approach which has generally been ignored due to the low sensitivity of HPTs at low input optical powers).

We now discuss in greater detail the specifics of these results.

2. Summary

i) Heterojunction offset theory

There have been long-standing controversies of the role that defects play in both heterojunction measurement and performance. Figure 1 shows a calculation of the apparent free carrier concentration profile in the presence of

various amounts of interfacial charge, σ_i. The effect of charge on the profile is readily apparent. We note that this variation in the profile has importance since it indicates a variation of the *diffusion potential* with σ_i, which is responsible for controlling charge transport in heterojunction devices. In Fig. 2 we show that the measured value of the offset energy, ΔE_c, depends strongly on the interface defect density. It would seem from this that extracting the "true" value of ΔE_c from C-V data (or any data) would be extremely difficult. However, in this ARO-sponsored program, we developed a very simple technique for determining ΔE_c even when charge exists at the heterojunction. Note that this technique is only valid if the charge is monopolar in nature -- dipolar defects would be indistinguishable from the intrinsic dipoles which form the heterojunction offset due to their spatially averaged charge neutrality. For this measurement technique, we generated a series of "universal" curves (Appendix 1) which are useful for obtaining an accurate determination of ΔE_c from the $n(x)$ profiles such as those shown in Fig. 1. The heterojunction diffusion potential for a defect-free heterojunction ($V_D(0)$) from which ΔE_c is directly related, is determined using the measured potential, V_{DK}, along with:

$$V_D(0) = V_{DK} + q/\kappa[\sigma_i(\Delta x_j - d/2) - (N_{D2} - N_{D1})\Delta x_j^2/2]$$

To obtain $V_D(0)$, therefore, all we need to do is measure V_{DK} and σ_i using a standard technique such as Kroemer's method, determine the interface width, d, using SIMS, for example, and plug the values into the above equation.

This procedure has been used on samples grown by hydride vapor phase epitaxy (VPE) and by liquid phase epitaxy (LPE). In Fig. 3, we show a typical measurement made on a VPE InGaAs/InP heterojunction, giving the most accurate value for such heterojunctions measured to date by C-V or other methods.

ii) InGaAs/InP heterojunctions with very low interface state densities

During the course of our investigations of heterojunctions, we grew many InGaAs/InP samples with remarkably low interface state densities. These samples were grown in our high uniformity LPE system, using ultra-high purity indium for the melt sources. In *all* previous work done both in our lab as well as

in other labs around the world [3,4,5], it has been found that InGaAs/InP heterojunctions have a high defect density (with $\sigma_i > 10^{11}$ cm^{-2})such that the apparent ΔE_C is observed to vanish as T -> 0! For our samples, it was found that this effect was either greatly reduced, or even eliminated due to a significant decrease in the interface state densities obtained by our growth techniques.

A sample which demonstrates a small decrease in the measured ΔE_C is shown in Fig. 4. Here, it is observed that there is no significant decrease in ΔE_C of approximately 70 meV at 150K -- already a significant improvement in the typically observed decrease of 200 meV reported by others. As proof that this decrease is in fact due to interface states filling at low temperature (a point which in itself has generated considerable controversy), we have used the simple theory and equation given above to "correct" the measured values of ΔE_C by subtracting the effects due to traps. Note that the traps were observed independently using DLTS. The corrected temperature dependence of ΔE_C is shown in Fig. 5. From these data we obtain the expected result -- i.e. the *intrinsic* value of ΔE_C is independent of temperature since it can only be a function of the dipolar character of the interfacial atoms at the heterojunction.

In addition to growing samples with low σ_i, we have also grown material which is evidently free of any significant defect density. This is confirmed by the plot in Fig. 6 which indicates no variation of the measured ΔE_C versus temperature or frequency. To our knowledge, this is the only demonstration of an InGaAs/InP heterojunction which has no significant defect density. Furthermore, we observe that there is no dependence of the offset energy on lattice mismatch, even though the mismatch was varied from sample-to-sample over the extremely large range of $\pm$ 0.25%! Indeed, the defect densities measured for these samples are the lowest ever reported (with $\sigma_i < 7 \times 10^9$ cm^{-2}) , again independent of lattice mismatch. We attribute this high quality interface to extremely good control of temperature during growth, and the elimination of defects due to the melt-back process. However, the main source of these high quality interfaces is probably a result of the use of very high purity In melts (with 7 9's+ purity). This may be an indication that LPE is still the growth technology capable of giving the lowest defect density growth attainable. One further interesting outcome of this work is the observation that defects resulting from misfit dislocations are not always electrically active at the heterojunction. We conclude that the energies of such defects might be "pulled" into the conduction or valence bands at the heterointerface, and hence they

remain permanently thermalized. This conclusion appears consistent with the observation in previous work that heterojunction defects are shallow [3].

iii) HgCdTe/CdTe heterojunctions

We also investigated IR materials after we discovered that certain organic compounds make good rectifying contact to the narrow band gap (0.24 eV) $Hg_{0.7}Cd_{0.3}Te$. The "traditional" compounds used in organic contacts, such as 3,4,9,10 perylenetetracarboxylic dianhydride (PTCDA), do not form rectifying contacts on these semiconductors, possibly due to the oxygen in the organic molecule reacting with the Hg. Thus, we chose a class of crystalline organic materials which did not contain oxygen -- i.e. the phthalocyanines (Pc's) -- and found that indeed, good rectifying organic-on-inorganic (OI) semiconductor devices were obtained. The *room temperature*, bipolar I-V characteristics of such devices are shown in Fig. 7. Note that reverse-biased breakdown voltages as high as 8V were observed at room temperature. This is to be compared with $< 0.5V$ observed for metal/HgCdTe junctions. Due to this observation, the prospects for room temperature IR device operation are quite promising.

The OI device is fabricated by first depositing, in vacuum, approximately 1000 Å of the pre-purified organic material onto the wafer surface following procedures described in detail elsewhere [6,7]. Next, ohmic contact is made to the substrate by depositing a suitable metal across the wafer surface. This is followed by depositing ohmic contact dots onto the organic material surface. The OI diode area is defined by the diameter of the contact dot due to the anisotropy in the organic film conductivity which confines current to flow only beneath the dot. We note that for semi-insulating substrates, the "back contact" can be deposited directly onto the wafer surface near to the contact dot. Alternatively, this back contact can also be deposited onto the organic film surface. As long as this back contact is larger than the dot contact, little or no error is incurred in data obtained using this structure.

Capacitance-voltage analysis is carried out using the OI structure along with analysis techniques which are applied to the study of Schottky barrier or p-n junction diodes. The OI diode provides the advantage of being easy to apply and non-destructively remove from the wafer surface (using positive photoresist

developer), and large reverse voltages can also be applied to allow for deep depletion into the wafer bulk.

We have used the OI diode to obtain information regarding doping and heterojunction offsets which have heretofore been inaccessible to C-V analysis. Figure 8 shows a composite free carrier concentration profile obtained on a taper-etched, n-HgCdTe/p-HgCdTe/P-CdTe sample. To obtain such a deep depletion profile (extending 10 μm below the surface) through both p and n-type materials, it was necessary to taper-etch the epitaxial layers in this sample prior to deposition of the H_2Pc organic thin film. These data indicate that the OI device is useful in probing both n and p-type material, and can also be used on narrow bandgap as well as wide gap semiconductors. A detailed view of the carrier concentration at the p-P heterojunction is shown in Fig. 9. Here, the results are truly surprising. It is apparent that hole depletion occurs on the HgCdTe side, whereas accumulation occurs on the CdTe side of the heterointerface, suggesting the band diagram shown in the inset of the figure. While the offset direction is opposite to that understood to be the case by conventional wisdom, the unique aspect of C-V analysis is that *the band structure does not have to be guessed at a priori* (as in the case of optical measurements, for example). Rather, the band structure and the dipole direction is directly inferred from the relative positions of the spike and notch in the free carrier concentration profile.

Once again, ΔE_c was measured from these data using our theory developed earlier. We obtained $\Delta E_c = 110 \pm 20$ meV and $\sigma_i = -6 \times 10^{10}$ cm^{-2}. These values were checked by a full solution to Poisson's Equation, shown by the dashed line fit in the figure.

iv) High sensitivity heterojunction bipolar phototransistors

We have also investigated the effects of interface charge on the operation of heterojunction phototransistors (HPTs). Here, we fabricated standard HPTs using an n-InP emitter/p-InGaAs base/n-InGaAs collector grown by LPE. Due to the high quality heterointerfaces, we fabricated transistors with very low output conductances, as shown in Fig. 10. Here, P_{in} is the input optical power. These transistors showed the common problem of decreased gain at low input power levels (Fig. 11). This is due to a combination of effects, most notable among which are bulk and surface recombination in the base-emitter

region. To make a transistor useful at very low input optical powers which are needed for detection in most photonic transmission systems, however, this effect at low P_{in} must be greatly reduced, or even eliminated.

The recombination current is exacerbated by the presence of the dip in the conduction band at the E-B junction. This provides a recombination site for electrons injected into the base region, thus decreasing the gain, especially at low injection levels. To eliminate this problem, we investigated the device shown in Fig. 12. This is only a minor modification of the standard HPT in that a very thin (100 - 500 Å) n-layer is inserted at the emitter side of the E-B junction. This results in a flattening out of the conduction band at the heterointerface eliminating the electron trap to a considerable degree. Also, it provides a higher "ramp" over which the electrons are injected at the E-B junction, thus allowing them to avoid trapping in the remaining dip. Finally, it also reduces E-B capacitance, thus improving high bandwidth response.

The effect on gain for this "novel" device is shown in Fig. 11. It is clearly apparent that the doping dip enhances the gain at low input power levels (corresponding to low collector currents). The ideality factor of these gain curves, which is related to the slope of the curves, is found to be equal to 1.2 at low current levels corresponding to the best values obtained to date for LPE heterojunction phototransistors. More important is the fact that the novel structure has a significantly lower ideality factor than the conventional structure (with a value of 1.7).

3. Conclusions

In conclusion, we have studied the properties of semiconductor heterojunctions using several novel analytical and experimental techniques. A new, and highly accurate means for .neasuring the properties of heterojunctions has been demonstrated, where the measurements of the band offset energies can be made even in the presence of high densities of interface charge. The techniques developed have been applied to study both InGaAs/InP as well as HgCdTe/CdTe heterojunctions, affording the most accurate measurements obtained to date for the band offset energies of these materials systems. These measurements were made possible via the use of novel test structures consisting of organic-on-inorganic semiconductor contact barrier diodes. Furthermore, we have grown InGaAs/InP heterojunctions with the lowest defect densities yet reported, and obtained the surprising result that the defect charge

density is independent of the degree of lattice mismatch. We observe that the defect density is strongly related to the purity of the source metals used in the semiconductor growth. Finally, we have employed our low defect density heterojunctions in novel, high sensitivity heterojunction bipolar phototransistors.

4. Acknowledgements

I would like to thank Mr. Len-yi Leu and Mr. Chia-di Lee for generating the theory, concepts and data used in this work. Also, I would like to thank Dr. Michael Stroscio for his steadfast support of this program.

5. References

1. H. Kroemer, Wu-Yi Chen, J. S. Harris and D. D. Edwall, Appl. Phys. Lett., **36**, 295 (1980).

2. H. Kroemer and W. Y. Chen, Solid-State Electron., **24**, 655 (1981).

3. S. R. Forrest and O. K. Kim, J. Appl. Phys., **52**, 5838 (1981).

4. P. S. Whitney and C. G. Fonstad, J. Crystal Growth, **83**, 219 (1987).

5. M. Ogura, M. Mizuta and K. Oraka, Japan. J. Appl. Phys., **22**, 1502 (1983).

6. S. R. Forrest, M. L. Kaplan and P. H. Schmidt, Ann. Rev. Mat. Sci., **17**, 189 (1987).

7. S. R. Forrest, P. H. Schmidt, R. B. Wilson and M. L. Kaplan, J. Vac. Sci. Technol., **B4**, 37 (1986).

FIGURE CAPTIONS

Fig. 1: Calculated free carrier concentration as a function of position for several values of fixed interface charge density. The heterojunction studied is shown in the inset.

Fig. 2: Dependence of the measured conduction band offset energy as a function of fixed interface charge density. Here, ΔE_{ck} is the measured value, ΔE_{c1} is due to the contribution from fixed charge only, and ΔE_c is the actual value.

Fig. 3: Calculated (dashed line) and measured (solid line) apparent free carrier concentration profiles for a VPE-grown InGaAs/InP heterojunction. SIMS profile of the heterojunction is shown in the inset.

Fig. 4: Dependence of the measured conduction band offset energy as a function of temperature for various measurement frequencies. Sample is a InGaAs/InP heterojunction grown by LPE.

Fig. 5: Data of Fig. 4 after correction using Eq. (1) in text.

Fig. 6: Dependence of the measured conduction band offset energy as a function of temperature for various lattice mismatches. Samples are InGaAs/InP heterojunctions grown by LPE using ultra-high purity indium.

Fig. 7: Bipolar current voltage characteristics of an H_2Pc/p-HgCdTe heterojunction measured at room and low temperatures.

Fig. 8: Composite free carrier concentration profile of a taper-etched *n*/p-HgCdTe/CdTe sample.

Fig. 9: Detail of the profile shown in Fig. 8 in the region of the HgCdTe/CdTe heterojunction. Inset is the inferred band diagram for this sample.

Fig. 10: Heterojunction bipolar phototransistor characteristics obtained using LPE growth.

Fig. 11: Photocurrent and dark current gains of novel (Fig. 12) and conventional InGaAs/InP HPTs as a function of collector current.

Fig. 12: Novel InGaAs/InP heterojunction bipolar phototransistor structure with low base recombination current.

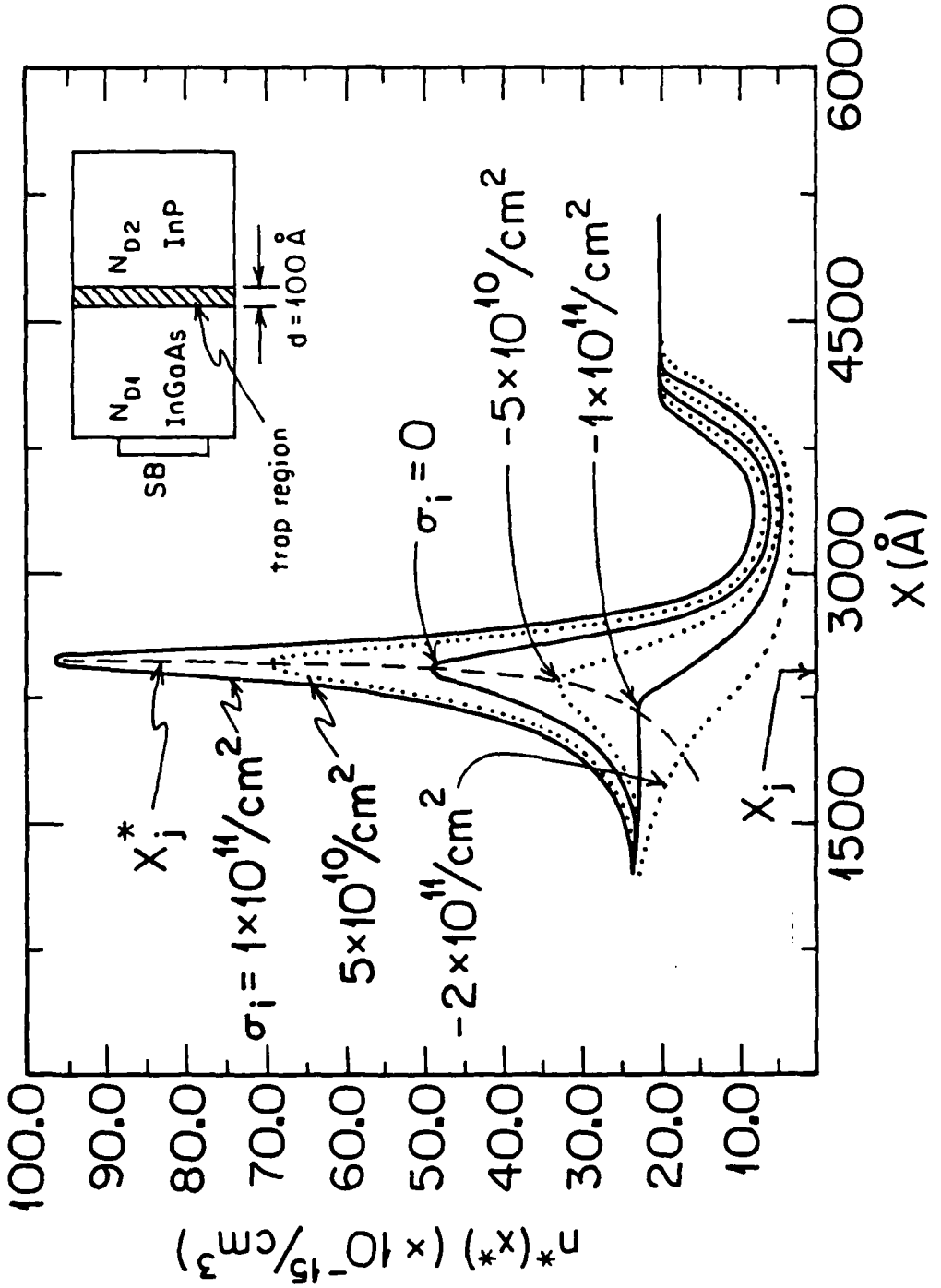
n*(x*) (x 10⁻¹⁵/cm³)
100.0
90.0
80.0
70.0
60.0
50.0
40.0
30.0
20.0
10.0
1500
3000
4500
6000
X (Å)
X*j
Xj
σi = 1×10¹¹/cm²
5×10¹⁰/cm²
-2×10¹¹/cm²
σi = 0
-5×10¹⁰/cm²
-1×10¹¹/cm²
trap region
SB
N_D1
InGoAs
N_D2
InP
d = 100 Å

Fig. 1

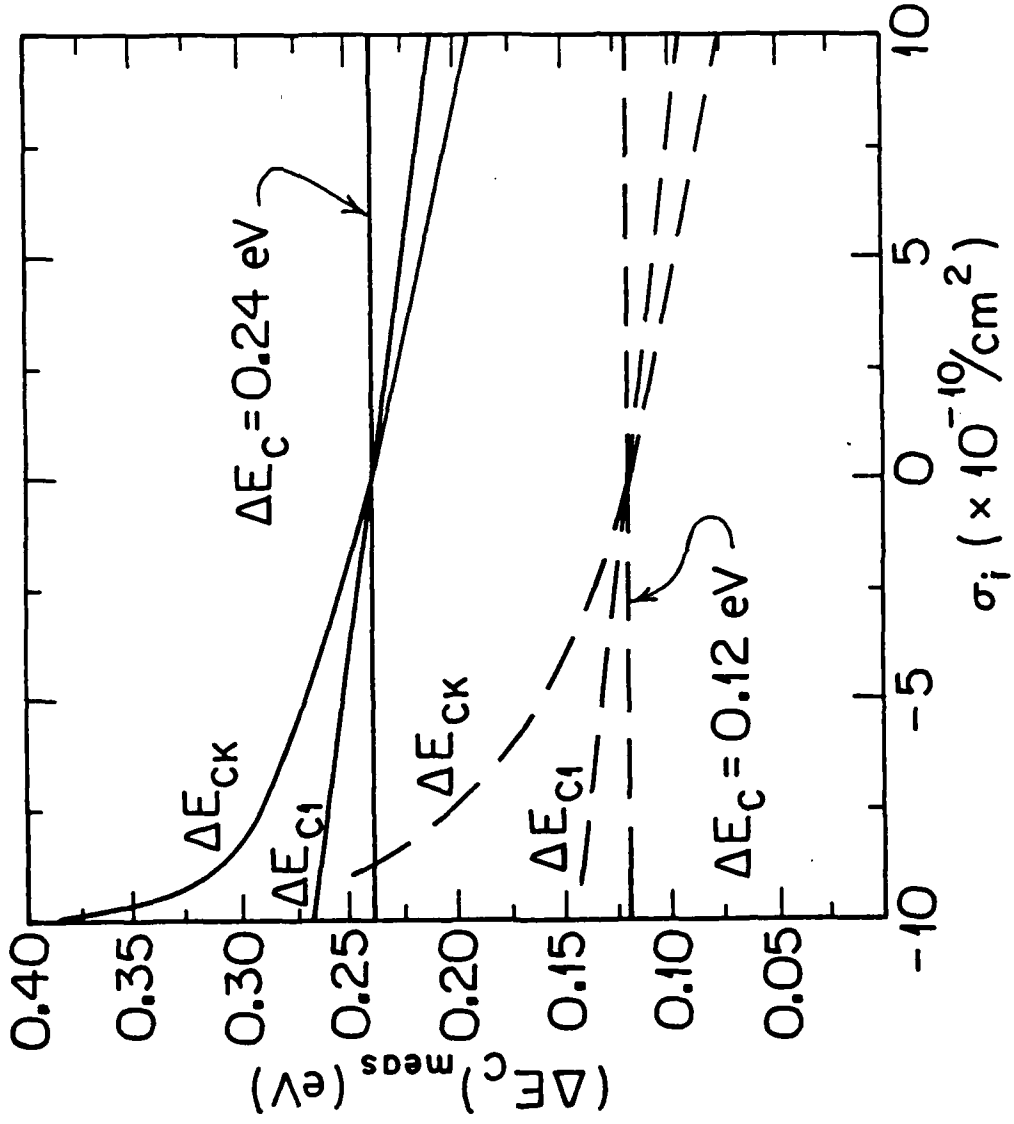
$\Delta E_c = 0.24$ eV
ΔE_{ck}
ΔE_{c1}
ΔE_{ck}
ΔE_{c1}
$\Delta E_c = 0.12$ eV
$(\Delta E_c)_{meas}$ (eV)
0.40
0.35
0.30
0.25
0.20
0.15
0.10
0.05
10
5
0
-5
-10
σ_i ($\times 10^{-10}$/cm^2)

Fig. 2

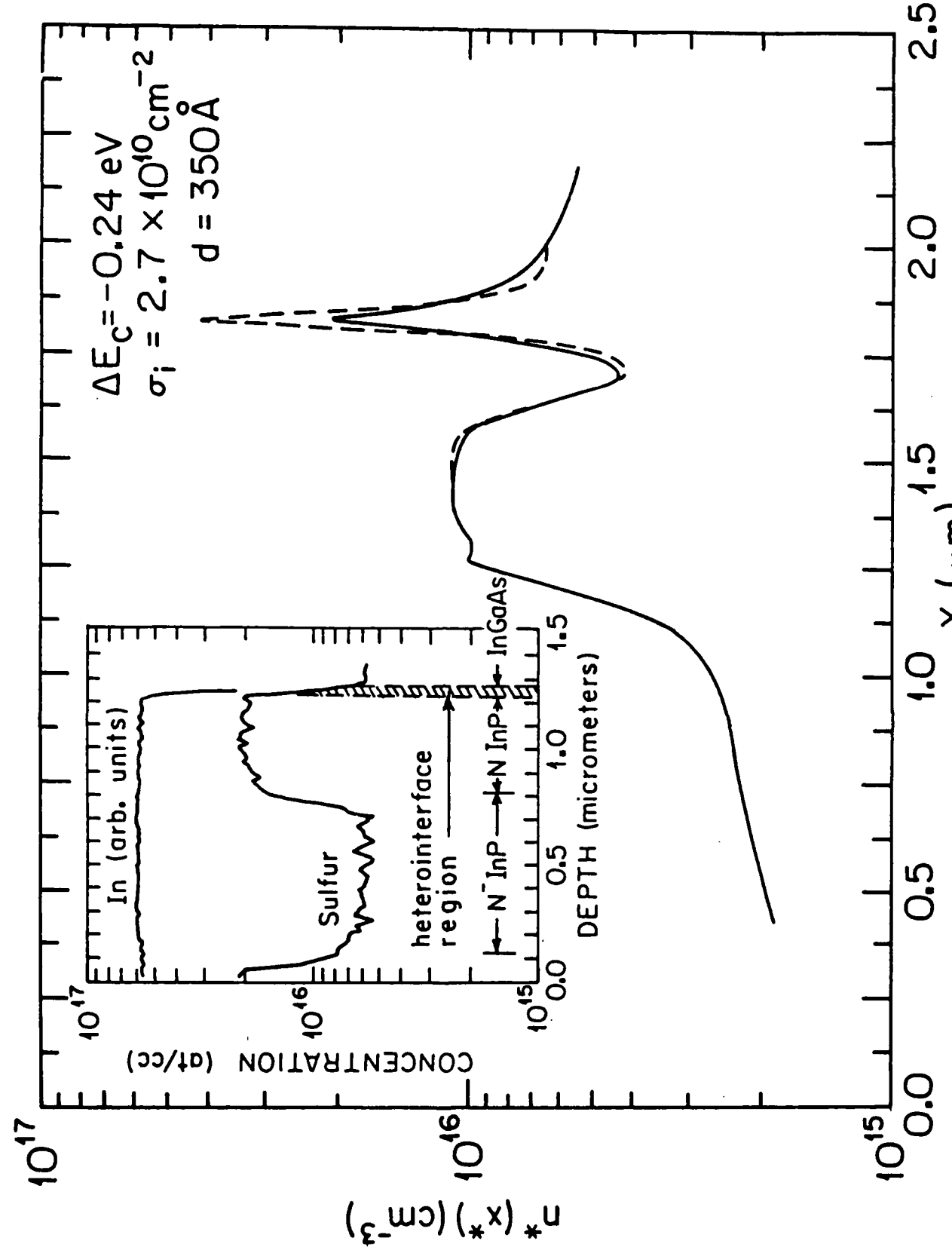
$\Delta E_c = -0.24$ eV
$\sigma_i = 2.7 \times 10^{10}$ cm^{-2}
d = 350Å
$n^*(x^*)$ (cm^{-3})
10^{17}
10^{16}
10^{15}
0.0
0.5
1.0
1.5
2.0
2.5
X (μm)
CONCENTRATION (at/cc)
In (arb. units)
Sulfur
heterointerface region
N$^-$ InP
N InP
InGaAs
DEPTH (micrometers)

Fig. 3

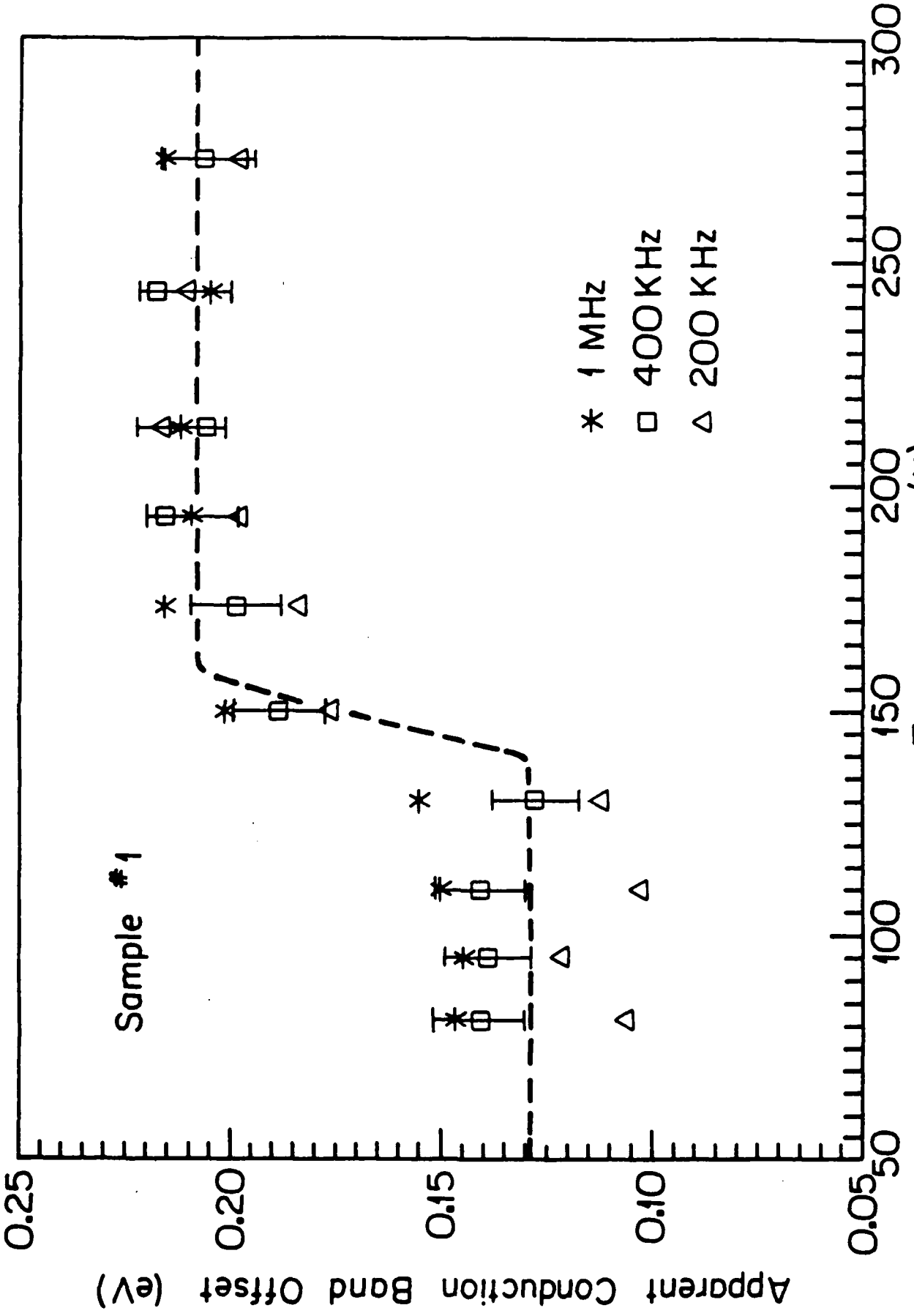
Apparent Conduction Band Offset (eV)
0.25
0.20
0.15
0.10
0.05
50
100
150
200
250
300
Temperature (K)
* 1 MHz
□ 400 KHz
△ 200 KHz
Sample #1

Fig. 4

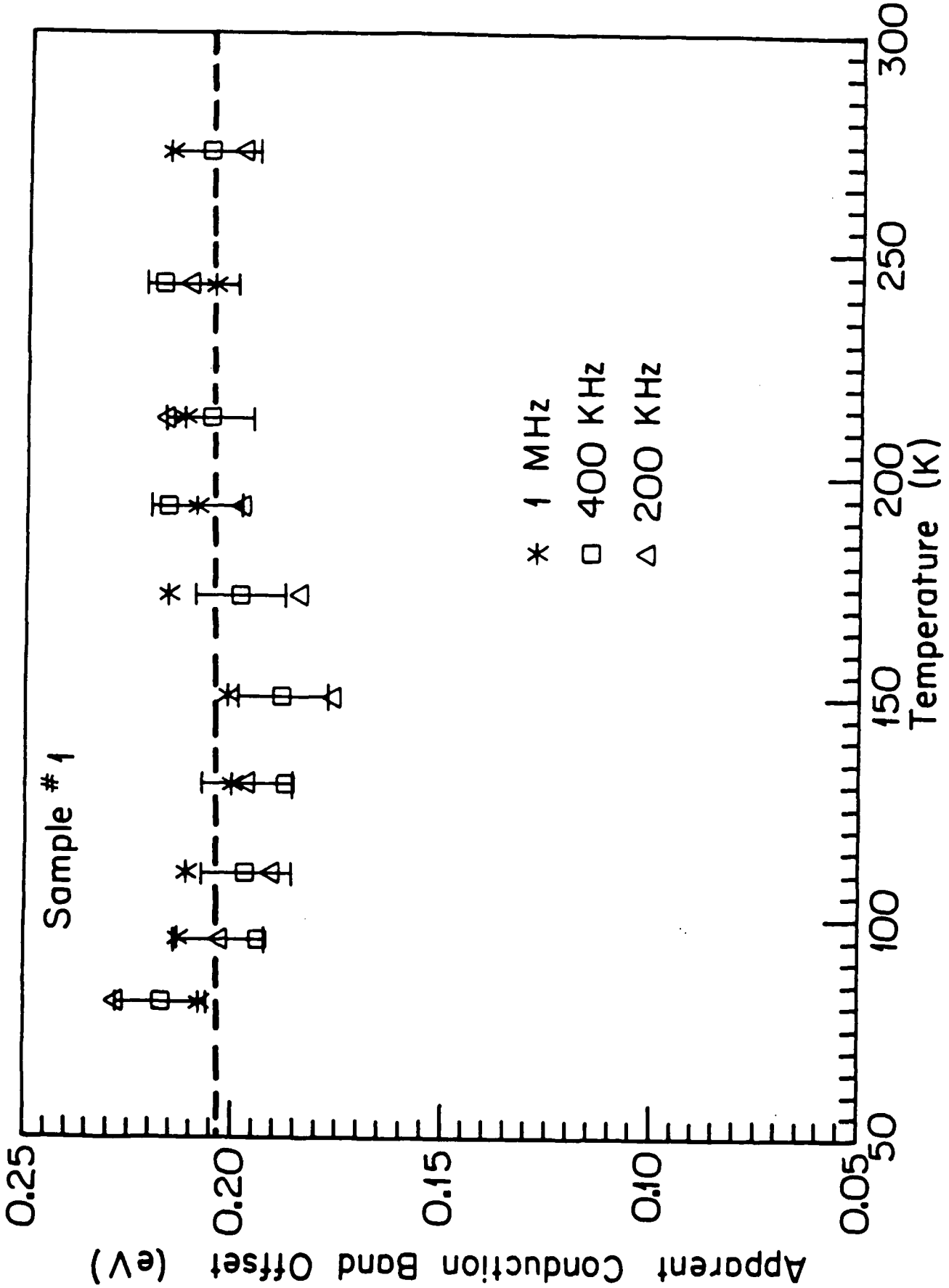
Apparent Conduction Band Offset (eV)
0.25
0.20
0.15
0.10
0.05
50
100
150
200
250
300
Temperature (K)
* 1 MHz
□ 400 KHz
△ 200 KHz
Sample # 1

Fig. 5

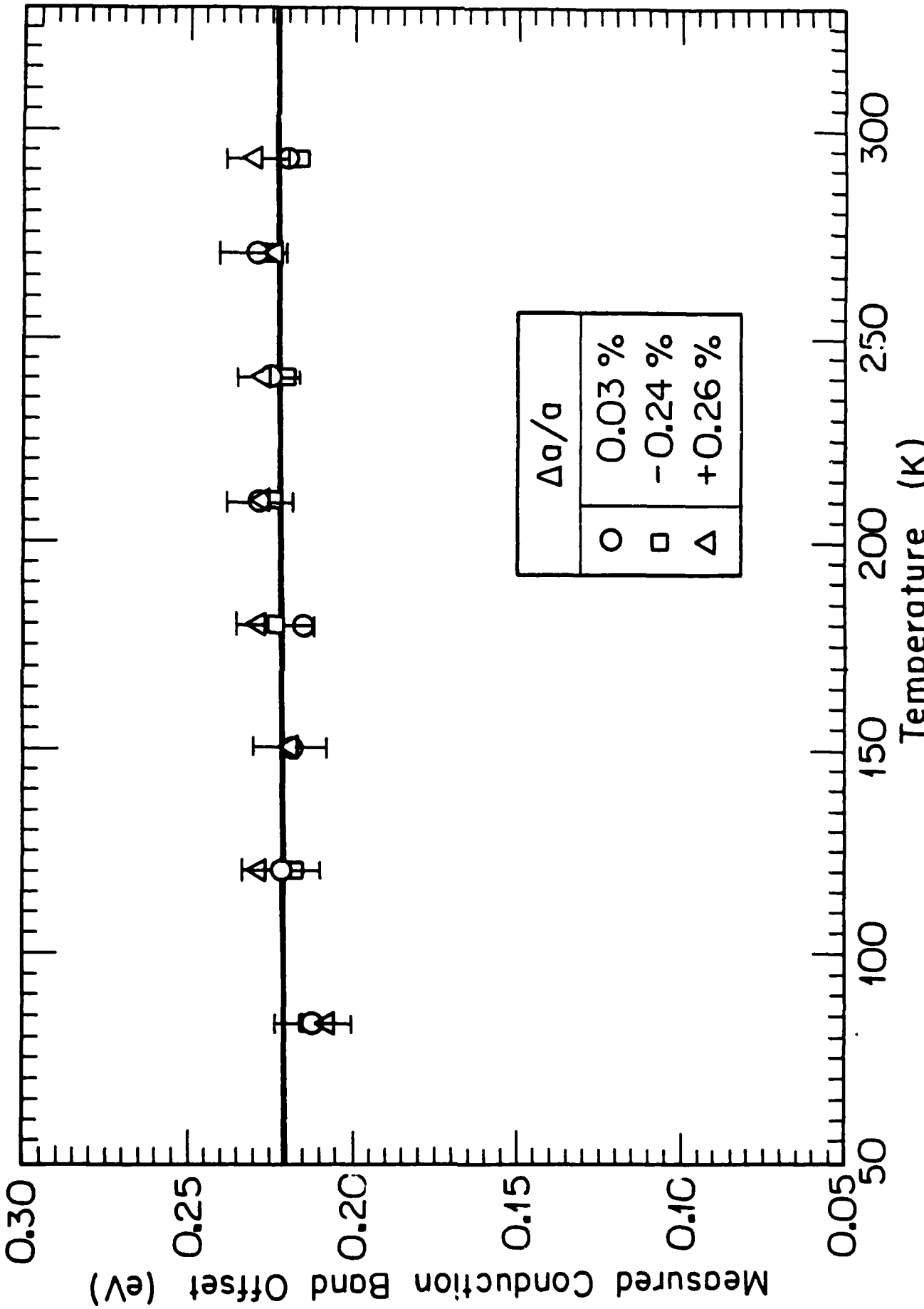
Measured Conduction Band Offset (eV)
0.30
0.25
0.20
0.15
0.10
0.05
50
100
150
200
250
300
Temperature (K)
Δa/a
O 0.03 %
□ -0.24 %
Δ +0.26 %

Fig. 6

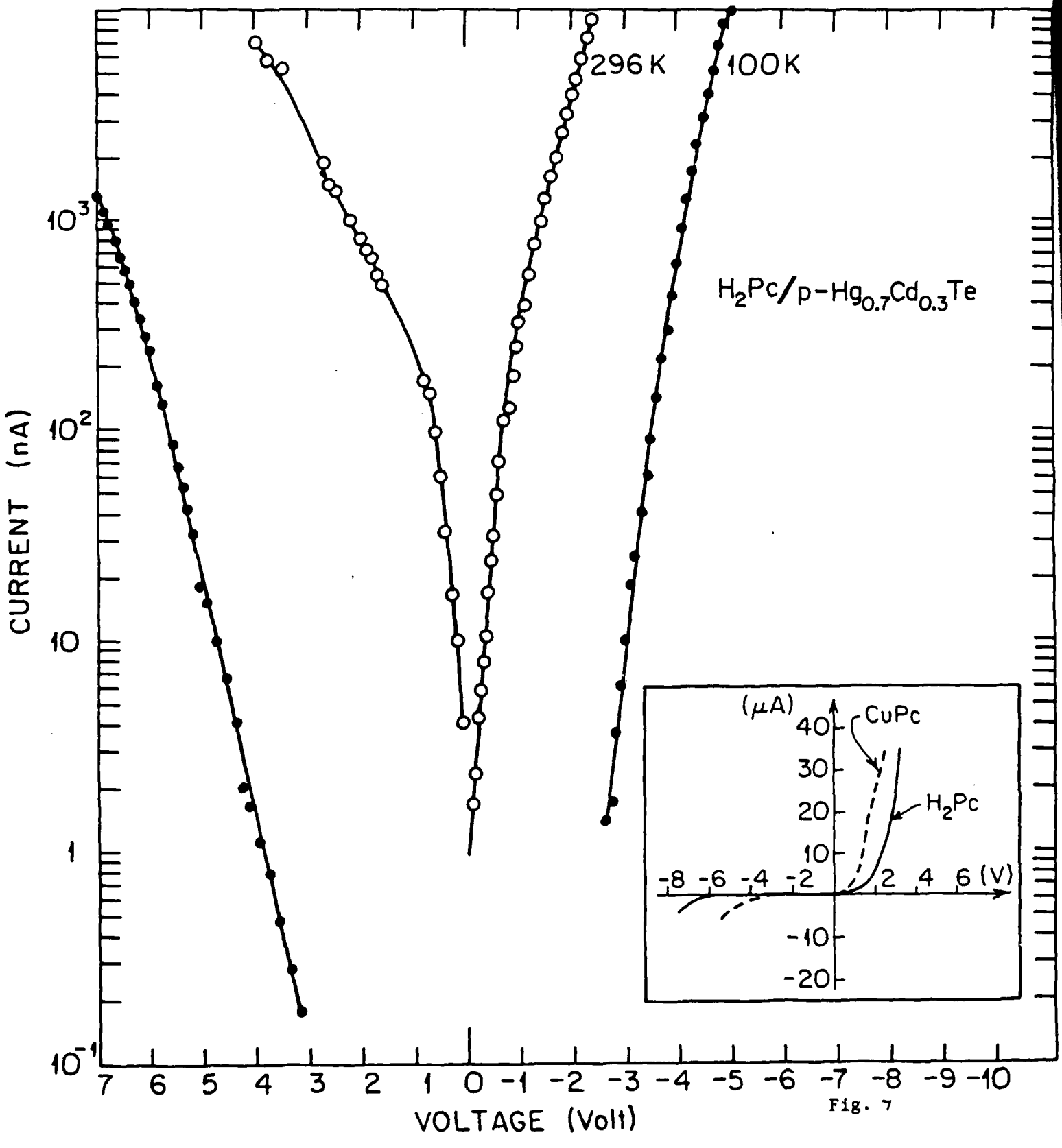
296K
100K
$H_2Pc/p-Hg_{0.7}Cd_{0.3}Te$
CURRENT (nA)
10^3
10^2
10
1
10^{-1}
7 6 5 4 3 2 1 0 -1 -2 -3 -4 -5 -6 -7 -8 -9 -10
VOLTAGE (Volt)
(μA)
CuPc
H_2Pc
40
30
20
10
-8 -6 -4 -2 2 4 6 (V)
-10
-20

Fig. 7

CARRIER CONCENTRATION (cm⁻³)
DEPTH (μm)
n – Hg1-y Cdy Te
p – Hg0,7Cd0,3Te
Cd(4%Zn)Te
X*j

Fig. 8

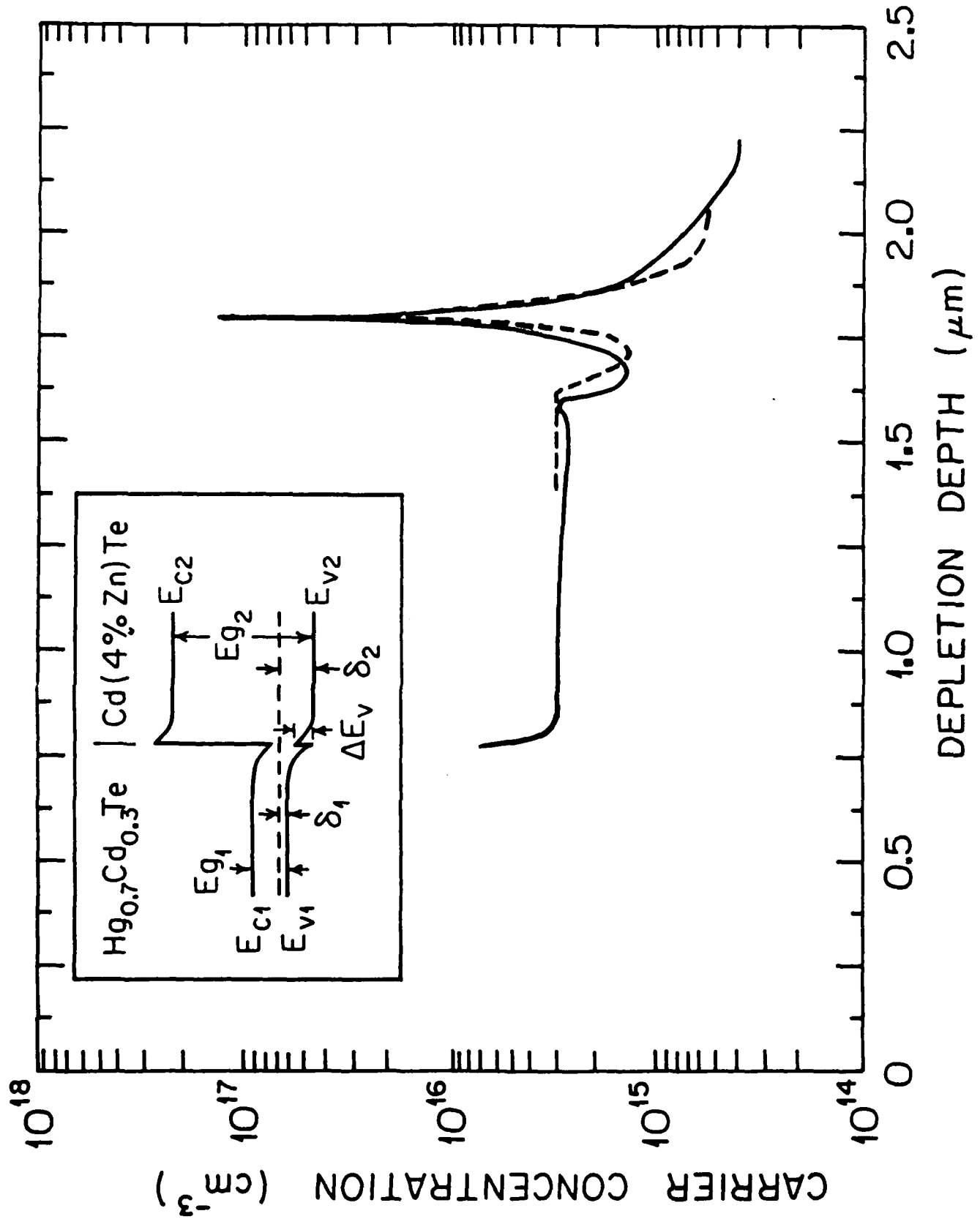
CARRIER CONCENTRATION (cm⁻³)
DEPLETION DEPTH (μm)
Hg0.7Cd0.3Te | Cd(4% Zn)Te
Ec2
Eg2
Ev2
δ2
ΔEv
δ1
Eg1
Ec1
Ev1

Fig. 9

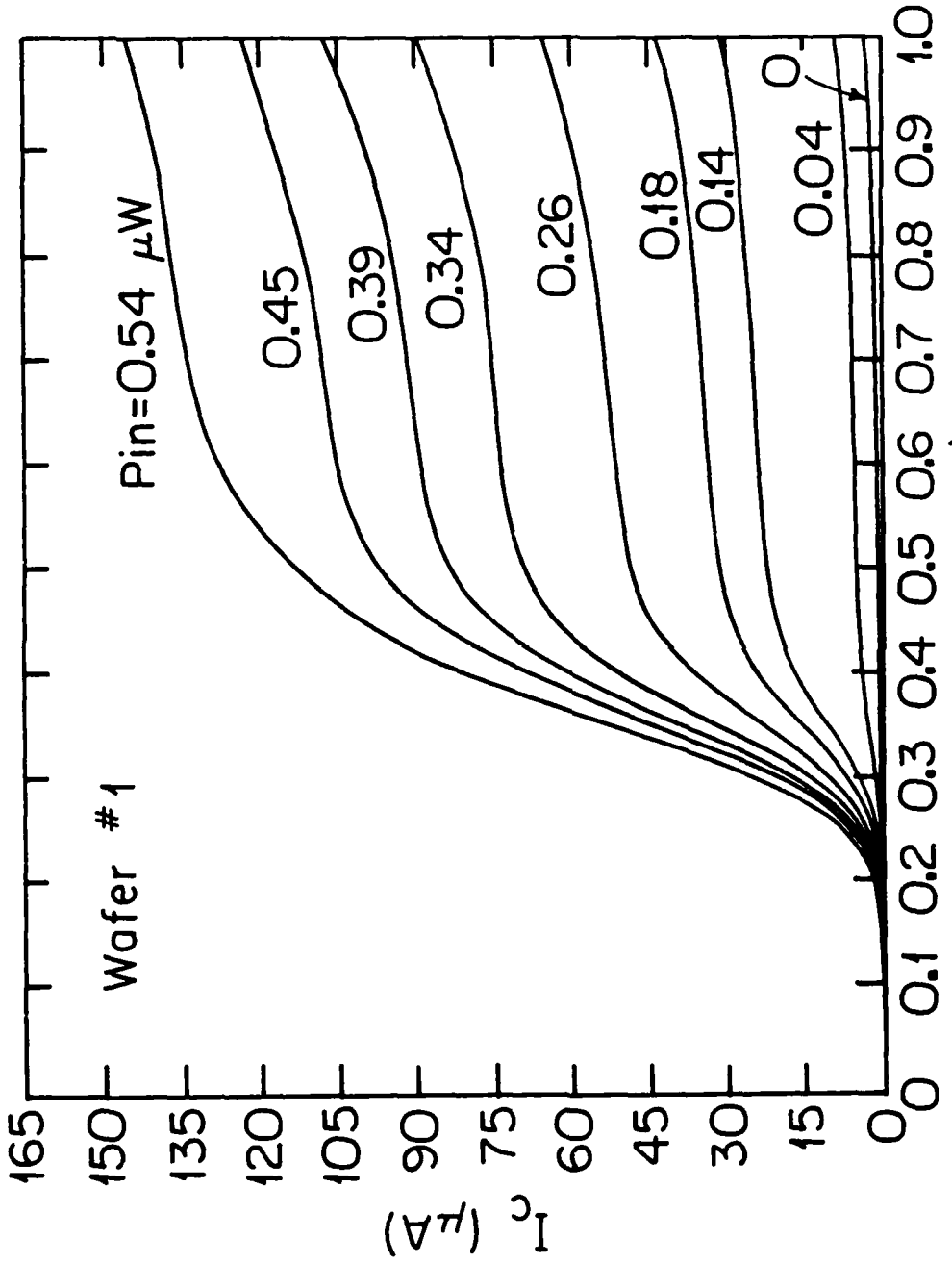
Pin=0.54 μW
0.45
0.39
0.34
0.26
0.18
0.14
0.04
0
Wafer #1
I_C (μA)
V_{CE} (Volts)
0
15
30
45
60
75
90
105
120
135
150
165
0.1
0.2
0.3
0.4
0.5
0.6
0.7
0.8
0.9
1.0

Fig. 10

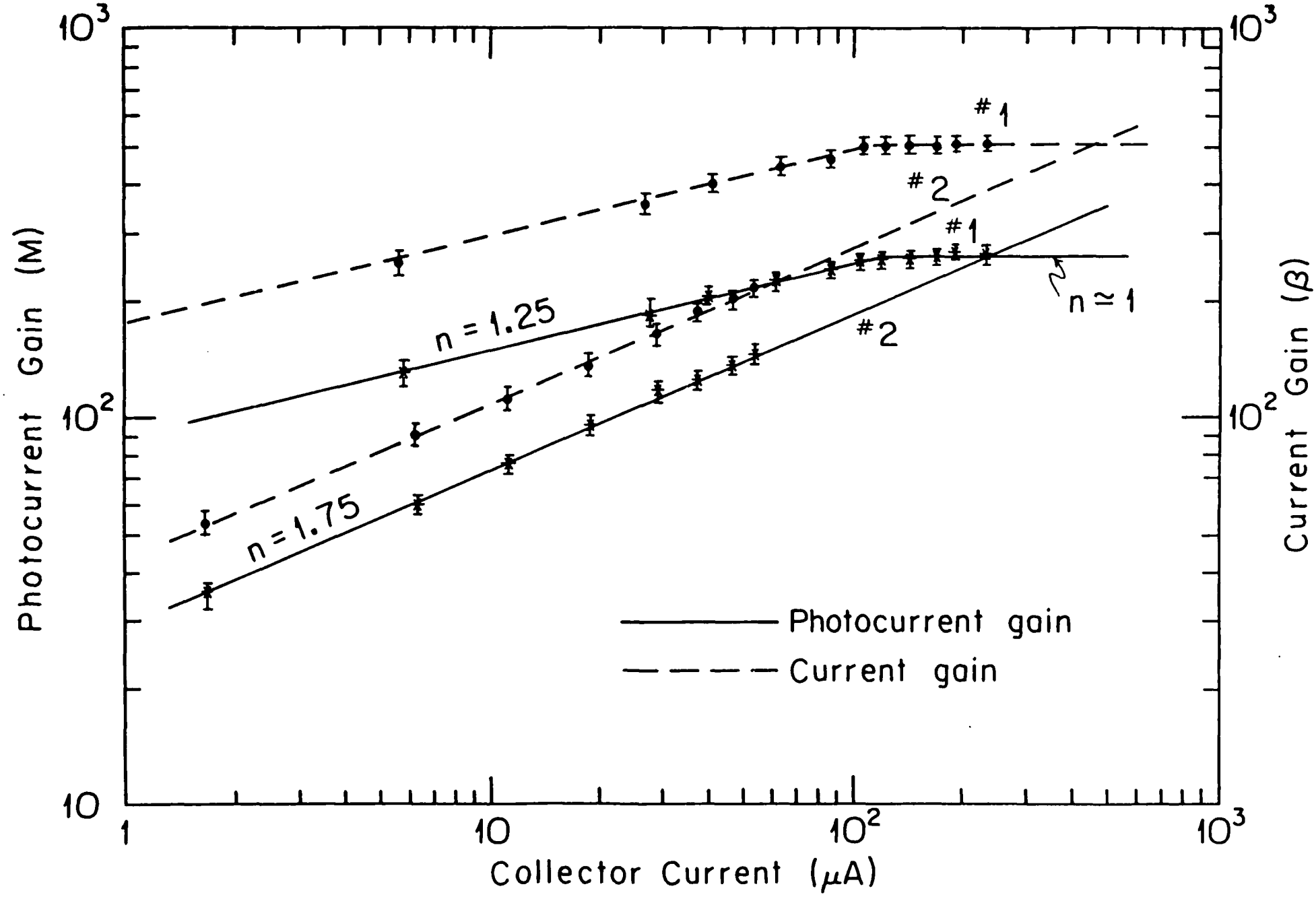
10^3
10^2
10
1
10
10^2
10^3
Photocurrent Gain (M)
Current Gain (β)
Collector Current (μA)
#1
#2
#1
#2
n = 1.25
n = 1.75
n ≃ 1
Photocurrent gain
Current gain

Fig. 11

STRUCTURE OF HETEROJUNCTION PHOTOTRANSISTOR

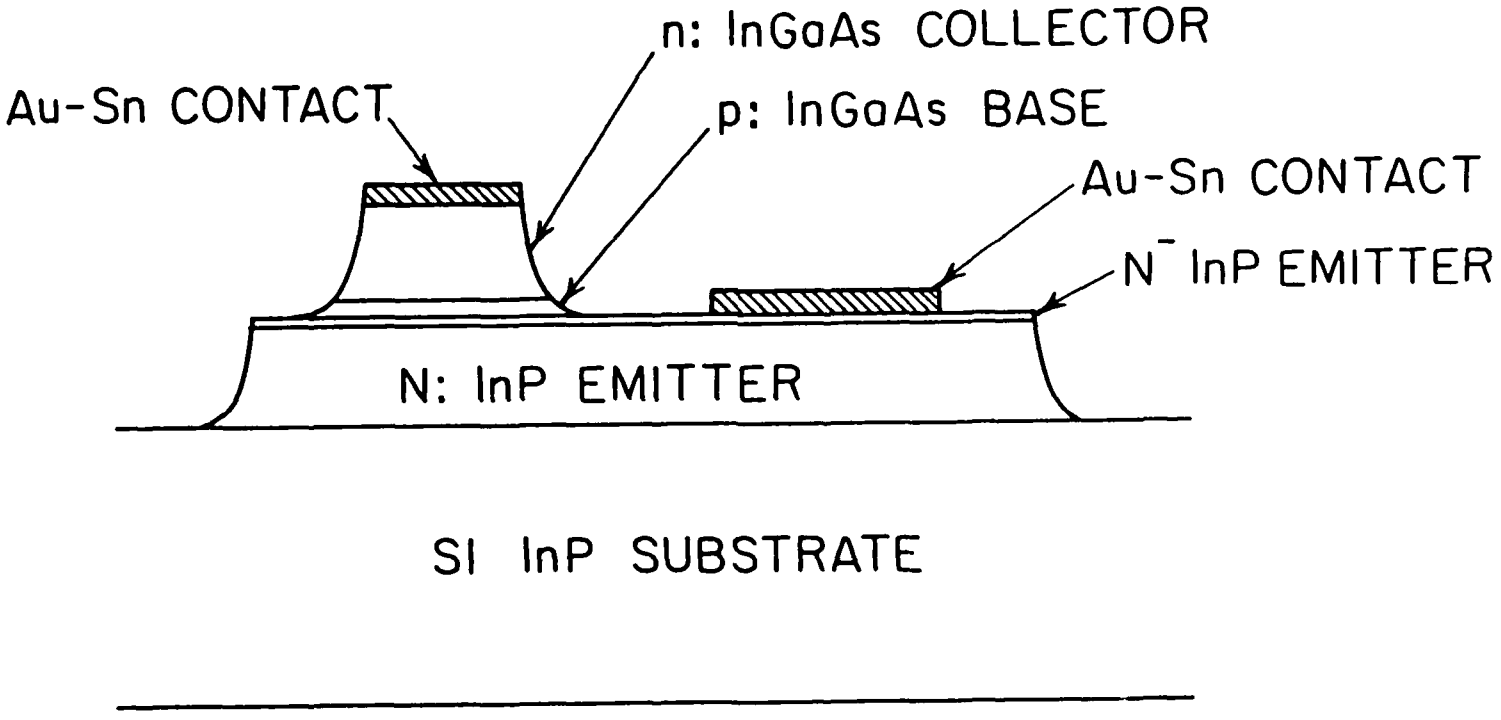

Fig. 12

APPENDIX 1

The determination of heterojunction energy band discontinuities in the presence of interface states using capacitance-voltage techniques

L. Y. Leu and S. R. Forrest
Departments of Electrical Engineering/Electrophysics and Materials Science, University of Southern California, Los Angeles, California 90089-0241

(Received 22 June 1988; accepted for publication 1 August 1988)

Effects of trapped interface charge on the determination of heterojunction energy band discontinuity energies using capacitance-voltage (C-V) techniques are analyzed both theoretically and experimentally. We show that for shallow traps, whose charge occupancy is unchanged by variations in the applied voltage, the measured conduction band discontinuity energy (ΔE_c) as determined by the depletion technique [Kroemer, Chien, Harris, and Edwall, Appl. Phys Lett. **36**, 295 (1980)] is a function of trap density (σ_i). This error source in determining ΔE_c is large for small values of ΔE_c due to distortions of the conduction band induced by the trapped interface charge. In addition, the analysis used for determining σ_i and ΔE_c via the depletion technique has been generalized to correct for the effects of both deep and shallow traps. We show that at low measurement frequency, the measured value of ΔE_c is nearly independent of σ_i, and this value is near to the exact value of ΔE_c measured in the absence of interface traps (i.e., for $\sigma_i = 0$). However, at high measurement frequency (or low temperature), the measured ΔE_c decreases with increasing σ_i or increasing trap energy depth from the conduction band minimum. These deviations from the actual value can be corrected by using the equations developed in this article. We apply these results to the understanding of $In_{0.53}Ga_{0.47}As$/InP heterojunctions. The computer-simulated apparent free carrier concentration profiles are used to fit experimental data at several temperatures. The best fit value of ΔE_c ($= 0.22$ eV) is in agreement with the value obtained via the emended equations. We explain the complex temperature dependence of these experimental profiles as due to donor traps near the heterojunction.

I. INTRODUCTION

The band discontinuity energy is one of the most important parameters needed to determine heterojunction (HJ) characteristics. Among the various measurement techniques available,[1-7] capacitance-voltage (C-V) analysis is among the most powerful.[8,9] In particular, using the C-V method first proposed by Kroemer *et al.*,[10] information regarding the HJ position (x_j), the fixed charge density (σ_i), and conduction band discontinuity energy (ΔE_c), can all be easily determined.

However, there are several phenomena which lead to inaccuracies in determining ΔE_c and related parameters by C-V methods. Among these are: compositional gradients between the contacting semiconductors[11,12]; doping nonuniformities due to interdiffusion near the HJ; and the inherent difference between the actual x_j, and the apparent heterojunction depth[10,13] x_j^* (as determined from the peak position of the apparent carrier concentration profile). As a result, the magnitude of the errors due to these factors needs to be studied in detail.

In particular, it has been observed[14-17] that both σ_i and ΔE_c obtained for $In_{0.53}Ga_{0.47}As$/InP heterojunctions measured by C-V techniques apparently depend strongly on both temperature and measurement modulation frequency, contradicting the fact that ΔE_c is an inherent property of the HJ, and therefore should be independent of these "environmental" parameters. Recently, Kazmierski *et al.*[16] pointed out that the dependence of ΔE_c on both temperature and frequency may arise from the dynamic behavior of interface traps. They suggest that the apparent carrier concentration profile, $n^*(x^*)$, with its characteristic peak and valley usually associated with the presence of the HJ dipole, can be generated entirely by deep donor traps, rather than due to a nonzero value of ΔE_c. However, Kazmierski[16] assumes that the donor traps are partially filled at low temperature, and completely filled at equilibrium at high temperature, which is opposite to what is expected for such traps. The dramatic shift of apparent (x_j^*) from the actual HJ position (x_j) used in their simulation was obtained by setting $\Delta E_c = 0$. This shift introduces large calculational errors, and thus the conclusion that $\Delta E_c = 0$ does not appear to be correct.

Lang *et al.*[18] measured the conduction band discontinuity of the same HJ system by admittance spectroscopy of quantum well structures. In that work, a value of $\Delta E_c = 250 \pm 10$ meV was obtained which agrees well with the C-V data reported by others.[14,15,17] On the other hand, Lang claims that C-V measurement yields a vanishing HJ diffusion potential at low temperature simply due to the presence of a parasitic temperature-dependent series resistance of the undepleted HJ region. This, however, contradicts data presented elsewhere.[19]

In order to study the error sources inherent in C-V measurements of HJ properties, and to understand the apparent paradoxes mentioned above, the effects of shallow, as well as deep traps are considered by analytical as well as numerical simulation methods. The original equations of Kroemer *et al.*[10] for the determination of the trap density (σ_i) and HJ diffusion potential (V_D), appear to be valid only for HJs

 0021-8979/88/225030-11$02.40

with a low density of shallow interface traps. It will be shown that $\Delta E_c(\sigma_i)$—i.e., the conduction band discontinuity energy measured for a HJ with a shallow interface charge density of σ_i— differs more from the actual value $\Delta E_c(0)$ as σ_i increases, independent of the polarity of σ_i. In addition, the deviation of $\Delta E_c(\sigma_i)$ from the value calculated using the original equations suggested by Kroemer (called ΔE_{cK} in this article) becomes nearly constant at high temperatures and low measurement frequencies. Modified equations are derived which can be used to correct for errors in $\Delta E_c(0)$ induced by the presence of charge at the heterojunction. Also, the measured trap density obtained from the original equations (called σ_{iK}) is found to deviate from the exact value of σ_i, depending on whether the traps are donor- or acceptorlike.

Two $In_{0.53}Ga_{0.47}As/InP$ heterostructure samples are studied by C-V techniques. For sample No. 1, we compare the experimental and theoretical C-V data measured at $T = 201$ and 102 K. The equations derived for determining the conduction band discontinuity were used to correct the measured value, ΔE_{cK}. After correction, the value of $\Delta E_c(0)$ is found to equal 0.22 eV, which is consistent with the consensus of values of ΔE_c for this HJ system reported in the literature. In a second sample, the apparent free carrier concentration profile shows a double-peak feature at room temperature. This feature has also been reported by Andre *et al.*[20] for $In_{0.53}Ga_{0.47}As/InP$ HJs and more recently by Jeong, Schlesinger, and Milnes[21] for InGaAs/GaAs heterojunctions. In our sample, a third peak also appears at $T = 200$ K. From analysis discussed in this article, we attribute the first and the second peaks to two deep donor traps, while the third peak is due to accumulation of electrons near the heterojunction (HJ).

The article is organized as follows: In Sec. II we present the theory of the dependence of ΔE_c on interface charge density, and hence derive new equations for determining σ_i and the HJ diffusion potential (V_D). The error sources inherent in using the original equations in Ref. 10 in the presence of deep traps are discussed. Furthermore, carrier concentration profiles as obtained from C-V data are numerically simulated for the case of both deep and shallow levels, and the effects of measurement frequency and temperature on determining V_{DK} in the presence of deep traps are considered. In Sec. III, methods for obtaining ΔE_c by use of the emended equations is presented. In Sec. IV, experimental data for $In_{0.53}Ga_{0.47}As/InP$ HJs are analyzed and in Sec. V, we present conclusions.

II. THEORY

Figure 1 shows the apparent $[n^*(x^*)]$ and actual free carrier concentration $[n(x)]$ profiles calculated for a Schottky barrier-on-heterojunction ($SB/In_{0.53}Ga_{0.47}As/InP$) structure. In this heterojunction system, $In_{0.53}Ga_{0.47}As$ and InP have band-gap energies of 0.75 and 1.35 eV, respectively. The apparent (or measured) free carrier concentration $[n^*(x^*)]$ is determined from C-V data obtained by depleting the HJ by applying reverse voltage to the adjacent rectifying SB contact. Hence,[22]

$$n^*(x^*) = \left(\frac{2}{q\kappa}\right)\frac{dV}{d(1/C^2)}, \tag{1a}$$

with

$$x^* = \kappa/C, \tag{1b}$$

where x^* is the apparent distance from the SB contact, q is the electronic charge, and κ is the semiconductor permittivity.

The actual free carrier concentration profile $n(x)$ is obtained by solving Poisson's equation. Due to the existence of a conduction band discontinuity (ΔE_c), the free carriers are accumulated at the $In_{0.53}Ga_{0.47}As$, and are depleted from the InP side of the HJ. The difference between $n^*(x^*)$ and $n(x)$ in the HJ region (Fig. 1) arises from the limited spatial resolution inherent in the C-V data.[23] Kroemer, and coworkers have shown[10,11] that the total number of free carriers, as well as the first moment of the charge distribution should be identical for both the measured and actual carrier concentration profiles when integrated across the entire HJ region. Based on these assumptions, the density of fixed interface charge, σ_{iK}, and the diffusion potential V_{DK}, of an isotype HJ can be expressed by

$$\sigma_{iK} = -\int_{-\infty}^{\infty}[N_D(x^*) - n^*(x^*)]dx^*, \tag{2}$$

$$V_{DK} = q/\kappa\int_{-\infty}^{\infty}[N_D(x^*) - n^*(x^*)](x^* - x_j)dx^*, \tag{3}$$

where $N_D(x^*)$ is the background doping concentration at apparent position x^*, and x_j is the actual position of the HJ as measured from the surface of the sample.

Now, the conduction band discontinuity (ΔE_{cK}) is obtained from the diffusion potential via:

$$\Delta E_{cK} = qV_{DK} + \delta_2 - \delta_1, \tag{4}$$

where δ_1 and δ_2 are the depths of the Fermi levels as measured from the conduction band minima for the two contacting materials.

Note that only shallow interface charge traps are con-

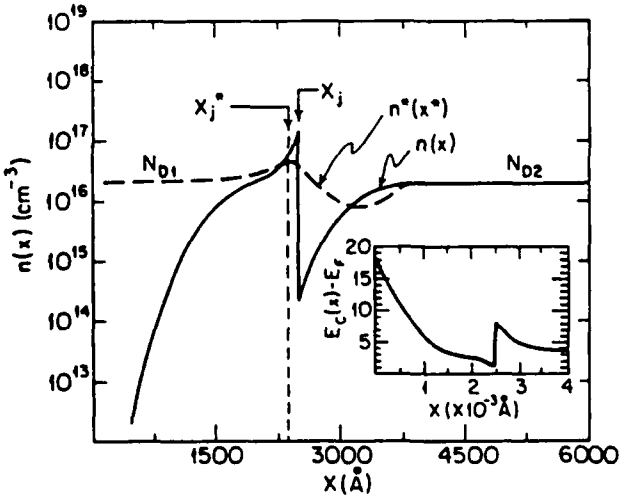

FIG. 1. Apparent $[n^*(x^*)]$ and actual free carrier concentration $[n(x)]$ profiles for a $SB/In_{0.53}Ga_{0.47}As/InP$ heterojunction. Inset: Conduction band diagram corresponding to the actual free carrier concentration profile. The ordinate is in units of k_BT.

sidered in the above analysis. For deeper traps, whose occupancies are a function of applied voltage, the density of ionized traps (σ_i) changes with bias according to Fermi–Dirac statistics. Hence, Eqs. (2) and (3) must be modified to account for variations in trap occupancy as the Fermi energy is swept through the band gap in the HJ region.

To explore the effects that deep levels have on measurements of ΔE_c, we assume that acceptor traps are negatively charged when occupied by electrons, becoming neutral after the electrons are excited into the conduction band. On the other hand, donor traps are positively charged when the electrons are excited to the conduction band, and are neutral when occupied. The density of ionized traps (σ_i) at each voltage can be expressed by an integral over the *ionized* trap concentration $\pm N_t(x)$ (+ for donor and − for acceptor traps). Hence, σ_i is given by

$$\sigma_i = \pm \int N_t(x)dx = \pm \int_{-\infty}^{\infty} \frac{N_{to}(x)dx}{1 + g\exp\{\pm[-E_c(x) + E_F + E_t]/k_BT\}}, \quad (5)$$

where E_t is the trap energy with respect to the conduction band minimum $E_c(x)$, and $N_{to}(x)$ is the total trap concentration at position x. A degeneracy factor (g) of 2 for donors and $\frac{1}{2}$ for acceptors is assumed. Note that $E_c(x)$ is a function of voltage, and thus σ_i is also voltage dependent.

Now, charge neutrality can be expressed by

$$\sigma_i = -\int_{-\infty}^{\infty} [N_D(x) - n(x)]dx \quad (6)$$

and the diffusion potential obtained for a HJ with traps is given by

$$V_D(\sigma_i) = q/\kappa \int_{-\infty}^{\infty} [N_D(x) - n(x)](x - x_j)dx. \quad (7)$$

Both Eqs. (6) and (7) differ from Eqs. (2) and (3) in that the actual [$n(x)$] rather than apparent [$n^*(x^*)$] free carrier concentration profiles and positions are used. Furthermore, note that Eqs. (6) and (7) may have an implicit voltage dependence in the presence of deep traps. This dependence arises via the means for determining $n(x)$ using C-V data. As voltage is increased, $E_c(x)$ changes, which will, in turn, contribute to $n(x)$ via the emission of trapped charge when $E_t > E_F$. Defining

$$n'(x) = n(x) \pm N_t(x) \quad (8)$$

as the total free carrier concentration due to shallow plus ionized deep donors (− sign) or acceptors (+), and substituting this along with Eq. (5) into Eq. (6) gives

$$-\int_{-\infty}^{\infty} [N_D(x) - n'(x)]dx = 0. \quad (9)$$

Replacing $n(x)$ with $n'(x)$ is equivalent to setting $\sigma_i = 0$. Making the transformation of $n(x) \rightarrow n'(x)$ therefore should allow for the determination of the "intrinsic" HJ diffusion potential V_D from the potential measured in the presence of defects. We will show that this can be accomplished without the detailed knowledge of $N_t(x)$ which, in fact, cannot be exactly obtained using C-V data due to their limited resolution.

The diffusion potential in the absence of traps near the HJ [$V_D(0)$], is found by invoking the conservation of total first moment of charge.[23] Hence:

$$V_D(0) = q/\kappa \int_{-\infty}^{\infty} [N_D(x) - n'(x)](x - x_j)dx,$$

which leads to

$$V_D(0) = V_{DK} \pm q/\kappa \int_{-\infty}^{\infty} N_t^*(x^*)(x^* - x_j)dx^*. \quad (10)$$

As will be shown below, the interface position apparently "shifts" to x_j^* from its actual position x_j, depending on the interface state density σ_i. Defining $\Delta x_j = x_j - x_j^*$, we can write Eq. (10) to obtain (for shallow or deep donor traps):

$$V_D(0) = V_{DK} + q/\kappa \int_{-\infty}^{\infty} N_t^*(x^*)(x^* - x_j^*)dx^* - q\Delta x_j/\kappa \int_{-\infty}^{\infty} N_t^*(x^*)dx^*, \quad (11)$$

where $V_{DK} = V_D(\sigma_i)$ is the diffusion potential measured in the presence of trapped charge. A similar expression can be obtained for deep acceptor traps (Appendix A). Once more, assuming conservation of charge, and using Eqs. (6), (8), and (9) we conclude that

$$\sigma_i = \sigma_{iK} = \pm \int_{-\infty}^{\infty} N_t^*(x^*)dx^*, \quad (12)$$

where the upper sign refers to donors, and the lower to acceptors. Equations (11) and (12) are emended forms of Eqs. (2) and (3). They can be used to determine the "intrinsic" HJ diffusion potential [$V_D(0)$] using C-V data obtained for HJs with a high density of trapped charge. We show below that the original analysis[10] is a special case of these equations.

A. Shallow interface traps

If the acceptor energy level is well below the Fermi level even at maximum applied voltage, or if the donor energy level is well above the Fermi level even at $V = 0$, all the traps are ionized. In this case, the total density of ionized traps (N_t) is bias independent, and these shallow traps are referred as "fixed charge traps." If we define the measured total trap concentration $N_{to}^*(x^*)$ in a manner analogous to the actual total trap concentration $N_{to}(x)$ [cf., Eq. (5)], then $N_{to}^*(x^*)$ can be written as $N_t^*(x^*) + N_t^{(0)*}(x^*)$, where $N_t^*(x^*)$ and $N_t^{(0)*}(x^*)$ are the measured ionized and neutral trap concentrations, respectively. For shallow traps, the ionized trap concentration is equal to the total trap concentration, and Eq. (12) becomes

$$\sigma_i = \pm \int_{-\infty}^{\infty} N_{to}^*(x^*)dx^* = \pm \int_{-\infty}^{\infty} N_{to}(x)dx = \sigma_{iK}. \quad (13)$$

Therefore, for shallow traps, Eq. (2) gives the exact trap density σ_i as concluded earlier.[10]

It is important to note, however, that the diffusion po-

tential calculated from Eq. (3) deviates from the exact value $[V_D(0)]$ since it neglects the last two terms on the right side of Eq. (11), which are the contributions to the total diffusion potential due to interface traps. We need to subtract this effect from V_{DK} to obtain the diffusion potential which is due only to the heterointerface dipole, and thus obtain $V_D(0)$. This last value then yields the correct value of ΔE_c via Eq. (4).

If $N_{to}(x)$ is uniformly distributed between x_j and $x_j + d$, Eq. (11) can be simplified to give

$$V_D(0) = V_{DK} + q\sigma_i d/2\kappa + q\Delta x_j \sigma_i/\kappa. \qquad (14)$$

Note that $V_D(0)$ approaches V_{DK} as d or σ_i is decreased. Thus, measurements of ΔE_c using the C-V depletion technique are only accurate in the absence of interface traps, although the effects of traps are small for very abrupt HJs. Note also that an accurate determination of the interface position, x_j, is also essential for the calculation of V_D from Eq. (3). Usually, x_j is assumed to be located at the peak position of the apparent carrier concentration profile (Fig. 1), although it has been shown[10,13] that x_j^* is shifted away from x_j, particularly when the rectifying contact is formed at the side of the larger band-gap material. However, from a measurement of $\sigma_i = \sigma_{iK}$, V_{DK}, and Δx_j from C-V data, and an estimate of d for the HJ sample, it is straightforward to obtain $V_D(0)$ (and hence ΔE_c) using Eq. (14). We will show how this is done in practice in the discussion below.

As a specific example illustrative of the effects of traps, we model $In_{0.53}Ga_{0.47}As$/InP HJs using materials parameters given in Table I. In this work, several assumptions were made to simplify the numerical simulations: (i) The total trap concentration N_{to} is assumed to be uniformly distributed within a thin region of width[21] d located on one side of the HJ; (ii) one trap at energy E_t was assumed for deep interface traps; and (iii) the quasi-Fermi level is assumed to be flat throughout the HJ region. No compositional or doping concentration gradients, image charge or quantum effects in the accumulation region are considered.

Figure 2(a) shows the calculated $n^*(x^*)$ profiles of an $In_{0.53}Ga_{0.47}As$/InP HJ with various values of σ_i located within 100 Å of the InP side of the HJ. For $\sigma_i < 0$, electrons are repelled from both sides of the HJ, and thus the peak of $n^*(x^*)$ decreases while x_j shifts toward the surface ($x = 0$). When $\sigma_i = -2\times10^{11}$ cm^{-2}, the peak vanishes completely due to depletion of carriers from both sides of the HJ. This is the so-called "double-depletion" characteristic sometimes observed for HJs with a high density of interface charge.[24–26] Positive trapped charge, however, attracts electrons to both sides of the HJ. In this case, the peak becomes higher, and x_j^* shifts toward x_j.

Table I. Parameters used for $In_{0.53}Ga_{0.47}As$/InP heterojunction calculations.

Quantity	Units	Value
E_{g1}	eV	0.75
E_{g2}	eV	1.35
m_1 [a]	m_0 [b]	0.04
m_2 [a]	m_0	0.07
ΔE_c	eV	0.24
κ	pF/cm	1.06
x_j	Å	2500
d	Å	100
ϕ_B [c]	eV	0.4
N_{D1}	cm^{-3}	2×10^{16}
N_{D2}	cm^{-3}	2×10^{16}

[a] Subscripts 1 and 2 refer to $In_{0.53}Ga_{0.47}As$ and InP, respectively.
[b] m_0 refers to units of free electron mass.
[c] Schottky barrier energy.

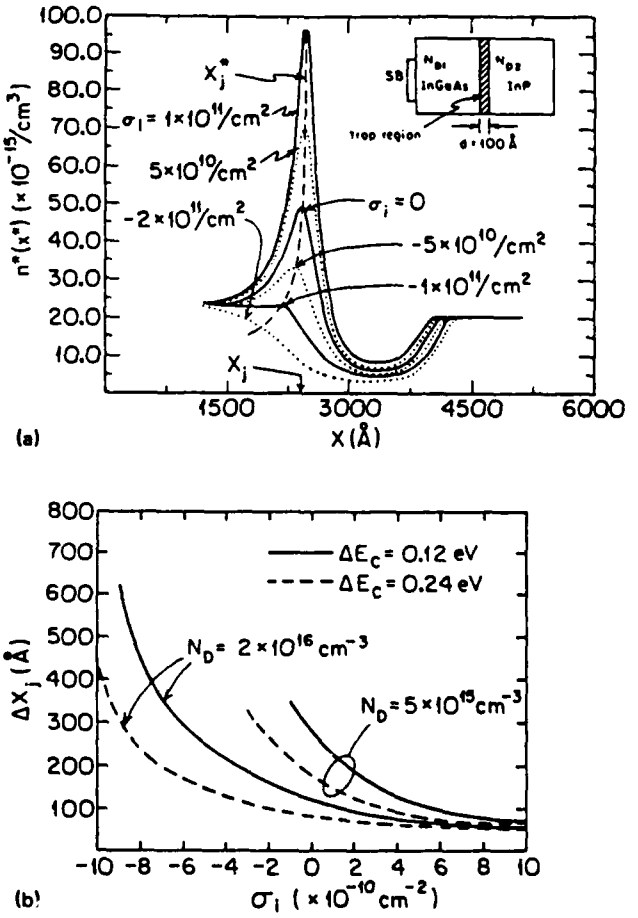

FIG. 2. (a) Apparent free carrier concentration profiles of a $In_{0.53}Ga_{0.47}As$/InP HJ for positive and negative shallow trap densities. The region with traps is located on the InP side within 100 Å of the HJ. (b) Shift in the apparent HJ position, $\Delta x_j = x_j - x_j^*$, as a function of defect density (σ_i) for two values of conduction band discontinuity energy.

Figure 2(b) shows the dependence of $\Delta x_j = x_j - x_j^*$ on interface charge density and conduction band discontinuity energy with two different background doping concentrations. From this figure, we note that for $\sigma_i > 0$, Δx_j is very small, independent of background doping. However, for acceptor traps where $\sigma_i < 0$, Δx_j is an increasing function of the trap density. Hence, for these traps, the contribution to $V_D(0)$ due to the shift in apparent HJ position must be taken into account. Indeed, Fig. 2(b) can be used to estimate the value of Δx_j to use in Eq. (14) given a background carrier concentration, N_D, σ_i, and ΔE_{cK} as obtained from Eqs. (1)–(3).

To estimate the dependence of the measured conduction

band discontinuity on defect charge density, in Fig. 3 we plot $(\Delta E_c)_{meas}$ [calculated using Eqs. (3) and (14)] vs σ_i with $\Delta E_c = 0.24$ and 0.12 eV. The curves labeled ΔE_{c1} correspond to calculations where we take $\Delta x_j = 0$ [in Eq. (14)], the curves labeled ΔE_c give the exact value which is obtained using all terms in Eq. (14), while ΔE_{cK} is the uncorrected value obtained using Eqs. (3) and (4). Observe that ΔE_{c1} and ΔE_{cK} deviate more from the exact value of ΔE_c as $|\sigma_i|$ increases. As shown in Fig. 2(b), Δx_j is larger for $\sigma_i < 0$, and thus the deviation of ΔE_{c1} is also larger than for positive σ_i. Furthermore, as ΔE_c decreases, the percentage of the deviation of the measured from the actual value of ΔE_c increases. For example, with $\sigma_i = -5\times10^{10}$ cm^2, ΔE_{c1} is greater than $\Delta E_c = 0.24$ eV by 8%, and is greater by 16% for $\Delta E_c = 0.12$ eV. The deviation of ΔE_{cK} is twice these values over the same range of ΔE_c.

B. Deep interface traps

Significant errors in the determination of the trapped charge density, and hence ΔE_c, can be introduced if deep interface traps exist whose occupancy changes during the course of the C-V measurement. During C-V measurement, most of the trapped electrons are emitted as the reverse bias is made sufficiently large. Thus, in the limit of large reverse bias $\sigma_{iK} \to \sigma_i$ for deep donor traps, which is identical to the case for shallow traps [cf., Eq. (13)]. Similarly, it can be shown (Appendix A) that $\sigma_{iK} \to 0$ for acceptor traps, leading to discrepancies between the measured and actual values of interface trap densities.

Due to the relatively long time response of deep traps, it is necessary to consider their dynamical nature to understand the measured C-V data. The emission rate of charge from the traps is given by

$$e_n = g\sigma_{cc}\langle v\rangle N_c \exp(-E_t/k_BT), \tag{15}$$

where σ_{cc} is the trap capture section, $\langle v\rangle$ the mean thermal velocity of electrons, and N_c is the effective conduction band density of states. If the ac capacitance measurement frequency is $\omega \ll e_n$, the measurement is defined as low frequency (LF), and if $\omega \gg e_n$, it is referred to as a high frequency (HF) measurement. According to Eq. (15), the emission rate can be decreased by lowering the sample temperature (T). Hence, a low frequency measurement may become a high frequency measurement by lowering T. Since the number of trapped electrons which are able to respond to the ac modulation signal decreases as frequency is increased, the resultant apparent profile $[n^*(x^*)]$ is distorted by changing either temperature or frequency, which ultimately affects the value obtained for V_{DK}.

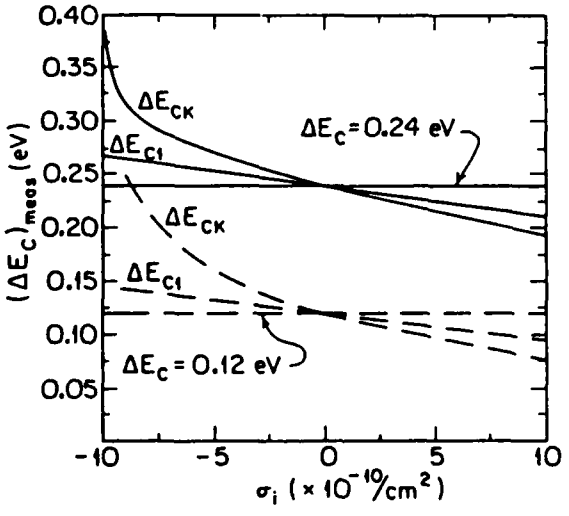

FIG. 3. Measured conduction band discontinuity energy $(\Delta E_c)_{meas}$ vs charge trap density (σ_i) for two values of ΔE_c. Here ΔE_{c1} is the corrected value obtained by setting $\Delta x_j = 0$.

The frequency dependence of the capacitance for homojunctions with deep traps has been studied previously.[27-29] Both the rate equation and Poisson's equation have to be solved simultaneously to obtain the frequency-dependent junction capacitance. In general, this makes the expression for the high frequency capacitance C_{HF} very complicated. In order to simplify the case of traps localized at a HJ, Kazmierski *et al.*[16] proposed a model which assumes that the occupancy of the traps is unchanged under small increments in the ac modulation voltage (dV). The occupancy of traps at V at HF is, therefore, the same as at $V - dV$. Furthermore, it was assumed that the sweep frequency of the reverse bias (Ω) is always $\Omega \ll e_n$—i.e., the trap occupancy is always in equilibrium with the "dc" voltage increment (DV). Therefore, this approach is valid for $\Omega \ll e_n \ll \omega$.

Another, somewhat different model proposed by Jeong *et al.*[21] was used to explain dependence of the $n^*(x^*)$ profile of InGaAs/GaAs HJs on temperature. The expression used to describe the occupancy traps [Eq. (10) in Ref. 21] is a function of e_n. It can be shown (Appendix B) that this model is only valid when $e_n \simeq \Omega$. Both the results of Kazmierski and Jeong are, therefore, applicable to different frequency regimes. In Appendix B, we derive a single result which is valid for all $\Omega < \omega$. In practice, we can arrange the experiment such that $\Omega \ll e_n \ll \omega$, in which case the results of Kazmierski are accurate, and hence, will be followed in the remainder of this section.

Figure 4 shows the apparent carrier concentration profiles for an $In_{0.53}Ga_{0.47}As$/InP HJ with a deep acceptor density $\sigma_i = -1\times10^{11}$ cm^{-2} calculated for both LF (solid line) and HF (dashed line) measurements. The energy of the trap from the InP conduction band minimum is 0.25 eV. Note that only one peak is observed for $\Delta E_c \simeq E_t$. This is different from the case treated by Jeong[21] where two peaks were observed: one due to electron accumulation and the other due to traps. However, we consider the case of $\Delta E_c \simeq E_t$ since it has been observed experimentally for this HJ system in the present, and in previous work.[9,15,17] The double-depletion characteristic of the apparent profile observed for the same *shallow* interface trap density [cf., Fig. 2(a)] disappears completely for both profiles. This difference is due to the emission of electrons from the deep traps during the course of the C-V measurement, whereas the charge state of shallow traps remains constant. Note also that V_{DK} [Eq. (3)] is reduced for the high frequency measurement. For the data shown, V_{DK} is found to equal 0.25 and 0.21 eV at low and high measurement frequency, respectively.

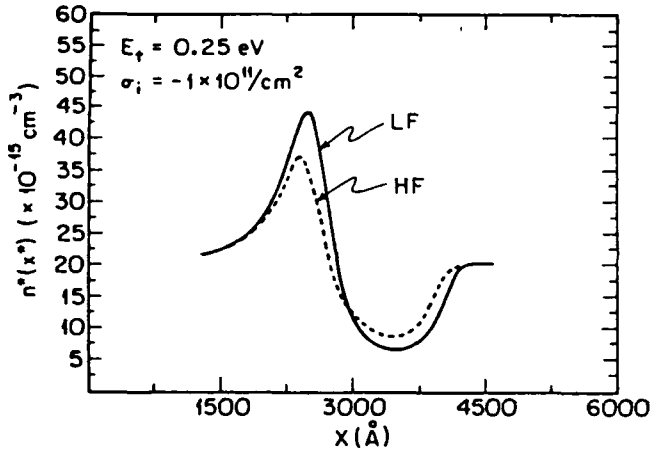

FIG. 4. Apparent free carrier concentration profile of deep acceptor traps at low frequency (solid line) and at high frequency (dashed line). The trap density (σ_i), acceptor energy depth (E_t) and conduction band discontinuity (ΔE_c) are assumed to be -1×10^{11} cm^{-2}, 0.25 eV, and 0.24 eV, respectively.

The measured trap densities (σ_{iK}) were calculated for these profiles. As expected, σ_{iK} is equal to σ_i for deep donors at all frequencies. On the other hand, for deep acceptor traps, σ_{iK} is nearly independent of σ_i, and is approximately equal to zero in both the HF and LF regimes. This result is consistent with theory, as discussed at the beginning of this section, and in Appendix A.

Figure 5 is a plot of ΔE_{cK} as a function of trap density. Both low frequency (LF) and high frequency (HF) cases are considered. For deep acceptor traps, ΔE_{cK} is nearly constant ($\sim$0.24 eV) at low frequency over the entire range of σ_i considered, and is close to the actual value [$\Delta E_c(0)$]. This implies that the energy bands are less distorted by deep rather than shallow traps (cf., Fig. 3). This results since deep traps can emit charge during the course of the *C-V* measurement, which reduces their contribution to the diffusion potential. At high frequency, ΔE_{cK} drops to 0.20 eV as σ_i increases to -1×10^{11} cm^{-2}.

Errors in measuring ΔE_c are also present for deep donor traps. Although ΔE_{cK} measured at LF is close to the exact value, in the HF regime large errors are incurred. For example, at $\sigma_i = 1\times10^{11}$ cm^{-2}, $\Delta E_{cK} \simeq 0.6\,\Delta E_c(0)$. This tendency appears to explain the often observed frequency dependence of ΔE_c obtained by *C-V* techniques,[14-17] with the most accurate values of ΔE_c obtained at low frequency (or alternatively high temperature).

Figure 6 is a plot of ΔE_{cK} versus temperature (T) assuming a donor trap density of $\sigma_i = 1\times10^{11}$ cm^{-2}. Note that ΔE_{cK} gradually drops with temperature, with the HF data being somewhat more temperature dependent. At 130 K, $\Delta E_{cK} = 0.075$ eV at HF, which is well below the exact value of 0.24 eV. As implied by the discussion above, there should exist a transition temperature (T_c) below which the value of ΔE_{cK} drops from the LF to the HF curve. The transition occurs when $e_n(T_c) = \omega$. The effect shown in Fig. 6 clearly explains the apparent dramatic drop of the measured conduction band discontinuity (ΔE_{cK}) to nearly zero at $T = 150$ K, which was observed by Forrest *et al.*[14] for $In_{0.53}Ga_{0.47}As/InP$ HJs.

The temperature dependence for acceptor traps was similarly explored. We found that, as for donor traps ΔE_{cK} drops with temperature, although the drop in the case of acceptors is not as severe as for donor traps (cf., Fig. 5). Indeed, the very strong dependence found for $In_{0.53}GaAs_{0.47}As/InP$ HJs is evidence that the effect is due to donor traps, contrary to conclusions made in previous work on this subject.[14-17]

III. CALCULATION OF ΔE_c USING THE EMENDED EQUATIONS

As mentioned above, Eq. (11) or (A4) can be used to correct the value of the measured diffusion potential (V_{DK}) in the presence of deep traps. However, the correction term involves the ionized trap concentration profile [$N_t^*(x^*)$] for donors, or the neutral trap profile $N_t^{(0)*}(x^*)$ for acceptors. Unfortunately, these are not easy to extract directly from the free carrier concentration profiles.

As shown in Eq. (5), the ionized trap concentration

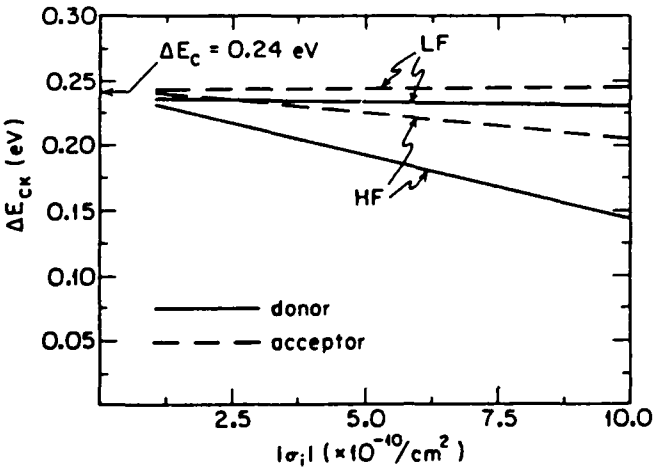

FIG. 5. Calculated conduction band discontinuity energy ΔE_{cK} vs the trap density σ_i at low and high frequency for both deep acceptor and donor traps.

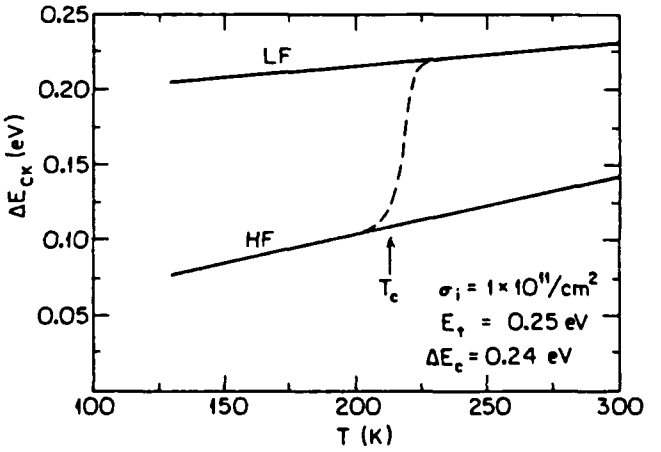

FIG. 6. Calculated conduction band discontinuity ΔE_{cK} vs temperature (T) for deep donor traps. The transition temperature (T_c) is shown at $T = 210$ K.

$N_t(x)$ is a function of bias due to the dependence of $E_c(x)$ on V. Figure 7 shows how the apparent trap concentration profile $[N_t^*(x^*)]$ is related to the actual ionized trap concentration $[N_t(x)]$ at different voltages for donor traps. In the figure, $\sigma_i = 1\times10^{11}$ cm^{-2}, $T = 130$ K, and $E_t = 0.25$ eV are assumed. Also, the trap region is taken to be 100 Å wide centered at 2550 Å, and the HJ is at $x_j = 2500$ Å. Figure 7(a) shows the occupancy of the traps at different reverse bias voltages. Apparently, the ionized trap concentration at each position increases as the voltage increases, finally becoming fully ionized at $V > 2.4$ V. In Fig. 7(b) we plot $\Delta N_t(x)$ vs V. Here, $\Delta N_t(x)$ is the change of occupancy in $N_t(x)$ obtained by increasing the reverse bias voltage by DV (= 0.06 V in this figure). The area under each curve (shaded for 1.20 V) is the number electrons emitted from the traps per unit area when the voltage is increased by DV. The charge distribution ionized by a small change DV in the voltage, $[\Delta N_t(x)]$ should be equal to the area of the corresponding strip of $N_t^*(x^*)$ between x^* and $x^* + dx^*$ which are evaluated at V and $V + DV$, respectively [Fig. 7(c)]. Therefore, for donorlike traps, we conclude that

$$N_t^*(x^*)dx^* = \int_{x_j}^{x_j+d} \Delta N_t(x)dx. \tag{16a}$$

Similarly, for acceptor traps with neutral trap density $N_t^{(0)*}(x^*)$, we have

$$N_t^{(0)*}(x^*)dx^* = -\int_{x_j}^{x_j+d} \Delta N_t(x)dx. \tag{16b}$$

Figure 8 shows the apparent free carrier concentration profiles $[n^*(x^*)]$ in the presence of acceptor traps. The apparent trap profiles $[N_t^{(0)*}(x^*)]$ are also shown. These latter profiles are obtained by the procedure discussed with respect to Fig. 7. As implied earlier, the areas under the $N_t^{(0)*}(x^*)$ profiles are equal to the actual trap density in both frequency regimes. Furthermore, the exact value of ΔE_c (= 0.24 eV) is recovered after correcting ΔE_{cK} using Eq. (A4) for acceptor traps.

It should be noted, however, that making such a correction to ΔE_{cK} using the integrals over the apparent trap distribution as in Eqs. (11) or (A4) is not useful since we need to be able to generate (by computer simulation) $n^*(x^*)$ to obtain $N_t^*(x^*)$. Once we have generated $n^*(x^*)$, we will have already obtained ΔE_c without the need for Eq. (11). Thus, in general, the emended forms of Eq. (3) as given by Eq. (14) are more often useful, providing that an estimate of d can be obtained. Typically, d can range from a few atomic layers for molecular beam epitaxially grown samples, to a few hundred angstroms for samples grown by liquid phase epitaxy (LPE). This distance can be independently obtained by Auger electron spectroscopy or several other direct microscopic techniques. Thus, to obtain $V_D(0)$, the $n^*(x^*)$ profile can be determined to good accuracy at LF (see Sec. II), thereby obtaining $\sigma_i = \sigma_{iK}$ using Eq. (2). From these results, Δx_j can be approximately obtained from Fig. 2(b), and using the estimate of d consistent with the growth processes employed, V_{DK} is easily corrected to give $V_D(0)$ using Eq. (14). This procedure is employed in Sec. IV for $In_{0.53}Ga_{0.47}As/InP$ HJs. One should keep in mind that such

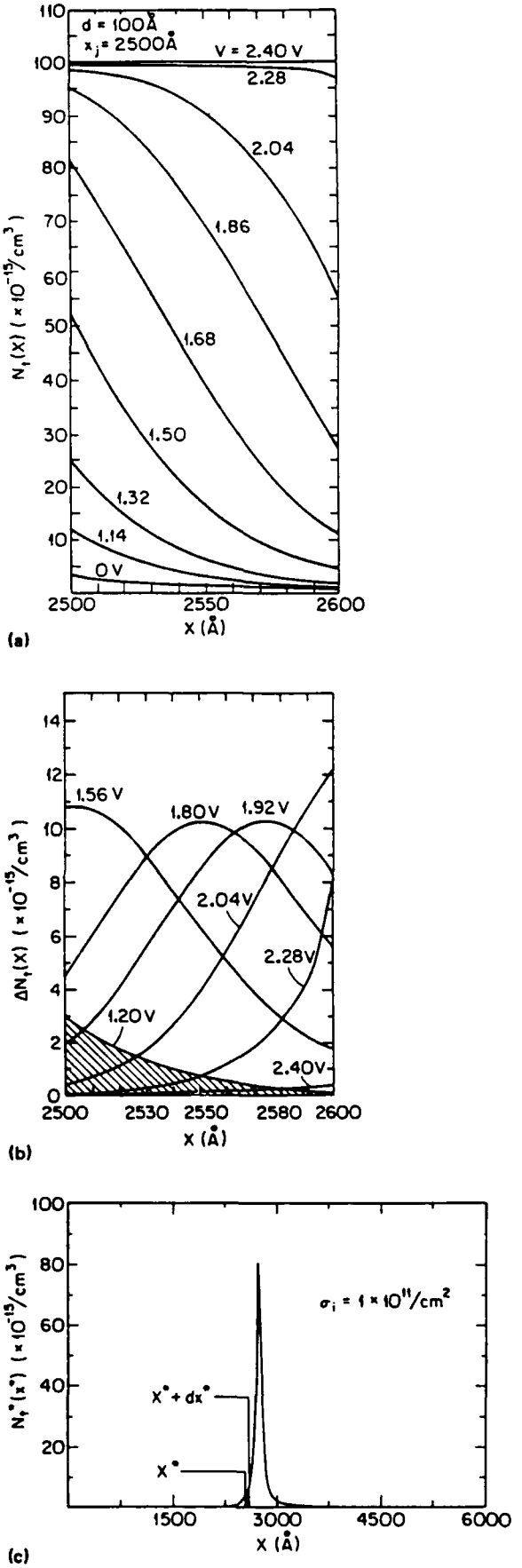

FIG. 7. (a) Ionized trap concentration profiles $[N_t(x)]$ vs position (x) at different applied voltages. (b) The increment of the trap concentration profiles $[\Delta N_t(x)]$ vs position (x) for the conditions used in (a). (c) Ionized apparent trap concentration profile obtained from (b).

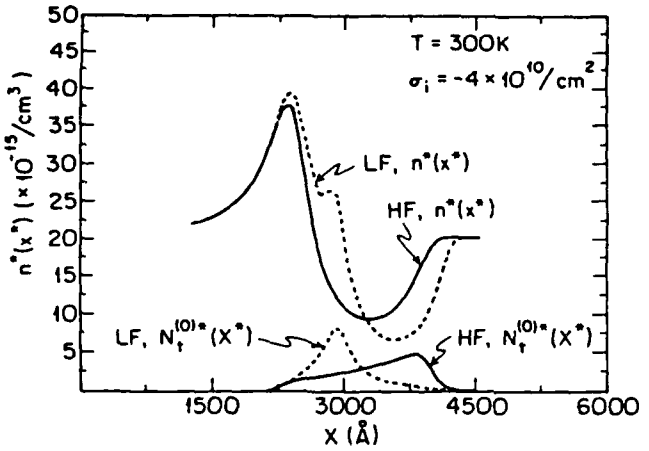

FIG. 8. The apparent free carrier concentration profiles at both low and high measurement frequency for an acceptor trap at $E_t = 0.30$ eV. The ionized trap concentration profiles are also shown at the bottom of the figure.

a procedure can correct the value of ΔE_{cK} by 10%–50%. However, if $\sigma_i > 10^{11}$ cm^2, the correction terms in Eq. (14) become comparable to V_{DK}. In this case, the values of $V_D(0)$ and V_{DK} should both be viewed with caution since under these conditions, the energy bands at the heterojunction are predominantly influenced by the trapped charge rather than the HJ dipole potential.

IV. EXPERIMENTAL RESULTS

Two $In_{0.53}Ga_{0.47}As$/InP HJ samples were investigated to test the results of Secs. II and III. Sample No. 1 was a mesa-type structure consisting of layers of adventitiously doped n-InP and n-$In_{0.53}Ga_{0.47}As$ successively grown by LPE on a (100) p-InP substrate with a Zn doping of $N_A = 6.5\times10^{16}$ cm^{-3}. The n-InP layer was 3 μm thick, and the free carrier concentration of both n-type layers was 4×10^{15} cm^{-3}. The lattice mismatch of the layers is 0.08%. Details of the fabrication and growth processes for this sample have been published previously.[14]

For sample No. 2, approximately 2.0 μm of n-$In_{0.53}Ga_{0.47}As$ with a carrier concentration of 2×10^{15} cm^{-3} was grown via LPE onto a 2.0-μm-thick n-InP layer, also with a carrier density of 2×10^{15} cm^{-3}. Lattice mismatch between the layers was less than 0.01%. In this case, the substrate was (100) sulfur-doped, n^+-InP with a carrier concentration $>2\times10^{18}$ cm^{-3}. A rectifying organic-on-inorganic (OI) semiconductor contact was then formed on $In_{0.53}Ga_{0.47}As$ side using the organic compound 3-, 4-, 9-, 10- perylenetetracarboxylic dianhydride (PTCDA).[30] Details of OI diode fabrication have also been presented previously.[31,32] Due to the large energy barrier at the OI/$In_{0.53}Ga_{0.47}As$ contact, the diode has a small reverse leakage current, and can be depleted far from the surface before breakdown. This allows one to quickly and easily obtain the free carrier concentration profiles.

For sample No. 1, there is a dramatic drop[14] of ΔE_{cK} as T is decreased from 170 to 135 K using a measurement frequency of 1 MHz. This implies that the transition from the LF to HF regime (Fig. 6) occurs at $T_c \simeq 150$ K at this measurement frequency. Thus, data at $T = 201$ K [Fig. 9(a)] are obtained at LF, while those taken at $T = 102$ K [Fig. 9(b)] corresponds to the HF regime.

Figure 9 also shows the computer simulated $n^*(x^*)$ profiles at $T = 201$ and 102 K. We obtain the best fit by assuming $d = 200$ Å, $x_j = 3$ μm, $\Delta E_c = 0.22$ eV, $\sigma_i = 3\times10^{10}$ cm^{-2}, and a *donor* trap at energy $E_t = 0.17$ eV. Here, d is inferred from optical response time measurements made for these HJ diodes.[33] These data are consistent with those reported earlier[14] [where $E_t = 0.20 \pm 0.02$ eV, $\sigma_i = (3.0 \pm 0.5)\times10^{10}$ cm^2]. The difference in ΔE_c between the measured ($\Delta E_{cK} = 0.20$ eV) and the best fit value obtained from the simulated $n^*(x^*)$ profile arises from positive interface charges near the HJ. Note that the fit at both low and high temperature is in reasonable agreement with the data, although the peak heights differ by a factor of 2. This discrepancy appears to arise from the resolution limit of the capacitance measurement. For example, the value of dC/dV at the $n^*(x^*)$ peak is equal to 0.03 pF/V. On the other hand, the value of dC/dV for the simulation result is 0.015 pF/V. Another error source may arise from compositional grading in the transition region between $In_{0.53}Ga_{0.47}As$ and InP which would tend to lower the measured peak due to a spatial broadening of the charge.

If Eq. (14) is used to correct the value of ΔE_{cK} by assuming $d = 200$ A, $\Delta x_j = 400$ A, and $\sigma_{iK} = 3\times10^{10}$ cm^2, the exact value of $\Delta E_c(0)$ is also found to be equal to 0.22

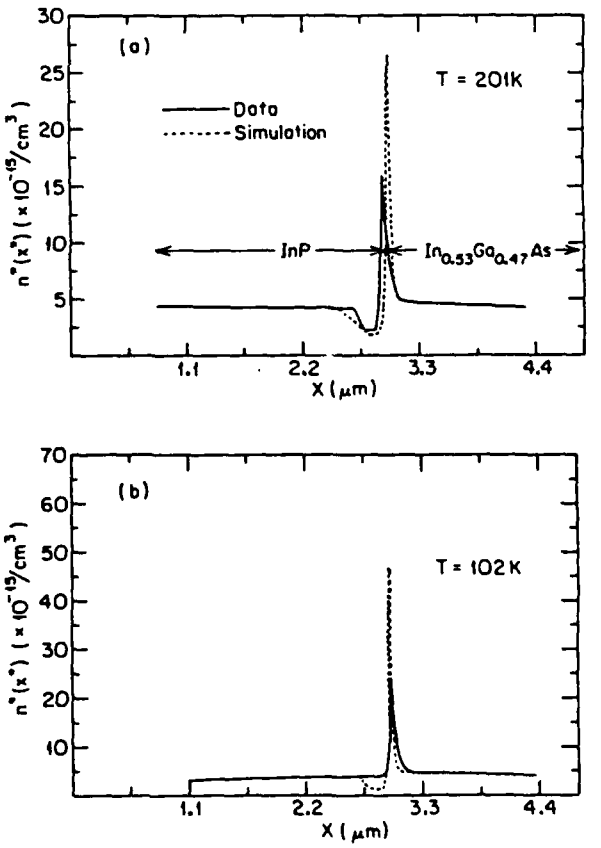

FIG. 9. Experimental and computer simulated apparent free carrier concentration profiles for an $In_{0.53}Ga_{0.47}As$/InP HJ at (a) $T = 201$ K and (b) $T = 102$ K. The best theoretical fit was obtained by using $\Delta E_c = 0.22$ eV, $E_t = 0.17$ eV, $\sigma_i = 3\times10^{10}$ cm^2, and $d = 200$ Å.

eV. This is consistent with the value obtained from the best fit of the experimental data and those obtained independently in other experiments.[15-18,31] Note also that the deep trap is assumed to be located on the InP site of the HJ. If a deep level with $E_t = 0.17$ eV is assumed to be located on the $In_{0.53}Ga_{0.47}As$ side, the accumulation electron peak and the deep trap peaks become separated as in Fig. 8. This differs with recent conclusions of Kazmierski *et al.*[16] regarding the origins of this trap.

A considerably different situation exists for sample No. 2, as shown in Fig. 10. At $T = 300$ K, the profile has two peaks, unlike the typical peak-valley profile shown in Fig. 2(a). According to simulation results for this HJ (taking $\Delta E_c = 0.24$ eV), the electron concentration due to accumulation at the HJ dipole should be $\sim 1\times10^{16}$ cm^{-3} at room temperature—a value which is too small to account for the observed peak heights of $\sim 2\times10^{17}$ cm^{-3}. Furthermore, as the temperature decreases to 270 K, both peaks A and B shift dramatically toward the InP side. These peaks can be explained as due to emission of charge from deep traps at the HJ.

Since the peak due to a trap is shifted further toward the substrate with increasing E_t, we expect that peak B is at larger E_t than peak A. Also note that both peak heights increase at lower temperature (270 K). A fit to the data at $T = 270$ K consistent with these assumptions is shown by the dashed line. Parameters used in the fit are given in Table II.

As the temperature decreases from 270 to 230 K, both peaks decrease in amplitude and move further toward the substrate. Peak B decreases continuously and finally disappears at $T = 150$ K. This indicates that, at low temperature, traps responsible for peak B are in the HF regime with a measurement frequency of 1 MHz (cf., Fig. 8). On the other hand peak A (with smaller E_t) has a higher emission rate (or lower transition temperature T_c). Since the height of peak A at $T = 150$ K is larger than at room temperature, this implies that T_c must be lower than 150 K.

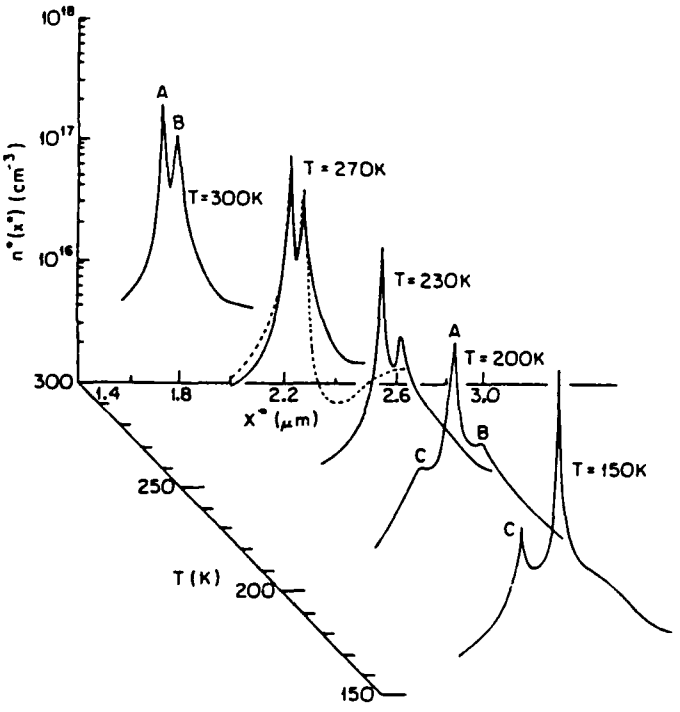

FIG. 10. Temperature-dependent apparent free carrier concentration profiles for an $In_{0.53}Ga_{0.47}As/InP$ HJ at several measurement temperatures. The dashed line shown at $T = 270$ K is the simulated apparent free carrier concentration profile using parameters listed in Table II.

Table II. The parameters[a] used in fitting of data obtained for sample No. 2.

Quantity	Units	Value
E_{t1} [b]	eV	0.03
E_{t2} [b]	eV	0.21
N_{t1} [a]	cm^{-3}	3×10^{17}
N_{t2} [c]	cm^{-3}	2×10^{17}
d	Å	200
ΔE_c	eV	0.24
x_j	μm	1.95
N_{D1}	cm^{-3}	2×10^{15}
N_{D2}	cm^{-3}	2×10^{15}

[a] Subscripts 1 and 2 refer to $In_{0.53}Ga_{0.47}As$ and InP, respectively.
[b] E_t = trap energy depth from $In_{0.53}Ga_{0.47}As$ conduction band minimum.
[c] N_t = integrated trap density = σ_t/d.

When the temperature decreases from 230 to 200 K, a third peak (C) appears. The position of peak C is independent of temperature from 200 to 150 K. Furthermore, the carrier concentration of this peak is $\sim 2\times10^{16}$ cm^3 at $T = 150$ K, which is close to the expected value (1.6×10^{16} cm^3) for the HJ accumulation electron concentration assuming $\Delta E_c = 0.24$ and $N_D = 2\times10^{15}$ cm^3. Therefore, peak C is attributed to accumulation of electrons due to the intrinsic heterojunction dipole potential.

From the data, we obtain $\sigma_t \sim 7\times10^{11}$ cm^2 for both peaks A and B, which is an anomalously high trap density. We speculate that these two deep traps are, therefore, due to extrinsic impurities or defects (e.g., anion vacancies) incurred during growth, although their source is not fully understood at present. Since $\sigma_t > 0$, the defects appear to be donors as in the case of sample No. 1, rather than acceptor-like as suggested previously.[14,15,17] Due to the large differences in σ_t for samples 1 and 2, it is not clear whether one or both peaks have the same origins for the two samples, although in both cases the peaks are due to a high density of donors. However, contrary to previous speculations on this matter, it is not due to lattice mismatch between layers. For sample No. 2, the mismatch is only 0.01% which could account for $\sigma_t < 10^7$ cm^{-2}. Further, the lattice mismatch for sample No. 2 is less than for sample No. 1, although the measured σ_t is greater for the former sample.

V. CONCLUSIONS

The accuracy of the widely used C-V technique proposed by Kroemer *et al.*[10] for the measurement of band-edge discontinuity energies has been investigated. Emended equations for determination of the trap density (σ_t) and conduction band discontinuity energy (ΔE_c) in the presence of both deep and shallow traps have been derived. The accuracy for determining the conduction band discontinuity ener-

gy can be improved by correcting the measured value according to these new expressions.

We have also shown that the magnitude of the discrepancy between ΔE_c and measurement is dependent on both temperature and measurement frequency. The difference between the measured conduction band discontinuity (ΔE_{cK}) and the actual value [$\Delta E_c(0)$] becomes large at low temperature, high measurement frequency, or for deep traps. From computer simulations of C-V measurements, we can explain the dramatic drop of ΔE_{cK} to zero at low temperature observed previously[14-17] for $In_{0.53}Ga_{0.47}As$/InP HJs as due to traps localized at the heterointerface.

The theoretical and experimental free carrier concentration profiles measured at low and high temperature for $In_{0.53}Ga_{0.47}As$/InP HJs were studied. We correct the measured conduction band discontinuity energy (ΔE_{cK}) by applying the emended equations to the C-V data at $T = 201$ K. The value of ΔE_c obtained using this technique is 0.22 eV, consistent with values obtained by other workers, as well as by numerical simulations. The temperature-dependent apparent profiles for a second sample show the existence of two deep levels. The source of these defects, however, is not fully understood at present. Other experiments (e.g., DLTS, admittance spectroscopy) have to be used to obtain more detailed information.

In summary, the use of the emended equations is straightforward and should lead to more accurate determination of ΔE_c measured in the presence of interfacial defects than has been possible using standard C-V techniques. Finally, the results presented in this work provide a means for understanding many complex phenomena which are observed in the course of HJ profiling using C-V data.

ACKNOWLEDGMENTS

We thank C. D. Lee for supplying samples for measurement. We thank the Army Research Office and the Powell Foundation without whose support this work would not have been possible.

APPENDIX A: TRAP CHARGE DENSITY AND CONDUCTION BAND DISCONTINUITY FOR DEEP ACCEPTOR TRAPS

If the reverse bias is made large enough, most of the electrons in the traps are emitted, and the traps become neutral with density, $N_t^{(0)^*}(x^*)$. Thus,

$$-\int_{-\infty}^{\infty} N_t^{(0)^*}(x^*)dx^* \to \sigma_i.$$

In substituting $N_t^*(x^*)$ with $N_{to}^*(x^*) - N_t^{(0)^*}(x^*)$, Eq. (12) becomes

$$\sigma_{iK} = -\int_{-\infty}^{\infty} N_t^*(x^*)dx^* = \sigma_i + \int_{-\infty}^{\infty} N_t^{(0)^*}(x^*)dx^*. \quad \text{(A1)}$$

Comparing the above equations, we conclude that $\sigma_{iK} \to 0$ for acceptorlike traps.

For calculating the diffusion potential, $N_t^*(x^*)$ in Eq. (11) should also be replaced with $N_{to}^*(x^*) - N_t^{(0)^*}(x^*)$. Thus, assuming charge conservation:

$$\begin{aligned} V_D(0) &= V_{DK} - q/\kappa \int_{-\infty}^{\infty} [N_{to}^*(x^*) - N_t^{(0)^*}(x^*)] \times (x^* - x_j)dx^* \\ &= V_{DK} - q/\kappa \int_{-\infty}^{\infty} N_{to}(x)(x - x_j)dx \\ &\quad + q/\kappa \int_{-\infty}^{\infty} N_t^{(0)^*}(x^*)(x^* - x_j)dx^*. \end{aligned} \quad \text{(A2)}$$

If $N_{to}(x)$ is uniformly distributed between x_j and $x_j + d$, Eq. (A2) becomes (for $\sigma_i < 0$)

$$V_D(0) = V_{DK} + \frac{q\sigma_i d}{(2\kappa)} + q/\kappa \int_{-\infty}^{\infty} N_t^{(0)^*}(x^*)(x^* - x_j)dx. \quad \text{(A3)}$$

Note that for shallow acceptor traps, $N_t^{(0)^*}(x^*)$ is zero since this term represents the total number of neutral traps. In this case, Eq. (A3) can be simplified to yield Eq. (14).

Defining Δx_j as the difference between x_j^* and x_j, Eq. (A3) becomes

$$\begin{aligned} V_D(0) &= V_{DK} + q/\kappa \int_{-\infty}^{\infty} N_t^{(0)^*}(x^*)(x^* - x_j^*)dx^* + \frac{q\sigma_i d}{(2\kappa)} \\ &\quad - q\Delta x_j/\kappa \int_{-\infty}^{\infty} N_t^*(x^*)dx^*. \end{aligned} \quad \text{(A4)}$$

Note also that the fourth term approaches zero for acceptor traps since all of the electrons in the traps are emitted during the C-V measurement.

APPENDIX B: FREQUENCY DEPENDENCE OF THE C-V DATA

In this Appendix, the HF models proposed by Kazmierski *et al.*[16] and Jeong *et al.*[21] are recast into a single expression. The rate equation describing electron capture at a defect can be written as[34]

$$\frac{\partial N_t}{\partial t} = N_{to}[c_n n(1 - f_t) + e_p(1 - f_t) - e_n f_t - c_p p f_t], \quad \text{(B1)}$$

where f_t is the occupancy of the trap, $n(p)$ is the free electron (hole) concentration, $c_n(c_p)$ is the electron (hole) capture coefficient, and $e_n(e_p)$ is the electron (hole) emission rate.

Applying an ac modulation signal, all the variables will have small variations about their steady-state values, viz.: $p = p_0 + \delta p$, $n = n_0 + \delta n$, and $N_t = N_t(0) + \delta N_t$. Here $N_t(0)$ is the number of ionized traps at $t = 0$. If only first-order terms are retained, Eq. (B1) becomes[27]

$$\frac{\partial \delta N_t}{\partial t} = -\frac{\partial N_t}{\tau}, \quad \text{(B2)}$$

where

$$\tau = 1/[c_n(n_0 + n_1) + c_p(p_0 + p_1)]$$

is the trap time constant and $n_1(p_1)$ is the electron (hole) density if $E_F = E_t$.

If the traps are located in the depletion region ($n_0 \to 0$), and the interaction with the valence band is ignored for n-

type material (where $p_1 \ll n_1$) the trap time constant can be simplified to

$$\tau = 1/c_n n_1$$
$$= 1/[\sigma_{cc}\langle v\rangle N_c \exp(-E_t/k_B T)] = 1/e_n$$

[cf. Eq. (15)].

The solution of Eq. (B2) can then be written as

$$N_t(t) = N_t(0) + [N_t(\infty) - N_t(0)](1 - e^{-t/\tau}). \quad \text{(B3)}$$

Case 1: Bias sweep frequency small ($\Omega \ll e_n \ll \omega$)

Assume at $t = 0$ that a reverse bias voltage V is applied to the sample. At $t = t_1$ the voltage increases to $V + dV$, where dV is the ac modulation signal. If the trap concentration is a function of position, $N_t(t)$ becomes $N_t(x,t)$ and Eq. (B3) becomes

$$N_t(x, V + dV)$$
$$= N_{to} f_t(x,V) + [N_t(\infty)$$
$$- N_{to} f_t(x,V)][1 - \exp(-t_1/\tau)]. \quad \text{(B4)}$$

Note that $N_t(0)$ has been replaced with $N_{to} f_t(x,V)$ since the charge (or discharge) of the traps can respond to the sweep frequency (Ω) of the dc bias. From this same argument, $N_t(\infty)$ can be replaced by $N_{to} f_t(x, V + dV)$. Furthermore, as $t_1/\tau \to 0$, $N_t(x, V + dV) \to N_{to} f_t(x,V)$. This is just the approach used by Kazmierski *et al.*[16]

Case 2: Bias sweep frequency large ($e_n \ll \Omega \ll \omega$)

If the temperature is low enough such that $e_n \ll \Omega$, the boundary condition $N_t(0) = N_{to} f_t(x,V)$ is no longer valid since the occupancy of electrons cannot follow the sweep frequency (Ω) of dc reverse bias V. As a boundary condition, assume that all the traps are occupied by electrons at $V = 0$ at $t = 0$ [i.e., $N_t(0) = N_{to}$]. On the other hand, as $t \to \infty$, $N_t(\infty)$ should be $N_{to} f_t(x, V + dV)$. If voltage $V + dV$ is applied at $t = \pi/\omega$ (half the period of ac small signal), Eq. (B3) becomes

$$N_t(x, V + dV)$$
$$= N_{to} - N_{to}[1 - f_t(x, V + dV)(1 - e^{-\pi/(\omega\tau)})]. \quad \text{(B5)}$$

Equation (B4) is the HF model proposed by Jeong *et al.*[21]

In conclusion, Eq. (B3) is the rigorous solution of which the previous treatments are special cases. However, the regime treated by Jeong is not practical and hence should not lead to correct results when applied to most experimental data. On the other hand, the approach of Kazmierski is valid to good approximation in most cases.

[1] F. Capasso and G. Margaritondo, *Heterojunction Band Discontinuities Physics and Device Applications* (North-Holland, Amsterdam, 1987).
[2] A. G. Milnes and D. L. Feucht, *Heterojunction and Metal-Semiconductor Junction* (Academic, New York 1972).
[3] H. Kroemer, Surf. Sci. **132**, 543 (1983).
[4] A. G. Milnes, Solid-State Electron. **30**, 1099 (1987).
[5] R. Dingle, A. C. Gossard, and W. Wiegmann, Phys. Rev. Lett. **34**, 1327 (1975).
[6] G. Margaritondo, Surf. Sci. **132**, 469 (1983).
[7] R. L. Anderson, Solid-State Electron. **5**, 341 (1962).
[8] A. R. Riben and D. L. Feucht, Solid-State Electron. **9**, 1055 (1966).
[9] S. R. Forrest and O. K. Kim, J. Appl. Phys. **52**, 5838 (1981).
[10] H. Kroemer, Wu-Yi Chien, J. S. Harris, and D. D. Edwall, Appl. Phys. Lett. **36**, 295 (1980).
[11] H. Kroemer, Appl. Phys. Lett. **46**, 504 (1985).
[12] M. A. Rao, E. J. Caine, H. Kroemer, S. I. Long, and D. I. Babic, J. Appl. Phys. **61**, 643 (1987).
[13] J. E. A. Whiteaway, IEE Proc. (London) **130**, 165 (1983).
[14] S. R. Forrest and O. K. Kim, J. Appl. Phys. **53**, 5738 (1982).
[15] M. Ogura, M. Mizuta, and K. Oraka, J. Appl. Phys. **22**, 1502 (1983).
[16] K. Kazmierski, P. Philippe, P. Poulain, and B. de Cremoux, J. Appl. Phys. **61**, 1941 (1987).
[17] P. S. Whitney and C. G. Fonstad, J. Cryst. Growth **83**, 219 (1987).
[18] D. V. Lang, M. B. Panish, F. Capasso, J. Allan, R. A. Hamm, and A. M. Sergent, Appl. Phys. Lett. **50**, 736 (1987).
[19] L. Y. Leu and S. R. Forrest (unpublished).
[20] J. P. Andre, J. N. Patillon, J. L. Gentler, E. P. Menu, D. Moroni, and G. M. Martin, Int. Symp. GaAs Related Compound Semicond., paper F6, Las Vegas (1986).
[21] J. Jeong, T. E. Schlesinger, and A. G. Milnes, IEEE Trans. Electron Devices **ED-34**, 1911 (1987).
[22] S. M. Sze, *Physics of Semiconductor Devices* (Wiley, New York, 1981), 2nd ed., p. 80.
[23] H. Kroemer and W. Y. Chien, Solid-State Electron. **24**, 655 (1981).
[24] W. G. Oldham and A. G. Milnes, Solid-State Electron. **7**, 153 (1964).
[25] J. P. Donnelly and A. G. Milnes, Solid-State Electron. **9**, 174 (1966).
[26] M. A. Haase, M. A. Emanuel, S. C. Smith, J. J. Coleman, and G. E. Stillman, Appl. Phys. Lett. **50**, 404 (1987).
[27] C. T. Sah and V. G. K. Reddi, IEEE Trans. Electron Devices **ED-11**, 345 (1964).
[28] E. Schibli and A. G. Milnes, Solid-State Electron. **11**, 323 (1968).
[29] W. G. Oldham and S. S. Naik, Solid-State Electron. **15**, 1085 (1972).
[30] S. R. Forrest, M. L. Kaplan, P. H. Schmidt, W. L. Feldmann, and E. Yanowski, Appl. Phys. Lett. **41**, 90 (1982).
[31] S. R. Forrest, P. H. Schmidt, R. B. Wilson, and M. L. Kaplan, J. Vac. Sci. Technol. B **4**, 37 (1986).
[32] S. R. Forrest, M. L. Kaplan, and P. H. Schmidt, Ann. Rev. Mater. Sci. **17**, 189 (1987).
[33] S. R. Forrest, O. K. Kim, and R. G. Smith, Appl. Phys. Lett. **41**, 95 (1982).
[34] W. Schockley and W. T. Read, Phys. Rev. **87**, 835 (1952).

Accurate determination of heterojunction band discontinuities in the presence of interface traps using capacitance-voltage techniques

L. Y. Leu and S. R. Forrest
Departments of Electrical Engineering/Electrophysics and Materials Science, University of Southern California, Los Angeles, California 90089-0241

(Received 24 October 1988; accepted for publication 22 February 1989)

The effects that interface traps have on the determination of the heterojunction band discontinuity energies ΔE_c measured via capacitance-voltage analysis are considered. We show that both the trap density σ_{iK} and conduction-band discontinuity energy ΔE_{cK} measured using the method of Kroemer, Chien, Harris, and Edwall [Appl. Phys. Lett. 36, 295 (1980)] are functions of the heterointerface width d, the difference between the actual and the measured heterojunction positions Δx_j, and the doping levels of the two contacting materials. These error sources can be corrected by using simple amended equations developed in this study. This amended technique improves the measurement accuracy of both trap density and heterojunction band discontinuity energy, is easy to use, and is relatively insensitive to variations in doping and trap density in the interface region. This technique is applied to the analysis of a vapor phase epitaxial N-n InP/$In_{0.53}Ga_{0.47}As$ heterojunction for which we find $\Delta E_c = (0.24 \pm 0.01)$ eV.

I. INTRODUCTION

The capacitance-voltage (C-V) technique proposed by Kroemer *et al.*[1] has been widely used to measure the energy band discontinuities of many isotype heterojunctions (HJs).[1-5] This method exhibits features which have advantages over many other techniques used in determining HJ band discontinuity energies. For example, the measurements are not sensitive to compositional gradients[6] in the heterointerface region, and are relatively insensitive to materials parameters such as effective mass and permittivity.[7] By comparison, photoluminescence spectroscopy of multiple quantum wells is strongly dependent on an accurate knowledge of effective mass, quantum-well width, and well profile.[8] Likewise, x-ray photoelectron spectroscopy[9] is subject to errors due to the need of subtracting large valence-bond energies ($\sim$10–15 eV) to obtain a small discontinuity energy ($\sim$0.1–0.5 eV). Furthermore, current-voltage measurements are vulnerable to errors induced by parasitic current sources.

In addition to determining the band discontinuity energy, the C-V technique is also useful for measuring the density of the shallow trapped charge near the heterojunction. With this information, the relative quality of a HJ can be assessed such that, *a priori*, the accuracy of the subsequent band discontinuity energy measurement can be ascertained.

II. THEORY

The HJ properties are determined by first obtaining the apparent (or measured) free-carrier concentration profile $[n^*(x^*)]$ from C-V data. These data result from depleting the HJ by applying reverse voltage to an adjacent rectifying contact. Hence,[10]

$$n^*(x^*) = \left(\frac{2}{q\kappa}\right)\frac{dV}{d(1/C^2)}, \tag{1}$$

where $x^* = \kappa/C$ is the apparent distance from the rectifying contact, q is the electronic charge, and κ is the permittivity. The density of the shallow trapped interface charge, σ_{iK}, and the diffusion potential, V_{DK}, of an n-type, isotype HJ can then be obtained using[1]

$$\sigma_{iK} = -\int_{-\infty}^{\infty}[N_D(x^*) - n^*(x^*)]dx^*, \tag{2}$$

$$V_{DK} = \frac{q}{\kappa}\int_{-\infty}^{\infty}[N_D(x^*) - n^*(x^*)](x^* - x_j^*)dx^*, \tag{3}$$

where $N_D(x^*)$ is the background donor concentration at the apparent position x^*, and x_j^* is the apparent position of the HJ as measured from the location of the charge accumulation peak in the carrier concentration profile. The conduction-band discontinuity energy ΔE_{cK} is calculated using the diffusion potential via $\Delta E_{cK} = qV_{DK} + \delta_2 - \delta_1$, where δ_1 and δ_2 are the Fermi energies (with respect to the conduction-band minima) in the bulk of the contacting semiconductors. Here, subscripts 1 and 2 refer to the different materials comprising the HJ.

There are several inherent problems with the C-V technique which can lead to systematic errors in determining both ΔE_c and the actual fixed interface charge density, σ_i. For example, the use of Eqs. (2) and (3) is based on the assumptions that the apparent HJ position (x_j^*) is equal to its actual position (x_j), and that the trap density σ_i is low enough such that it does not significantly perturb the often small intrinsic heterojunction dipole potential. However, due to the limited spatial resolution inherent in C-V data,[1] x_j^* is shifted away from x_j, toward the electron accumulation region at the HJ. In order to correct for this effect, Rao *et al.*[11] calculated a series of pairs of σ_{iK} and ΔE_{cK} for (Ga,In)P/GaAs HJs by assuming different values of x_j, and then choosing the actual position of the HJ to minimize σ_{iK}. Since this approach assumes that the HJ has a very low density of interface states, it can only be reliably applied to sam-

 0021-8979/89/124818-05$02.40

ples where σ_i has been independently determined to be small.

On the other hand, we can expect that a high density of defects will influence the values obtained for V_{DK}, particularly if the diffusion potential is small.[12,13] This situation is made worse if the doping levels on both sides of the HJ are different. To illustrate this last point, in Fig. 1 we show the calculated apparent free carrier concentration profile of an InP/$In_{0.53}Ga_{0.47}As$ HJ with background dopings of $N_{D1} = 1.1\times10^{16}$ cm^{-3} and $N_{D2} = 3\times10^{16}$ cm^{-3} for InP and $In_{0.53}Ga_{0.47}As$, respectively. The calculation is accomplished by numerically solving Poisson's equation starting at the rectifying Schottky barrier contact made to the InP layer, and assuming that $\Delta E_c = -0.24$ eV, where the negative sign implies that the conduction-band energy is greater on the InP side than on the InGaAs side of the HJ.[2,14] Furthermore, for this calculation we assume that the Schottky barrier height is 0.4 eV and the interface trap density is $\sigma_i = -5\times10^{10}$ cm^{-2}, which is confined to a region of width $d = 200$ Å on the InP side of the heterointerface.

In using the C-V depletion technique, the background doping levels of both materials are obtained from the $n^*(x^*)$ profile at distances x^* far from either side of the HJ, and the integrals in Eqs. (2) and (3) are then evaluated by assuming that N_{D1} and N_{D2} are uniform in the HJ region. An abrupt step in doping between these values is assumed to occur at the HJ whose position is determined from x_j^*. As can be seen from the cross-hatched box in the figure, the integral in Eq. (2) will be incorrect due to the excess area arising from the difference between x_j^* and the actual position x_j. The error thus incurred is increased with an increasing difference between N_{D1} and N_{D2}. We can calculate the magnitude of the error by rewriting Eq. (2) as

$$\sigma_{iK} = -\int_{-\infty}^{x_j} [N_{D1} - n^*(x^*)]dx^* - \int_{x_j}^{x_j^*} [N_{D1} - n^*(x^*)]dx$$

$$- \int_{x_j}^{x_j^*} [N_{D2} - n^*(x^*)]dx^* - \int_{x_j}^{\infty} [N_{D2} - n^*(x^*)]dx^*, \quad (4)$$

The first and last integrals on the right-hand side of Eq. (4) are just σ_i, whereas the middle integrals arise since $\Delta x_j = x_j - x_j^*$ is not zero. Evaluating these integrals for the profile in Fig. 1 indicates that $\sigma_{iK} = -5.8\times10^9$ cm^{-2}, or about an order of magnitude less than the actual value. Hence, these effects cannot be ignored without inducing large errors in the fixed interface charge density as obtained using previous methods.

These errors can be reduced or eliminated by solving the integrals in Eq. (4). Grouping terms we obtain

$$\sigma_i = \sigma_{iK} - (N_{D1} - N_{D2})\Delta x_j. \quad (5)$$

By a similar analysis,[12] we obtain for the diffusion potential due only to the HJ dipole,

$$V_D(0) = V_{DK} + q/\kappa[\sigma_i(\Delta x_j - d/2) - (N_{D2} - N_{D1})\Delta x_j^2/2]. \quad (6)$$

In deriving Eq. (6), we assume the interface traps are uniformly distributed in a region of width, d. In other words, V_{DK} is the total potential drop due to the superposition of the intrinsic heterojunction electrostatic potential $[V_D(0)]$, and the potential due to monopolar interface defects $[(q/2\kappa)\sigma_i d]$. Interface states which are dipolar in nature, however, are indistinguishable from the intrinsic HJ dipole and can potentially induce error in the determination of $V_D(0)$, provided such defects are present.

Note that $V_D(0)$ approaches V_{DK} as d or σ_i are decreased. Thus, measurements of ΔE_c using the depletion technique along with Eqs. (2) and (3) are only accurate in the absence of interface traps, or for very abrupt HJs. On the other hand, if d is large and V_{DK} is small, the second and third terms on the right in Eq. (6) may become larger than the measured value of V_{DK}. One example of HJs in which V_{DK} differs significantly from $V_D(0)$ is p-P $Hg_{0.7}Cd_{0.3}Te$/Cd(4% Zn)Te heterojunctions measured in recent work.[15] There it was found that $d\sim0.3$ μm and $\Delta E_v = 100$ meV. In that case, $V_D(0)$ was found to be five times larger than V_{DK}.

Also note that monopolar defects (either donors or acceptors) are indistinguishable from shallow dopants. Thus, the net trap charge density calculated via Eq. (2) may arise from the wrong choice of N_{D1} or N_{D2}. Indeed, one problem with using Eqs. (2) and (3) is the assumption that N_{D1} and N_{D2} are known in the interface region, and that these values change abruptly at x_j^* (see Fig. 1). However, if any doping nonuniformities occur over the heterointerface width, d, we can use both Eqs. (5) and (6) to eliminate this error source to obtain the exact value of $V_D(0)$. In many cases the assumption that variations in doping occur over a distance d is justified since diffusion of dopants, semiconductor constituents, and defects will probably be most pronounced over the same spatial region. Indeed in most experiments reported using Eqs. (2) and (3), a value of $\sigma_{iK}\sim(1\text{–}3)\times10^{10}$ cm^{-2} is often observed. While this value may in fact be due to the

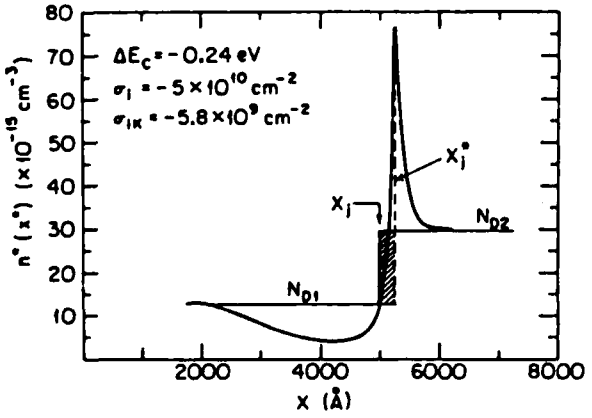

FIG. 1. A calculated apparent free-carrier concentration profile $[n^*(x^*)]$ of an N-InP/n-$In_{0.53}Ga_{0.47}As$ isotype heterojunction. The doping levels used for the InP and $In_{0.53}Ga_{0.47}As$ layers are 1.1×10^{16} and 3×10^{16} cm^{-3}, respectively.

presence of interfacial defects or even arise from limited experimental resolution,[12] it can also be explained as simply due to deviations of N_{D1} and N_{D2} from their bulk values in the heterointerface region.

As inferred from Eqs. (5) and (6), Δx_j and d are the only two unknowns needed to obtain the exact trap density and diffusion potential using the measured values of σ_{iK}, V_{DK}, N_{D1}, and N_{D2}. The width of the interface region (d) can be measured independently; for example, using secondary ion mass spectroscopy (SIMS) or other microscopically obtained data. Also, Δx_j can be found using Fig. 2(a) where it is plotted versus both σ_{iK} and N_{D1}. These curves, which have been determined via a computer solution to Poisson's equation for HJs where rectifying contact is made to the semiconductor layer which is depleted at the heterointerface, assume that $\Delta E_c = -0.12$ and -0.36 eV. These curves are independent of N_{D2} in the range $1\times10^{15} < N_{D2} < 5\times10^{16}$ cm^{-3}. Here, each curve is obtained by specifying values of d and ΔE_c, although Δx_j is found to be relatively insensitive to d. For example, as d is varied from 50 to 500 Å, the variation of Δx_j is less than 2%. Furthermore, $|\Delta x_j|$ decreases linearly as ΔE_c increases from 0 to -0.5 eV, independent of doping level and interface charge density (σ_{iK}). Hence, for any value of ΔE_c within this range, the dependence of $|\Delta x_j|$ on σ_{iK} can be found by interpolation from the values shown in this figure. The error incurred by obtaining Δx_j for a particular σ_{iK} via interpolation is less than 5%. Finally, note that Δx_j is relatively insensitive to the effective conduction band density of states N_c of both HJ materials. For example, as N_c increases from 3×10^{17} to 3×10^{18} cm^{-3}, the variation of Δx_j is only 4% (where $N_{D1} = N_{D2} = 6\times10^{15}$ cm^{-3} and $\sigma_i = 5\times10^{10}$ cm^{-2} are assumed).

In Fig. 2(b) we plot Δx_j vs σ_{iK} for a HJ with the opposite symmetry to that in Fig. 2(a). Thus, in this plot the rectifying contact is made to the material which is accumulated at the heterointerface (e.g., n-$In_{0.53}Ga_{0.47}As$). In comparison with Fig. 2(a), Δx_j is positive, and the absolute value of the shift in x_j^* is smaller for this HJ type. Hence, the deviation of V_{DK} from $V_D(0)$ can be reduced by preparing samples where the rectifying contact is made to the material which has carrier accumulation in the HJ region. Finally, also note that these curves are insensitive to N_{D1} as compared with N_{D2}, as shown in Fig. 2(a). This indicates that Δx_j is strongly determined by the doping concentration of the material which is depleted near the HJ, where the Debye length is larger.

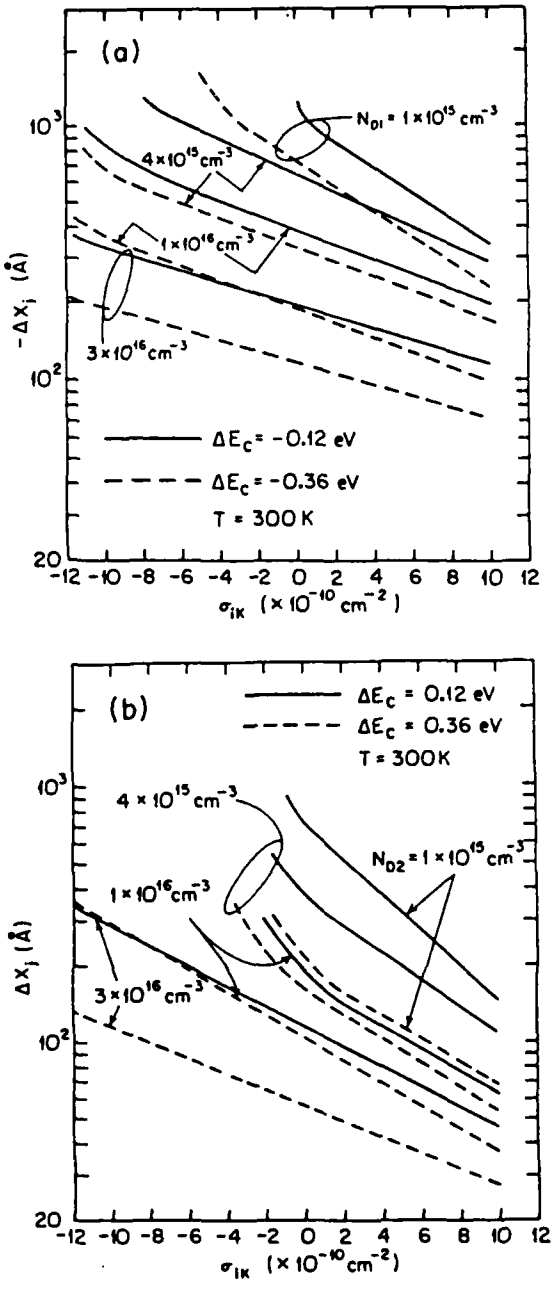

FIG. 2. (a) The difference between the apparent heterojunction position x_j^* and the actual position x_j vs the measured trap density σ_{iK} for samples where the rectifying contact is made to the semiconductor layer which is depleted at the HJ. Each curve corresponds to different doping levels, N_{D1}. Here $\Delta E_c = -0.12$ and -0.36 eV are assumed, and $\Delta x_j < 0$ for all values of σ_{iK}. (b). Same as (a) except where the contact is made to the layer with carrier accumulation at the heterointerface. Here, $\Delta E_c > 0$ results from this HJ symmetry.

III. EXPERIMENT

Using Eqs. (5) and (6) in conjunction with Fig. 2(a), $V_D(0)$ and σ_i were obtained for a N-n InP/$In_{0.53}Ga_{0.47}As$ isotype heterojunction grown by hydride vapor phase epitaxy[16] (VPE) on (100) n^+-InP substrates S-doped to 5×10^{18} cm^{-3}. The first layer grown was an approximately 1-μm-thick InP buffer layer, followed by 4 μm of adventitiously doped n^--$In_{0.53}Ga_{0.47}As$. Next, a 0.6-μm-layer of S-doped N-InP was grown, and the final layer was a 1.2-μm-thick, undoped N^--InP cap. A rectifying organic-on-inorganic (OI) semiconductor contact was formed on the top N^--InP surface using the organic compound, 3,4,9,10-perylenetetracarboxylic dianhydride via fabrication techniques discussed previously.[13,17] The free carrier concentration profile for the sample which was obtained by reverse biasing the OI contact is shown by the solid line in Fig. 3.

SIMS data for this sample are shown in the inset of Fig. 3. From the indium and sulfur concentration profiles, the N^--InP, N-InP, and n^--$In_{0.53}Ga_{0.47}As$ layers can be identified. The heterointerface region width (cross-hatched area)

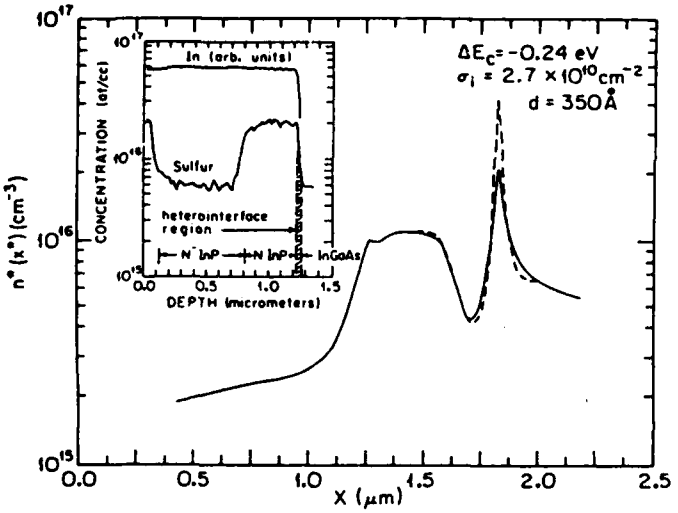

FIG. 3. Experimental (solid line) and calculated (dashed line) apparent free carrier concentration profiles of an N-n InP/$In_{0.53}Ga_{0.47}As$ sample. For the calculation, $\Delta E_c = -0.24$ eV, $d = 350$ Å, and $\sigma_i = 2.7 \times 10^{10}/cm^2$ are assumed. Inset: SIMS data for the same sample showing In and S concentrations. The cross-hatched area indicates the heterointerface region.

is inferred from the gradual drop of both the indium and sulfur concentrations at the N-InP/n-$In_{0.53}Ga_{0.47}As$ interface. The heterointerface width is estimated from these data to be $d = (350 \pm 50)$ Å.

From the free carrier concentration profile of Fig. 3, we obtain $N_{D1} = (1.00 \pm 0.02) \times 10^{16}$ cm^{-3}, $N_{D2} = (6.00 \pm 0.05) \times 10^{15}$ cm^{-3}, and $x_j^* = (1.83 \pm 0.01)$ μm. Using Eqs. (2) and (3), we calculate $\sigma_{iK} = (1.8 \pm 0.3) \times 10^{10}$ cm^{-2} and $V_{DK} = -(0.21 \pm 0.01)$ V. Taking the electron effective masses[18] of InP and $In_{0.53}Ga_{0.47}As$ as $0.07m_0$ and $0.04m_0$, where m_0 is the free-electron mass, we obtain $\Delta E_{cK} = -(0.22 \pm 0.01)$ eV.

Using σ_{iK} and ΔE_{cK}, we determine σ_i and ΔE_c as follows: From Fig. 2, Δx_j is obtained by linear interpolation using the curve corresponding to $\Delta E_c = \Delta E_{cK}$—the latter value being our first best estimate for the band discontinuity energy. In this manner, we obtain $\Delta x_j = -(250 \pm 12)$ Å. Substituting[19] d, Δx_j, σ_{iK}, and ΔE_{cK} into Eqs. (5) and (6), we get $\Delta E_c = -(0.24 \pm 0.01)$ eV and $\sigma_i = (2.7 \pm 0.4) \times 10^{10}$ cm^{-2}. More accuracy in these latter two parameters can be achieved by iteratively repeating the process, always replacing σ_i and ΔE_c in Eqs. (5) and (6) with the new values of σ_i and ΔE_c thus obtained. The iterations are discontinued when the difference between both sides of Eq. (6) becomes negligibly small. In the present example, only a single iteration was required. Note that while ΔE_{cK} and ΔE_c differ by only 10% for this sample, σ_i is roughly twice σ_{iK}, consistent with our discussion of Fig. 1 due to the sensitivity of this parameter to the choice of N_{D1} and N_{D2}.

The ability of Eqs. (5) and (6) to correct for the effects of fixed charge was further tested using a more extreme, albiet artificial example by assuming $N'_{D1} = 7 \times 10^{15}$ cm^{-3} for the sample in Fig. 3 instead of its actual value of $N_{D1} = 1 \times 10^{16}$ cm^{-3}. In this case, we set $d = d'$ equal to the integration limit on the InP side of the HJ, thereby "assigning" the difference between N'_{D1} and N_{D1} to fixed interface charge. Following this procedure, we obtained $V_{DK} = -0.06$ V, and after two iterations using Eqs. (5) and (6) and Fig. 2, we obtain, once more, the actual value of $V_D(0) = -0.23$ V and $\sigma_i = (N_{D1} - N_{D1})/d' + \sigma_i$. This example, although somewhat contrived, indicates the ability of the approach to achieve accurate values for ΔE_c even in the presence of a very high density of fixed charge.

In order to check the accuracy of σ_i and ΔE_c obtained for the InP/$In_{0.53}Ga_{0.47}As$ HJ, the apparent free carrier concentration profile [$n^*(x^*)$] near the HJ was calculated assuming $\Delta E_c(0) = -0.24$ eV, $d = 350$ Å, and $\sigma_i = 2.7 \times 10^{10}$ cm^{-2}. This calculated $n^*(x^*)$ profile is shown by the dashed line in Fig. 3. The agreement between the experimental and calculated profiles is quite good, except that the peak value at x_j^* for the experimental data is lower. This also represents an improved fit over that which was obtained using σ_{iK} and ΔE_{cK} inferred from Eqs. (2) and (3). We attribute the difference in peak values at x_j^* to the interfacial compositional gradient which tends to lower the measured peak due to a spatial broadening of the HJ dipole.

To our knowledge, these are the first measurements of the conduction-band discontinuity energy of hydride VPE grown N-n InP/$In_{0.53}Ga_{0.47}As$ HJs. These data are consistent with data[20] for molecular-beam epitaxially grown samples for this same heterojunction, and furthermore, they are consistent with data for liquid phase epitaxially grown n-N $In_{0.53}Ga_{0.47}As$/InP HJs.[13] This implies that the measured conduction-band discontinuity energy is independent of growth sequence for (100) $In_{0.53}Ga_{0.47}As$/InP heterojunctions.

IV. SUMMARY AND CONCLUSION

In conclusion, we have described a means for improving the measurement accuracy of the interface trap density and band-edge discontinuity energy obtained from capacitance-voltage analysis, and have used it to study hydride vapor phase epitaxially grown InP/$In_{0.53}Ga_{0.47}As$ HJs. This approach is especially useful for the measurement of band discontinuity energies of samples with high densities of shallow acceptor traps ($\sigma_i < 0$), or with large differences in free carrier concentrations between the contacting materials. The diffusion potential obtained from this improved C-V technique is insensitive to variations in doping and trap density in the interface region.

The technique is simple to use, and can give an *a priori* estimate of the accuracy of the band offset measurement. For relatively trap-free HJs whose offset magnitude is much greater than kT, the values for ΔE_c obtained using the conventional depletion technique[1] can be accurate to within 10–20 meV. For smaller offsets, or for HJs which have a non-negligible trap density (e.g., HgCdTe/CdTe), the conventional methods can lead to large inaccuracies. In these cases, the techniques discussed here can give an accurate value for ΔE_c which is several times larger than the measured values using previous methods. To our knowledge, this improved capacitance-voltage technique is the most accurate means available for determining the interface trap density and band discontinuity energies of semiconductor heterojunctions.

ACKNOWLEDGMENTS

We thank G. Erikson for supplying samples for measurement. Also, we express our appreciation to the Army Research Office (Michael Stroscio) and the Powell Foundation for their support of this research.

[1]H. Kroemer, W. Y. Chien, J. S. Harris, and D. D. Edwall, Appl. Phys. Lett. **36**, 295 (1980).
[2]S. R. Forrest and O. K. Kim, J. Appl. Phys. **53**, 5738 (1982).
[3]R. People, K. W. Wecht, K. Alavi, and A. Y. Cho, Appl. Phys. Lett. **43**, 118 (1983).
[4]H. Okumura, S. Misawa, S. Yoshida, and S. Gonda, Appl. Phys. Lett. **46**, 377 (1985).
[5]M. O. Watanabe and Y. Ohba, Appl. Phys. Lett. **50**, 906 (1987).
[6]H. Kroemer, Appl. Phys. Lett. **46**, 504 (1985).
[7]D. I. Babic and H. Kroemer, Solid-State Electron. **28**, 1015 (1985).
[8]G. Duggan, in *Heterojunction Band Discontinuities: Physics and Device Applications*, edited by F. Capasso and G. Margaritondo (North Holland, Amsterdam, 1987), Chap. 5, p. 207.
[9]R. W. Grant, E. A. Kraut, J. R. Waldrop, and S. P. Kowalcyk, *ibid.*, Chap. 4, p. 167.
[10]S. M. Sze, *Physics of Semiconductor Devices*, 2nd ed. (Wiley, New York, 1981), p. 80.
[11]M. A. Rao, E. J. Caine, H. Kroemer, S. I. Long, and D. I. Babic, J. Appl. Phys. **61**, 643 (1987).
[12]L. Y. Leu and S. R. Forrest, J. Appl. Phys. **64**, 5030 (1988).
[13]S. R. Forrest, P. H. Schmidt, R. B. Wilson, and M. L. Kaplan, J. Vac. Sci. Technol. B **4**, 37 (1986).
[14]M. Ogura, M. Mizuta, K. Onaka, and H. Kukimoto, J. Appl. Phys. **22**, 1502 (1982).
[15]S. J. Chang, L. Y. Leu, S. R. Forrest, and C. E. Jones, Appl. Phys. Lett. **54**, 1040 (1989).
[16]G. H. Olsen, in *GaInAsP Alloy Semiconductor*, edited by T. P. Pearsall (Wiley, New York, 1982), Chap. 1, p. 43.
[17]S. R. Forrest, M. L. Kaplan, and P. H. Schmidt, Ann. Rev. Mater. Sci. **17**, 189 (1987).
[18]H. Brendecke, H. L. Stormer and R. J. Nelson, Appl. Phys. Lett. **35**, 772 (1979).
[19]Equation (6) can be rewritten in terms of ΔE_c and ΔE_{cK} simply by replacing $V_D(0)$ and V_{DK}, respectively, with these band offset energies.
[20]D. V. Lang, M. B. Panish, F. Capasso, J. Allam, R. A. Hamm, A. M. Sergent, and W. T. Tsang, Appl. Phys. Lett. **50**, 736 (1987).

Determination of free carrier concentration profiles and the valence-band discontinuity energy of $Hg_{0.7}Cd_{0.3}Te$/Cd(4% Zn)Te heterojunctions using organic semiconductor layers

S. J. Chang, L. Y. Leu, and S. R. Forrest
Departments of Electrical Engineering/Electrophysics and Materials Science, University of Southern California, Los Angeles, California 90089-0241

C. E. Jones
Santa Barbara Research Center, Goleta, California 93117

(Received 22 August 1988; accepted for publication 4 January 1989)

Capacitance-voltage data are utilized to obtain the free-carrier concentration in *n*- and *p*-type $Hg_{1-y}Cd_yTe$ layers, and to measure the valence-band discontinuity energy of a *p*-type $Hg_{0.7}Cd_{0.3}Te$/Cd(4% Zn)Te isotype heterojunction. To facilitate measurement, rectifying contact was made to the $Hg_{1-y}Cd_yTe$ layers using one of two organic materials—metal-free phthalocyanine and copper phthalocyanine. Contrary to previous results with this heterojunction system, we find that holes are accumulated near the Cd(4% Zn)Te side (rather than $Hg_{1-y}Cd_yTe$ side). We obtain a valence band discontinuity energy (ΔE_v) equal to (110 ± 20) meV, and a fixed interface charge density of $\sigma = -(5.9 \pm 0.3) \times 10^{10}$ cm^{-2}.

Heterojunctions (HJ) in the $Hg_{1-y}Cd_yTe$ (MCT) materials system are assuming increased importance for a number of device applications such as photovoltaic and photoconductive infrared detectors. Since the lattice parameters of HgTe and CdTe are nearly equal ($\Delta a/a = 0.003$), approximately lattice-matched epitaxial growth of $Hg_{1-y}Cd_yTe$ for all values of y may be obtained on CdTe substrates, thus minimizing the density of defects associated with misfit dislocations. Moreover, it is found that lattice matching can be further improved by using $Cd_{1-x}Zn_xTe$ with $x \sim 0.04$ instead of CdTe for the substrate.

Band-edge discontinuities are of central importance in determining device behavior. However, our understanding, both theoretical and experimental, of the valence-band discontinuity in MCT heterojunctions is far from being complete. From the phenomenological common anion rule[1] and Harrison's linear combination of atomic orbitals (LCAO) calculations[2] without dipole contributions, it is deduced that the valence-band offset at the CdTe-HgTe interface is small (with $\Delta E_v < 0.1$ eV). Magneto-optical measurements[3] and resonant Raman spectra[4] obtained at low temperature on HgTe-CdTe superlattices also indicate that ΔE_v is small. On the other hand, a larger valence-band offset of 0.35 eV has been obtained at room temperature by x-ray photoemission spectroscopy[5] (XPS), consistent with values predicted by Tersoff's interface quantum-dipole model[6] (where $\Delta E_v = 0.5$ eV), and the LCAO calculation which includes the contribution due to dipoles[7] ($\Delta E_v = 0.49$ eV). In addition, recent tight binding calculations which include the contribution of the cation *d* orbitals[8] give a natural valence-band offset of 0.36 eV, which is very close to the XPS results.

The discrepancy between the experimental results obtained by these several techniques has been suggested to be due to the temperature dependence of the valence-band discontinuity.[9] For example, temperature-dependent data of the valence-band discontinuity obtained from direct electrical measurement[10] have been reported. However, the existence of parasitic transport mechanisms which were not considered in that work may lead to erroneous values of ΔE_v.

In our work, capacitance-voltage analysis combined with the use of organic thin-film contacts is used to obtain free-carrier concentrations deep into the bulk of the sample. In addition, the depletion method proposed by Kroemer *et al.*[11] is utilized to measure the band offset of MCT HJs. This technique is relatively insensitive to compositional gradients[12] at the heterojunction, and therefore it is particularly useful for studying $Hg_{1-y}Cd_yTe$/CdTe heterojunctions which can have a significant grading length due to the interdiffusion of Hg and Cd atoms at the heterointerface. Another property of this technique is that the band bending near the HJ can be inferred from the carrier concentration profile simply by observing the location of the carrier accumulation and depletion regions. This is different from optical techniques which only measure the relative energy levels of the valence- (or conduction-) band edges of the two contacting materials.

The *C-V* measurements are accomplished by depleting the semiconductor in the region of the heterojunction by applying reverse bias voltage across an adjacent rectifying contact. The apparent free-hole concentration $p^*(x^*)$ at the edge of the depletion region a distance x^* away from the contact is obtained using

$$p^*(x^*) = \frac{2}{q\kappa A^2} \frac{dV}{d(1/C_D^2)}, \tag{1}$$

with $x^* = \kappa A/C_D$, where A is the junction area, C_D is the diode capacitance, κ is the permittivity of the semiconductor, V is the reverse bias voltage, and q is the electronic charge. The background carrier concentration (N_A) on both sides of the *p-P* HJ can be determined by measuring $p^*(x^*)$ at distances far removed from the heterointerface. The apparent position of the HJ (x_j^*) is obtained from the location of the peak in $p^*(x^*)$ corresponding to charge accumulation in at the HJ. Using these data, the density of fixed charge in the heterointerface region and the built-in potential V_{DK} of the HJ dipole can be calculated using

$$\sigma = \int [N_A(x^*) - p^*(x^*)]\, dx^*, \tag{2}$$

 0003-6951/89/111040-03$01.00

$$V_{DK} = \frac{q}{\kappa} \int [N_A(x^*) - p^*(x^*)](x^* - x_j^*) dx^*. \quad (3)$$

It has been shown[13,14] that V_{DK} can differ significantly from that due solely to the HJ dipole potential, V_D, in the presence of a sufficiently high density of interface charge. In addition, due to inherent limitations of the spatial resolution of C-V data,[11] the actual HJ position (x_j) is shifted from x_j^* by $\Delta x_j = x_j - x_j^*$, which depends on the magnitude of σ and V_{DK}. When these factors are considered, the HJ dipole potential can be obtained using[13]

$$V_D = V_{DK} + q\sigma(d/2 + \Delta x_j)/\kappa, \quad (4)$$

where d is the width of the heterointerface region. The relationship between the valence-band discontinuity energy and V_D can finally be calculated using $\Delta E_v = \delta_2 - \delta_1 - |qV_D|$, where δ_1 and δ_2 are the depths of the Fermi levels as measured from the valence-band maxima in the $Hg_{1-y}Cd_yTe$ and Cd(4% Zn)Te bulks, respectively.

One impediment to the measurement of free-carrier concentrations is the difficulty in forming a rectifying contact to MCT. Schottky barrier diodes are subject to low voltage breakdown, hence giving rise to large reverse leakage currents which degrade the accuracy of the capacitance measurement. Therefore, we use organic-on-inorganic (OI) contact barrier[14,15] diodes to form rectifying contacts to the $Hg_{1-y}Cd_yTe$. Due to the anisotropy of the conductivity of the organic film, current is confined to the region under the contact pad, thus avoiding low-voltage edge-related breakdown. Thus, the diode can be depleted far from the surface prior to breakdown, allowing for free-carrier concentration profiles to be obtained deep into the semiconductor bulk.

For our experiment, an ~ 8 μm thick layer of p-type $Hg_{0.7}Cd_{0.3}Te$ was grown by LPE onto a (111), lightly p-type Cd(4% Zn)Te substrate, followed by a 1-μm-thick n-type cap layer of $Hg_{1-y}Cd_yTe$ whose composition varied from $y = 0.4$ at the p-n junction to $y = 0.3$ at the wafer surface. These samples could be depleted to approximately 3 μm from the surface before breakdown, falling considerably short of the nearly 10 μm total layer thickness. In order to further extend the profile depth, the wafer surface was taper etched by slowly dipping it in a bromine-methanol solution.[16] Once the taper was formed, an array of OI diodes was deposited along the taper direction, and a composite profile was constructed which correlated the individual profiles to their depth from the original, as-grown surface. To measure the depth of the taper as a function of position along the wafer, an array of mesas was formed during etching using a photolithographically defined SiO_2 mask. The taper depth from the original wafer surface was obtained using a surface profiler measurement of the mesa height.

To fabricate the OI diodes, the sample was solvent cleaned, and then placed in a vacuum of $\sim 10^{-6}$ Torr where 500 Å of the prepurified organic material was deposited via sublimation from a resistively heated source.[15] Two organic materials, namely, metal-free phthalocyanine (H_2Pc) and copper Pc (or CuPc), were used to form rectifying contacts to the n- and p-type MCT layers. Next, ohmic metal contacts were deposited through a shadow mask to form contacts with areas of 5.5×10^{-4} cm^2. To contact the MCT, an In strip was deposited alongside the organic film directly onto the wafer surface.

Typical room-temperature bipolar current-voltage characteristics for H_2Pc/p-$Hg_{0.7}Cd_{0.3}Te$ and CuPc/n-$Hg_{0.7}Cd_{0.3}Te$ diodes are shown in the inset of Fig. 1. Detailed characteristics obtained for the H_2Pc/MCT device are shown in Fig. 1. Soft breakdown is observed at 8 V and $T = 100$ K. The breakdown voltage of 8 V at $T = 100$ K (defined at reverse dark current of 10 μA) is considerably larger than the < 1 V breakdown observed for metal/MCT Schottky barrier diodes. Majority carrier types are deduced from the polarity of the I-V characteristics, and are consistent with the doping of the MCT layers during growth.[15] From these data we deduce[17] a H_2Pc/p-$Hg_{0.7}Cd_{0.3}Te$ barrier energy of $\phi_B = 0.41 \pm 0.04$ V.

Carrier concentration profiles taken from diodes along the taper were obtained from C-V data measured at 1 MHz at different temperatures (down to 91 K). No appreciable temperature dependence of the carrier concentration is observed. From the room-temperature profiles, the composite carrier concentration profile from the top n layer through the p layer to the Cd(4% Zn)Te substrate is obtained as shown in Fig. 2. The location of the peak in the concentration profile indicates that the $Hg_{0.7}Cd_{0.3}Te$/Cd(4% Zn)Te HJ is at 8.5 μm, consistent with microscopic measurement. Further, we obtain a free-carrier concentration of $(1-2) \times 10^{16}$ cm^{-3}, 4×10^{16} cm^{-3}, and 5×10^{14} cm^{-3} for the n-$Hg_{1-y}Cd_yTe$, p-$Hg_{0.7}Cd_{0.3}Te$, and p-Cd(4% Zn)Te layers, respectively.

The free-carrier concentration profile shown in Fig. 3 was measured at 91 K using a device located 6.6 μm from the original surface. We observe that holes are accumulated at the Cd(4% Zn)Te side giving rise to a peak in $p^*(x^*)$, and depleted from the $Hg_{0.7}Cd_{0.3}Te$ side of the HJ. This implies that the band bending of both materials near the HJ is as

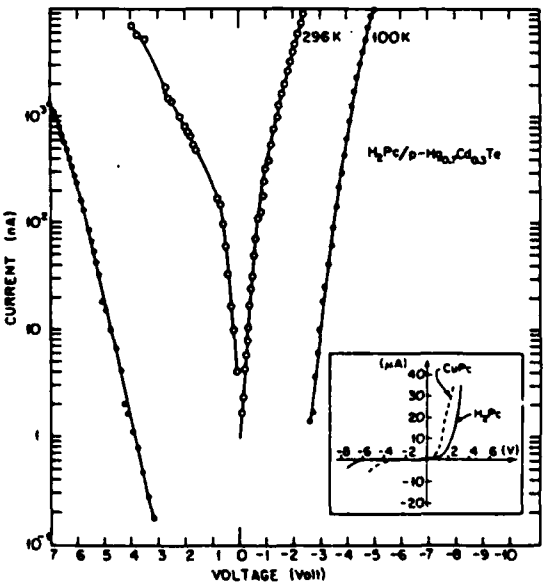

FIG. 1. Bipolar current-voltage characteristics of an In/$H_2PcHg_{0.7}Cd_{0.3}Te$ OI diode at two different temperatures. Open circles: 296 K, solid circles: 100 K. Inset: Typical bipolar current-voltage characteristics of an In/H_2Pc/P-$Hg_{0.7}Cd_{0.3}Te$ (solid line) and In/CuPc/$n$$Hg_{0.7}Cd_{0.3}Te$ OI diodes (dashed line). The two are plotted using opposite bias polarity for comparison. Scales are vert: 10 μA/div, horiz: 2 V/div.

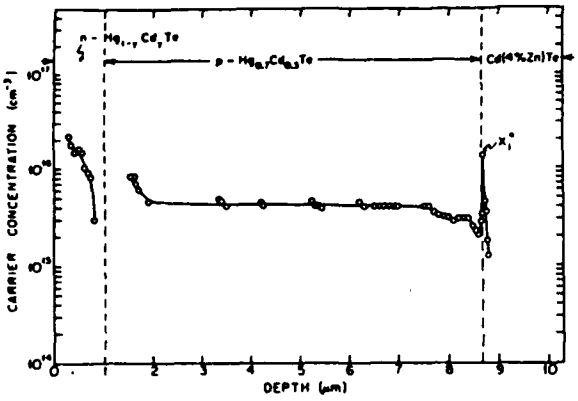

FIG. 2. Apparent free-carrier concentration profile measured by using *C-V* technique on the taper etch sample.

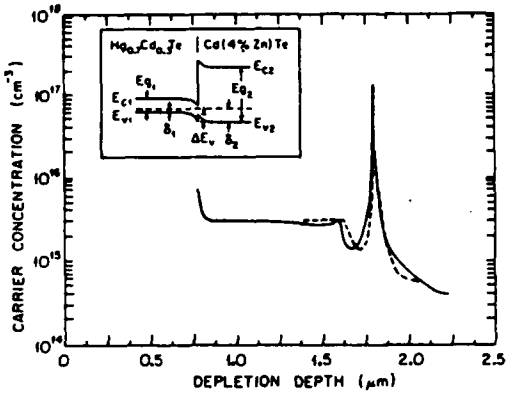

FIG. 3. Experimental (solid line) and reconstructed (dashed line) carrier concentration profiles in the vicinity of the *p-P* $Hg_{0.7}Cd_{0.3}Te$/ Cd(4% Zn)Te heterojunction. Inset: Band diagram showing the conduction band minimum E_c and valence-band maximum E_v vs position for the *p-P* $Hg_{0.7}Cd_{0.3}Te$/Cd(4% Zn)Te heterojunction.

shown in the inset, i.e., the valence band of Cd(4% Zn)Te lies above that of $Hg_{0.7}Cd_{0.3}Te$ at the HJ. This is contrary to previous work indicating that the valence band of CdTe is lower in energy than that of HgTe.[3,18,19]

From the profile shown in Fig. 3, a valence-band potential energy of $qV_{DK} = (25 \pm 4)$ meV is obtained via Eqs. (2) and (3). The density of fixed charge is calculated via Eq. (2), giving $\sigma = -(5.9 \pm 0.3) \times 10^{10}$ cm^{-2}; the negative sign indicating that the interface traps are acceptor-like. Using these values of σ and V_{DK} in Eq. (5), we obtain a valence-band offset[13,20] of $\Delta E_v = (110 \pm 20)$ meV.

To check the accuracy of the measured ΔE_v, the carrier concentration profile was "reconstructed" by solving Poisson's equation using the valence-band energy ΔE_v and interface charge density given above. To accomplish this fit, we assume a width[20] for the interface region of $d \simeq 3000$ Å. We note, however, that the quality of the fit is not strongly dependent on the value of d chosen. As shown in Fig. 3, the agreement between the measured hole concentration profile and the simulation result is quite good, providing an independent check of our values for ΔE_v and σ.

In conclusion, H_2Pc and CuPc are found to form rectifying contacts to HgCdTe. This allows the use of the *C-V* depletion technique to measure the free-carrier concentrations and the valence-band discontinuity energy of HgCdTe/Cd(4% Zn)Te heterojunction samples. A valence-band discontinuity, ΔE_v, equal to (110 ± 20) meV is obtained at 91 K, with the hole accumulation region at the Cd(4% Zn)Te side, rather than the $Hg_{0.7}Cd_{0.3}Te$ side of the heterointerface. Because the direction of the offset is different from that reported in the literature, several alternative explanations have been considered. If impurity buildup at defects in the junction region had caused an *n*-type region to be present in the HgCdTe, this would introduce a *p-n* junction above the heterojunction. If this were the cause of the structure in $p^*(x^*)$, the apparent carrier concentration would be expected to increase at the *p-n* junction to a very large value, and the profile on the far side would not be observed. Alternatively, the acceptor concentration might vary in the narrow HJ region in such a way as to "mimic" a typical HJ profile as shown in Fig. 3. However, this is considered unlikely because of the complicated "dipolar" form of the impurity concentration which would be required to produce such a peak. While these interpretations cannot be ruled out completely, the data presented for the HgCdTe/Cd(Zn)Te heterojunction are of a quality comparable to the best data taken on the GaAs/AlGaAs[11] and InGaAsP/InP[14] systems that did give verifiable offsets.

We are grateful to F. F. So for many helpful suggestions during the course of this work. Also, we thank the Army Research Office (M. Stroscio), Rome Air Development Center (J. Lorenzo), and the Air Force Wright Aeronautical Laboratories (Capt. W. Harris) without whose support this work could not have been accomplished.

[1] J. O. McCaldin, T. C. McGill, and C. A. Mead, Phys. Rev. Lett. **36**, 56 (1975).
[2] W. A. Harrison, Phys. Rev. B **24**, 5835 (1981).
[3] Y. Guldner, G. Bastard, J. P. Vieren, M. Voos, J. P. Faurie, and A. Million, Phys. Rev. Lett. **51**, 907 (1983).
[4] D. J. Olego, J. P. Faurie, and P. M. Raccah, Phys. Rev. Lett. **55**, 328 (1985).
[5] S. P. Kowalczyk, J. T. Cheung, E. A. Kraut, and R. W. Grant, Phys. Rev. Lett. **56**, 1605 (1985).
[6] J. Tersoff, Phys. Rev. Lett. **56**, 2755 (1986).
[7] W. A. Harrison and J. Tersoff, J. Vac. Sci. Technol. B **4**, 1068 (1986).
[8] S. H. Wei and A. Zunger, J. Vac. Sci. Technol. B **5**, 1239 (1987).
[9] J. P. Faurie, C. Hsu, and T. M. Duc, J. Vac. Sci. Technol. A **5**, 3074 (1987).
[10] D. H. Chow, J. O. McCaldin, A. R. Bonnefoi, T. C. McGill, I. K. Sou, and J. P. Faurie, Appl. Phys. Lett. **51**, 2230 (1987).
[11] H. Kroemer, Wu-Yi Chien, J. S. Harris, Jr., and D. D. Edwall, Appl. Phys. Lett. **36**, 295 (1980).
[12] H. Kroemer, Appl. Phys. Lett. **46**, 504 (1985).
[13] L. Y. Leu and S. R. Forrest, J. Appl. Phys. **64**, 5030 (1988).
[14] S. R. Forrest, P. H. Schmidt, R. B. Wilson, and M. L. Kaplan, J. Vac. Sci. Technol. B **4**, 37 (1985).
[15] S. R. Forrest, M. L. Kaplan, and P. H. Schmidt, Ann. Rev. Mater. Sci. **17**, 189 (1987).
[16] J. P. Rosbeck and M. E. Harper, J. Appl. Phys. **62**, 1717 (1987).
[17] S. R. Forrest and F. F. So, J. Appl. Phys. **64**, 399 (1988).
[18] T. N. Casselman, A. Sher, J. Silberman, W. E. Spicer, and A. B. Chen, J. Vac. Sci. Technol. A **1**, 1692 (1983).
[19] R. W. Grant, E. A. Kraut, J. T. Cheung, and S. P. Kowalczyk, J. Vac. Sci. Technol. A **5**, 3070 (1987).
[20] For this calculation, we take $d = 3000$ Å which is typical of our samples.

A Reprint from the

PROCEEDINGS

Of SPIE-The International Society for Optical Engineering

Volume 944

Growth of Compound Semiconductor Structures

15-16 March 1988
Newport Beach, California

Growth and characteristics of organic-on-inorganic semiconductor heterostructures

F. F. So, S. R. Forrest
Departments of Electrical Engineering and Materials Science
University of Southern California, Los Angeles, CA 90089-0241

Growth and Characteristics of Organic-on-Inorganic Semiconductor Heterostructures

F. F. So and S. R. Forrest
Departments of Electrical Engineering and Materials Science
University of Southern California
Los Angeles, CA 90089-0241

ABSTRACT

Recently, several crystalline organic semiconductors have been found to form rectifying heterojunctions when deposited onto inorganic semiconductor substrates. In this paper, we discuss the growth and characterization of these organic-on-inorganic (OI) heterostructures. Both the purification of organic materials, and the fabrication procedures for OI heterostructures are described in detail. The electrical properties, as well as the microstructure of the organic material are found to be very sensitive to the deposition conditions. The valence band discontinuity at the OI heterojunction is measured for the first time, using both forward current-voltage characteristics and internal photoemission. The interface state densities have been studied for several different organic semiconductors deposited on p-Si substrates. A model is proposed to account for the observed results.

I. Introduction

In the past ten years, considerable effort has been focused on the study of semiconductor heterojunctions[1]. Understanding of the nature of these heterojunctions (HJ's) is essential if we are to use them to advantage in many semiconductor devices such as lasers and photodetectors. More recently, there have been a few reports on an entirely new class of semiconductor heterostructures[2-5] which are also potentially useful for optoelectronic device applications[6-7]. These HJ's consist of an organic (crystalline molecular or polymeric) semiconductor in contact with an inorganic semiconductor, which form rectifying energy barriers at the organic-on-inorganic (OI) semiconductor interface. The resulting rectifying characteristics of the OI-HJ's have been attributed to the low reactivity between the deposited organic materials and the inorganic substrate, and to the low energy associated with the deposition of the thin films. These factors enable one to use OI heterostructures in non-destructive surface analysis of inorganic semiconductors.[8-9]

In this paper, we discuss the different aspects of the growth of OI heterostructures, including the purification of organic materials and the techniques for device fabrication. The nature of the OI heterointerface and band discontinuities also be discussed in detail.

II. Growth of OI-HJ Heterostructures

Purification Organic Material

The organic materials that have been used most extensively in OI-HJ's are aromatic compounds, such as 3,4,9,10 perylenetetracarboxylic dianhydride (PTCDA)[2-4]. These materials are crystalline molecular solids which are both thermally and hydrolytically stable.[11] We present here the purification procedures for PTCDA; and it is noted that the procedures for purifying other organic materials are similar. It is critical that all organic materials be purified prior to deposition onto inorganic substrates. This ensures highly stable and reproducible electrical and optical characteristics of the resulting devices.

PTCDA is available commercially[12] in powder form. Among the different methods to purify PTCDA, gradient sublimation[11,13] gives the highest purity source material. To purify PTCDA, a few grams of powder are put into the sealed end of a quartz tube. The tube is evacuated to about 10^{-5} torr, and the closed end of the tube is inserted into a preheated furnace. The sample is kept at 425-450°C (i.e. just below the sublimation temperature of PTCDA) during the process of purification, which proceeds for between 24 and 48 hours. After this period, the tube is cooled while the sample is maintained under vacuum. The wall of the tube shows bands of different colors. Only the dark red, unsublimed source material is used for fabrication of OI heterostructures.

Crystal and Molecular Structure of the Organic Thin Films

In order to understand the electrical properties of the OI heterojunction, it is necessary to study the crystal structure of these organic materials. For example, PTCDA is a monoclinic crystal[14], that forms infinite stacks of planar, uniformly spaced molecules in which the atoms of one molecule are located directly above adjacent molecules, as shown in Fig. 1. The interplanar spacings for several crystalline organic solids used in OI diodes are shown in Table I. The most important aspect of the crystal structure of PTCDA is its extremely small interplanar spacing of 3.21 Å, which is even smaller than that of graphite (3.37 Å). Thus, the π-orbitals overlap to the extent that car-

riers moving along the stacking axis are highly delocalized, giving rise to a significant anisotropy of electrical conductivity when measured with respect to the crystalline axes. Typical anisotropies range from 10-1000.

Anistropy can also be caused by the presence of grain boundaries in the organic films. The deposited organic films are polycrystalline, with a grain size on the order of several thousand angstroms. Carriers moving in the vertical direction are not likely to cross the grain boundaries if the organic film is thin enough (<2000Å). On the other hand carriers moving along any in-plane directions will be trapped at the grain boundaries and therefore the mobility is drastically reduced, resulting in additional anisotropy in conductivity.

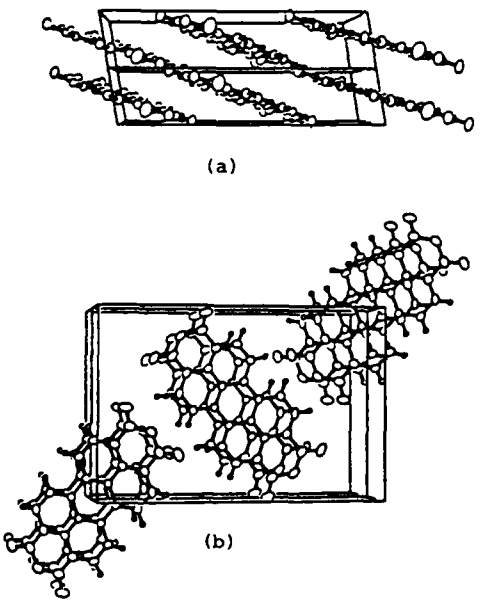

Fig. 1: Perspective view of the unit cell of PTCDA looking from (a) a-axis and (b) b-axis.

Table I
Interplanar spacing and ohmic contact metals used for some organic semiconductors

	PTCDA	NTCDA	CuPc	H_2Pc
Interplanar Spacing (Å)	3.21	3.51	3.38	3.40
Contact metal	In, Ti	In	Au	In

III. Fabrication of OI Heterostructures

Many molecular semiconductors such as PTCDA, 3,4,7,8 naphthalenetetracarboxylic dianhydride (NTCDA) and the phthalocyanines (Pc's)[3,10] have been used to form OI-HJ's with a variety of inorganic semiconductor substrates[15]. Here we give a brief outline of the fabrication procedures with additional detail given in the literature[2,3,9]. The first step in the fabrication of the OI heterostructure is wafer cleaning[11]. Organic solvents are used for degreasing, which is followed by native oxide etching in a dilute HF solution. For some III-V compounds such as InP and related materials, enhancement of the contact barrier can be achieved by oxidizing the samples in a solution such as HNO_3 and H_2O_2. Table II gives the cleaning sequence used to prepare several common inorganic semiconductors. The final step in surface preparation is a rinse in deionized water, followed by drying of the wafer with filtered nitrogen gas.

Table II
Cleaning Sequence For Some Semiconductors[a]

	1:4 $HF:H_2O$ (30s)	HNO_3 (conc.) (10s)	30% H_2O_2 (30s)
Si	X		
GaAs	X		X
InP	X	X	

[a]Surface treatments all follow a thorough organic solvent cleaning. Wafers should be rinsed in D.I. water for 5 min. after etching with acid.

Immediately after cleaning, the sample is loaded into a vacuum chamber which is pumped down to < 10^{-6} torr. Next, 1000-2000 Å of the organic material is vacuum sublimed onto the pre-cleaned top surface of the wafer. Organic materials generally have low sublimation temperature in the range between 100°C and 600°C. Good control of the deposition parameters can be achieved by using a two chamber source boat such as that employed for silicon monoxide deposition. Typical deposition rates for organic materials are 30-40 Å/s. Next, ohmic contact metal pads 2000-3000 Å thick are evaporated onto the organic film. The contact metals used for some organics are also listed in Table I. Finally, a full surface ohmic contact metal is evaporated onto the back side of the wafer.

It has been found that the microstructure[4] and surface morphology[5] of some aromatic compounds are very sensitive to both deposition rate and substrate temperature. For instance, thin films of PTCDA deposited at high deposition rates (50-100 Å/s) show strong preferred orientation. The crystalline perfection of films deposited at a high rate is demonstrated by the x-ray pole figure for the (102) interplanar diffraction peak as shown in Fig. 2(a). In sharp contrast, no preferred orientation is observed for films deposited slowly (2 Å/s), as shown in Fig. 2(b). It is noted that Kim et. al.[16] have observed that the surface morphology is better for organic films deposited at low substrate temperatures than those deposited at high temperatures. Therefore, substrate temperature also plays an important role in determining the microstructure of the organic film.

The effect that the microstructure of PTCDA has on electrical properties is apparent from Fig. 3. For films deposited at 100 Å/s, the carrier mobility can be as high as 1.4 cm^2/V-s, which is an order of magnitude larger than that for the films deposited at lower deposition rates. These results can be explained in view of the crystalline order of the films. A higher order implies fewer grain boundaries, and hence a reduced charge trapping at these imperfections. The existence of traps in the more disordered film is consistent with the hysterysis often observed in the current-voltage characteristics[4].

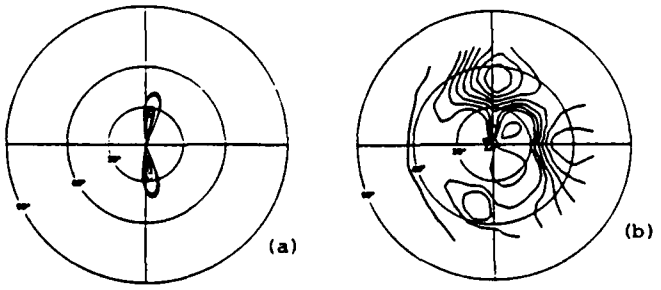

Fig. 2: X-ray pole figure of the (102) reflection intensity of PTCDA deposited at (a) >50Å/s and (b) approximately 2Å/s. Each contour represents a 10% and 2% change in peak intensity for (a) and (b) respectively.

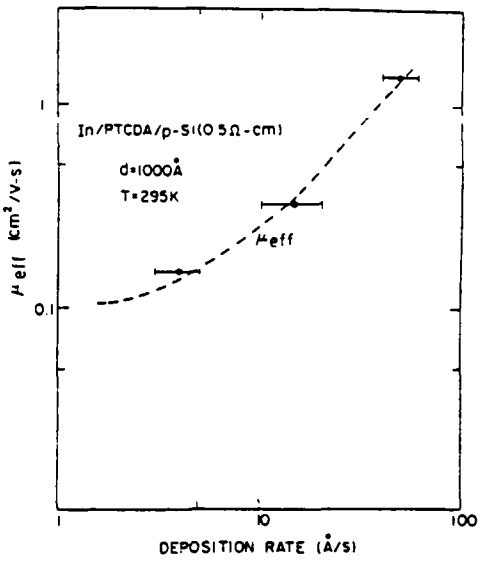

Fig. 3: Carrier mobility in PTCDA as a function of deposition rate.

IV. Measurement of Valence Band Discontinuity Energies

Knowledge of the band discontinuity energies is essential to the understanding of any semiconductor heterojunction.[17] For the first time, we have measured the energy band discontinuity of an OI-HJ. In this experiment, the sample was an isotype (p-P) PTCDA/p-Si heterojunction investigated using the temperature dependence of the I-V characteristics as well as internal photoemission spectroscopy.

It can be shown that the forward I-V characteristics are described[2,8,18] by

$$J = J_o \exp(-q\phi_{Bp}/kT)[\exp(qV_D/kT)-1]$$
$$= J_s[\exp(qV_D/kT)-1] \quad (1)$$

Here, k is the Boltzmann's constant, T is the temperature, q is the electronic charge, J_s is the saturation current and ϕ_{Bp} is the OI-HJ barrier potential. Also, V_D is the voltage drop across the depletion layer of the inorganic semiconductor which is taken to be positive under forward bias.

From Eq.(1), it is apparent that a measurement of the saturation current as a function of temperature will give its activation energy. A plot of $\log(J_s)$ as a function of 1/T is shown in Fig. 4. A schematic cross-sectional drawing of an organic-on-inorganic semiconductor heterojunction device is shown in the inset. A

least square fit to the data, as indicated by the straight line, gives ϕ_{Bp} = 0.56 ± 0.02 eV. The valence band discontinuity energy, ΔE_v, for this isotype heterojunction is obtained from ϕ_{Bp} using[19]

$$\Delta E_v = q\phi_{Bp} + \delta_s - \delta_o \qquad (2)$$

where δ_s and δ_o are the differences between the Fermi-level and the valence band maximum in the inorganic and organic bulk semiconductors. Taking the p-Si hole concentration to be 5×10^{15} cm^{-3}, a hole concentration[3] of $5\times10^{14}cm^{-3}$ for PTCDA, and assuming the effective hole mass (m*) in PTCDA is equal to the free electron mass, we obtain ΔE_v=(0.48±0.2)eV for a PTCDA/p-Si heterojunction. Note that the band gap of PTCDA is[3] 2.2eV. Therefore, $\Delta E_c = \Delta E_g - \Delta E_v$ = 0.6eV where ΔE_g is the difference in band gap energies between PTCDA and Si.

We have also measured ΔE_v directly by internal photoemission spectroscopy. In this experiment, a PTCDA/p-Si heterostructure was illuminated through the Si substrate using a chopped light source, such that light with energy greater than 1.1 eV is filtered by the substrate. Further attenuation of short wavelength light was achieved by inserting a second Si wafer between the sample and the light source. The short circuit photocurrent was then measured as a function of photon energy. Fig. 5(a) shows a photoemission spectrum where a peak is found at $h\nu$ = 0.57eV. The results can be interpreted as follows: At $h\nu$<0.57eV, holes in the organic film are photo-excited, and subsequently emitted over the OI energy barrier. This photoemission current is expected to follow: $I_{ph} \propto (h\nu - \Delta E_v)^2$. Fig. 5(b) shows a plot of the square root of photocurrent versus $h\nu$ for the data taken on the long wavelength side of the emission peak. A least squares fit to these data gives ΔE_v=(0.50+0.1)eV-- a value which agrees with that obtained from the forward I-V characteristics.

Note that at $h\nu$ >0.57eV, I_{ph} drops rapidly to zero. This can be understood using the band diagram shown in the inset of Fig. 5(a). Molecular semiconductors are characterized by narrow bandwidths, as indicated by the cross-hatched region in the figure. For PTCDA, the total bandwith (BW), which is the sum of highest occupied molecular orbital (HOMO) and lowest unoccupied molecular orbital (LUMO) bandwidths, is only 0.9 eV. Thus, transition "b" beyond the BW is forbidden, resulting in a drop in I_{ph} for high energy photons.

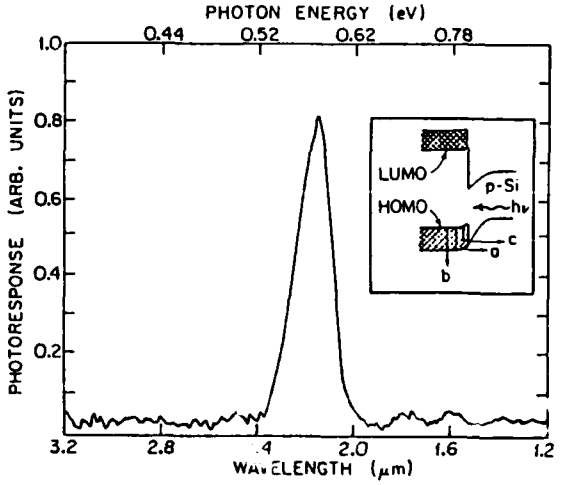

Fig. 5a: Photocurrent spectrum for an In/PTCDA/p-Si heterojunction illuminated via the p-Si substrate. The organic film thickness is 1000 Å.
Inset: Band diagram of a PTCDA/p-Si heterojunction showing allowed ("a" and "c") and forbidden ("b") photoemission transitions resulting in the spectrum shown.

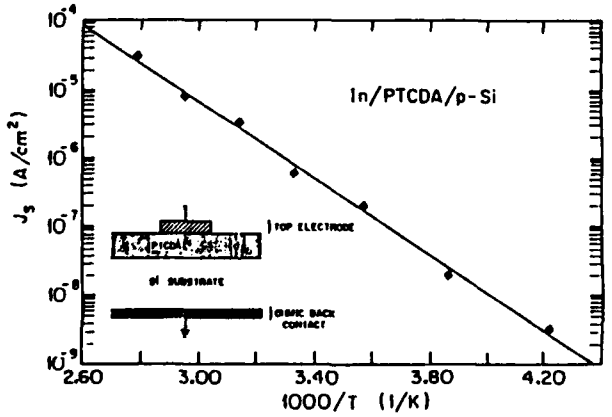

Fig. 4: Saturation current density (J_s) versus 1/T for an In/PTCDA/p-Si heterojunction. The solid line is a linear least squares fit to the data points.
Inset: Schematic view of an organic/inorganic semiconductor heterojunction device.

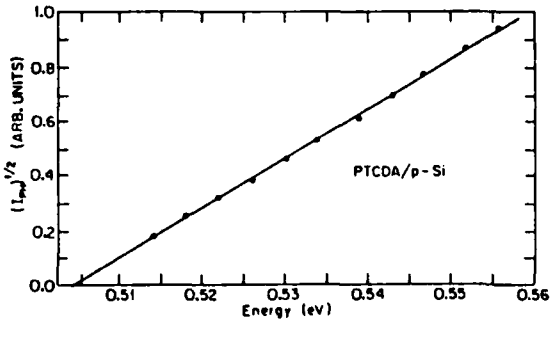

Fig. 5b: Square root of the photocurrent versus photon energy for the data on the long wavelength side of the peak shown in 5a. The solid line is a linear least squares fit to the data points.

IV. Effects of Interface Charge at the OI-HJ

Dianhydride containing compounds (such as PTCDA), have been used for semiconductor surface analysis[8,9] due to their inert nature when deposited onto inorganic semiconductor surfaces. In efforts to study the interactions between the substrate and the organic layer, we have investigated OI-HJs formed using NTCDA, PTCDA and two phthalocyanines (H_2Pc and CuPc) deposited on p-Si substrates. The interface state density as a function of surface potential was derived from the 1 MHz capacitance-voltage characteristics[10]. Figure 6 shows the interface state density (D_{ss}) at the Si surface for several OI-HJ's using these four organic semiconductors. It is apparent that the D_{ss} spectra for the PTCDA and NTCDA-containing diodes are qualitatively different from those for H_2Pc and CuPc. For example, D_{ss} for the former compounds are at a relatively low value of $10^{12}cm^{-2}eV^{-1}$, which is a typical value for silicon with a thin surface native oxide[20]. In contrast, CuPc, and to a lesser extent H_2Pc, show a pronounced peak at about 0.5 eV above the valence band edge. This peak is nearly two orders of magnitude higher than the background value of $10^{12}cm^{-2}eV^{-1}$. The existence of the high D_{ss} observed at the CuPc/p-Si interface can be explained in terms of the following mechanism: Water molecules can diffuse into the organic film in the laboratory environment and react with CuPc via:

$$H_2O + CuPc \longrightarrow H_2Pc + CuO \qquad (3)$$

The Gibbs free energy (ΔG^o) for this reaction is large and negative, implying the reaction is energetically favorable. The CuO molecules formed then diffuse through the surface native oxide layer and participate in the following reaction:

$$2CuO + Si \longrightarrow SiO_2 + 2Cu \qquad (4)$$

Once again, ΔG^o is negative, indicating the reaction is probable. It should be noted that the interface state density of the CuPc/p-Si heterostructure is peaked at 0.5eV above the valence band maximum, which corresponds[21] to one of the Cu deep acceptor levels of Si. This peak is likely to be due to the presence of free copper, or Cu-O-Si complexes at the Si surface. A similar reaction might occur at the H_2Pc/p-Si interface where H_2 molecules leave the organic molecules and form H-O-Si complexes, resulting in a high D_{ss} at about the mid-gap of Si. The existence of a high D_{ss} has the effect of pinning the surface Fermi level at the peak in charge density near $\phi_B = 0.5eV$.

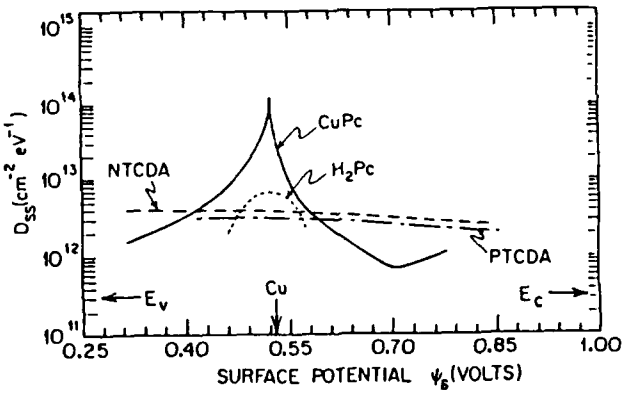

Fig. 6: Density of interface states (D_{ss}) as a function of surface potential in the Si band gap for four different organic/p-Si heterojunctions. The energy is with respect to the conduction (E_c) and valence (E_v) band edges of the Si substrate.

V. Conclusions

We have described the growth procedures for OI heterostructures. The microstructure and electrical properties of the organic films are very sensitive to the deposition conditions used. We have measured, for the first time, the valence band discontinuity energy for the PTCDA/p-Si heterojunction. This was accomplished using the forward I-V characteristics and internal photoemission spectroscopy data. Finally, we have analyzed the interface state densities of some organic-on-Si devices. In contrast to observations concerning dianhydride-based compounds which are relatively inert, CuPc has been found to react strongly with silicon, resulting in the presence of a high density of interface states which pin the Fermi level at the inorganic substrate surface.

The authors would like to thank the Rome Air Development Center, the Army Research Office, and the Powell Foundation for their support of this work.

References

1. F. Capasso and G. Margaritondo, Eds. Heterojunction Band Discontinuities: Physics and Device Application, North-Holland, Amsterdam, (1987).

2. S.R. Forrest, M.L. Kaplan, P.H. Schmidt, W.L. Feldmann, and E. Yanwoski, Appl. Phys. Lett., 41, 708 (1982).

3. S.R. Forrest, M.L. Kaplan, P.H. Schmidt, J. Appl. Phys., 55, 1492 (1984).

4. S.R. Forrest, M.L. Kaplan, P.H. Schmidt, J. Appl. Phys., 56, 543 (1984).

5. M. Ozaki, D. Peebles, B.R. Weinberger, A.J. Heeger, and A.G. MacDiarmid, J. Appl. Phys., 51, 4252 (1980).

6. F.F. So, S.R. Forrest, H.J. Garvin and D.L. Jackson, Integrated and Guided Wave Optics Tech. Dig., Santa Fe, 1988 (Optical Society of America, Washington, D.C., 1988).

7. C.-L. Cheng, S.R. Forrest, M.L. Kaplan, P.H. Schmidt, and B. Tell, Appl. Phys. Lett., 47, 1217 (1985).

8. S.R. Forrest and P.H. Schmidt, J. Appl. Phys., 59, 513 (1986).

9. S.R. Forrest, M. L. Kaplan, and P. H. Schmidt, J. Appl. Phys. 60, 2406 (1986).

10. F.F. So and S.R. Forrest, J. Appl. Phys. 63, 442 (1988).

11. S.R. Forrest, M.L. Kaplan, and P.H. Schmidt, Ann. Rev. Mater. Sci. 17, 189(1987).

12. Aldrich Chemical Co., Inc., Milwaukee, WI 53233.

13. F. Gutmann and L.E. Lyons, Organic Semiconductors (Wiley, New York, 1967).

14. A.J. Lovinger, S.R. Forrest, M.L. Kaplan, P.H. Schmidt, and T. Venkatesan, J. Appl. Phys., 55, 476 (1984).

15. P.H. Schmidt, S.R. Forrest, and M.L. Kaplan, J. Electrochem. Soc., 133, 769 (1986).

16. K.K. Kam, M.K. Debe, R.J. Poirier, and A.R. Drube, J. Vac. Sci. Technol., A5, 1914 (1987).

17. F.F. So and S.R. Forrest, Appl. Phys. Lett. 52, 1341 (1988).

18. S.R. Forrest and F.F. So, J. Appl. Phys., (June, 1988).

19. A.G. Milnes and D.L.Feucht, Heterojunctions and Metal-Semiconductor Junctions, Academic, N.Y. (1972).

20. J. Maserjian and N. Zamani, J. Appl. Phys. 53, 559 (1982).

21. A. G. Milnes, Deep Impurities in Semiconductors, Wiley, N.Y. (1973).

APPENDIX 2

The Effects of Lattice Mismatch on $In_{0.53}Ga_{0.47}As/InP$ Heterojunctions

C. D. Lee and S. R. Forrest

Departments of Electrical Engineering/Electrophysics

and Material Science

Center for Photonic Technology

University of Southern California

Los Angeles, CA 90089-0241

Abstract

The conduction band discontinuities and interface charge densities of several n-N isotype $In_xGa_{1-x}As/InP$ ($x \simeq 0.53$) heterojunctions with lattice mismatches ($\Delta a/a$) ranging from +0.26% to -0.24% were measured using capacitance-voltage (C-V) techniques. To facilitate these measurements, organic-on-inorganic contact barrier diodes were used. Extremely low interface charge densities ($< 1x10^{10}$ cm^{-2}) are obtained for all the samples, which are approximately one order of magnitude lower than previously reported values for these heterojunctions. We find that the interface charge density is independent of the magnitude of lattice mismatch and temperature. All the samples show a clear peak-and-notch in their apparent free carrier concentration profiles at temperatures as low as 83K. This is in contrast to results reported previously where the notch is observed to disappear at low temperature. The measured heterojunction conduction band discontinuity is also found to be temperature independent, with a value of (0.22 ± 0.02) eV.

The Effects of Lattice Mismatch On $In_{0.53}Ga_{0.47}As/InP$ Heterojunctions

C. D. Lee and S. R. Forrest

Departments of Electrical Engineering/Electrophysics

and Material Science

Center for Photonic Technology

University of Southern California

Los Angeles, CA 90089-0241

It is well known that defects at heterojunctions can affect the performance of optoelectronic devices. For example, lattice-mismatch induced dark-line defects at AlGaAs/GaAs heterojunctions are known to be a principle source of laser degradation [1]. In heterojunction (HJ) systems such as InGaAs(P)/InP where there is no "natural" lattice match condition, great care must be taken during growth to ensure that the composition of the quaternary semiconductor gives a near perfect lattice match. If such a condition is not met, a large number of defects can be generated which propagate from the heterointerface. Other researchers [2,3] have speculated that this lattice mismatch in InGaAs(P)/InP HJs results in a very high density of locallized defect charge. The presence of the charge is inferred from a severe distortion in the free carrier concentration profiles of these HJs obtained at low temperature [2,3] using capacitance-voltage (C-V) techniques [4]. To date, however, there has been no systematic study which indicates that this fixed charge, which has

been universally observed in $In_{0.53}Ga_{0.47}As/InP$ HJs, is in fact due to lattice mismatch.

In this study, we have grown a series of $In_xGa_{1-x}As/InP$ heterojunctions in which the lattice mismatch was varied over a very broad range; i.e. from -0.24% to +0.26%. Here, positive mismatch corresponds to compositions of $In_xGa_{1-x}As$ whose lattice constant is larger than that of InP. Using C-V techniques, we find that there is no correlation between lattice mismatch and fixed interface charge density. Furthermore, the charge densities measured in our samples are significantly lower than 10^{10} cm^{-2}, which to our knowledge represent the lowest values yet reported for $In_{0.53}Ga_{0.47}As/InP$ HJs. We observe, for the first time, that the free carrier concentration profile measured in the heterointerface region is temperature independent, indicative of the high quality of the HJs studied. From these results, we conclude that the source of the widely observed temperature dependence of these profiles is a result of native defects or impurities introduced during growth, which are noticably absent in our growth process.

As noted above, a good measure of the heterointerface quality is the density of the fixed charges which reside at the heterointerface. The dangling bonds and defects caused by the lattice mismatch, *if* they are electrically active, should trap free carriers and create fixed interface charges. Kroemer, et al. [4] have shown that the conduction band discontinuity and interface charge density can be determined from the apparent free carrier concentration profiles

obtained from C-V measurements. The band diagram of an n-N isotype Type 1 heterojunction, such as $In_{0.53}Ga_{0.47}As/InP$, is shown in the inset of Fig. 1. From this diagram, it is apparent that the conduction band offset energy is related to the diffusion potential V_D across the heterojunction via:

$$\Delta E_c = qV_D + \delta_1 - \delta_2. \tag{1}$$

Here, q is the electronic charge, and δ_1 and δ_2 are the depths of the Fermi levels as measured from the conduction band edges in the large and small band gap layers, respectively. The diffusion potential across the heterojunction, V_D, is given by [4]:

$$V_D = q/\epsilon \int_{-\infty}^{\infty} [N_d(x^*) - n^*(x^*)](x^* - x_j)dx^*. \tag{2}$$

The fixed charge density at the heterojunction, σ, is determined using:

$$\sigma = \int_0^{\infty} [\, N_d(x^*) - n^*(x^*) \,]\, dx^*, \tag{3}$$

where ϵ is the semiconductor permittivity, and $n^*(x^*)$ is the measured apparent free carrier concentration determined using standard C-V analysis methods [5]. Also, $N_d(x^*)$ is the background doping concentration which is equal to $n^*(x^*)$ in the InP and $In_{0.53}Ga_{0.47}As$ layers far away from the heterojunction, and x_j is the actual distance of the heterojunction from the rectifying contact.

Three liquid phase epitaxially (LPE) grown samples have been studied in this experiment. Double crystal x-ray diffraction was used to determine the lattice mismatch between the $In_xGa_{1-x}As$ layer ($x \approx$

0.53) and the underlying InP layer. The lattice mismatches of these three samples are -0.24%, -0.03%, and +0.26%, corresponding to sample #1, #2, and #3, respectively. The variation of lattice mismatch across a $(15\ mm)^2$ wafer was found to be less than ±0.03%, for the worst case sample.

The InP and $In_xGa_{1-x}As$ layers were grown on (100) S-doped n^+ InP substrates with an electron concentration of approximately $3x10^{18}$ cm^{-3}. Prior to growth, the substrates were organic solvent cleaned, etched in a solution of 3:1:1 $H_2SO_4:H_2O_2:H_2O$ for four minutes, and finally rinsed in deionized water immediately before loading into a graphite boat. For surface preservation during heat-up and melt homogenization, the substrate was kept under a Sn-InP melt [6] using a basket inserted into the graphite boat. The growth melt for the $In_xGa_{1-x}As$ layer was prepared using ultra-high purity (99.99999+%) [7] In prebaked for 24 hours at 700°C. After the bake, 99.9999% pure polycrystalline InAs and GaAs were added to the melt. Lattice mismatch was achieved by varying the percentage of Ga in the melt. We grew seven wafers with different lattice mismatches, and found that the lattice mismatch was almost linearly related to the atomic percentage of Ga in the melt. For a melt liquidius temperature of 650°C, as X^l_{Ga} is changed from 2.51% to 2.30%, the lattice mismatch ($\Delta a/a$) varied from -0.24% to +0.26%. Here, X^l_{Ga} is defined as the atomic percentage of Ga in the melt. The growth solutions were baked prior to growth for 48 hours at a temperature 20°C higher than the liquidus temperature to reduce the background doping concentrations

of the layers. The In-InP melt was prepared using prebaked, 99.99999+% In. The melt was then baked for an additional 48 hours after adding a small amount of InP for saturation purposes. The substrate was slid through an undersaturated In-InP melt just before growth to obtain a fresh surface.

A 2-3 μm thick InP buffer layer was grown by the two-phase method [8] at a rate of 0.3 $\mu m/^{o}C$, followed by an $In_xGa_{1-x}As$ layer grown with $3^{o}C$ of supercooling at $647^{o}C$. The growth rate of the $In_xGa_{1-x}As$ layer is strongly depending on the sign and magnitude of the lattice mismatch, varying from 0.6 $\mu m/^{o}C$ for $\Delta a/a = +0.26\%$, to 2.1 $\mu m/^{o}C$ for $\Delta a/a = -0.24\%$. This result is expected since the growth rate is limited by the diffusion of Ga within the melt. To obtain a uniform layer thickness and smooth surface morphology, the furnace was calibrated to obtain a uniform temperature profile to within $\pm$ $0.1^{o}C$ over a 25 cm length. We found that the surface morphology of negatively lattice mismatched $In_xGa_{1-x}As$ layers are generally better than those of positively lattice mismatched ones. In addition, the growth melt can not be wiped off from the wafer surface for $In_xGa_{1-x}As$ layers with $|\Delta a/a| > 0.3\%$.

To facilitate the C-V measurement, organic-on-inorganic (OI) semiconductor contact-barrier diodes were fabricated to form a rectifying contact with the top semiconductor layer [9,10]. These diodes were made in the following manner: A 100Å Cr followed by a 2000Å Au layer were vacuum-deposited to form the contact on the substrate surface. Next, a 1000Å thick layer of the pre-purified

organic semiconductor was vacuum-sublimed onto the epitaxial layer surface of the wafer. The organic compound employed was 3, 4, 9, 10 perylenetetracarboxylic dianhydride (PTCDA). Finally, 5.3 x 10^{-4} cm^2 circular In contacts were deposited onto the PTCDA surface through a shadow mask. The organic layer forms a rectifying HJ barrier with the underlying semiconductor such that large reverse bias voltages can be applied to the diode (typically 18V for $In_xGa_{1-x}As$ with a doping of 1 x 10^{15} cm^{-3}) without inducing large reverse leakage currents. Usually, the reverse saturation current is less than 10 mA/cm^2, and the sample under study can be deeply depleted prior to undergoing breakdown. A detailed description of the technique of using organic films for wafer analysis is presented elsewhere [9,10].

Capacitance-voltage measurements were performed at temperatures ranging from 293K to 83K. The measurement frequency used was 1 MHz, and the ac test signal amplitude was 10 mV_{rms}. The apparent free carrier concentration profiles of samples #1, #2 and #3 measured at 83K are shown in Fig. 1. As shown in this figure, the peak and notch are clearly evident for all three samples, and no distortion of these profiles from room to low temperature are observed. This result contradicts that of Lang, et al. [11] who suggested that HJ series resistance causes the notch in the $In_{0.53}Ga_{0.47}As$/InP HJs to vanish at low temperature. By that assumption, this distortion should be observed in all low temperature C-V measurements made on this HJ system, in clear contradiction to our results.

The low and flat free carrier concentrations on both sides of the HJ observed in the profiles in Fig. 1 provide an accurate determination of the background doping concentration (N_d). This minimizes the error in calculating the diffusion potential, V_D, and conduction band offset energy, ΔE_c, using Eq's. (1) and (2). Figure 2 shows the *measured conduction band offset energies of these three* samples as a function of temperature. As expected, the measured conduction band offset is independent of temperature, and has an average value of (0.22 ± 0.02) eV. The error bars in the figure are due to the uncertainties in choosing the background doping (N_d) on the $In_xGa_{1-x}As$ side of the heterojunction. This measured band offset value is consistent with previous reports of ΔE_c for $In_{0.53}Ga_{0.47}As/InP$ HJs measured at room temperature [2,3,11-13]. *However, to our knowledge, this is the first time that such a value* is found to be completely temperature independent, even though in some cases the lattice mismatch is quite large.

The fixed charge density at the heterointerface is shown in Fig. 3 as a function of temperature. The error bars here are also due to uncertanities in determining N_d. Although there is a small variation in σ at different temperatures, the value of σ is at least one order of magnitude smaller than the values reported previously *for* $In_{0.53}Ga_{0.47}As/InP$ HJs [2,3,12,13]. Since the value of σ is so small, the variation in σ with temperature can be attributed to the limitation on capacitance measurement accuracy. The small σ values in our samples also confirm that the filling in of the notch region

in previously reported data [2,3,12,13] is due to charge trapping at a high density of defects at the heterointerface at low temperature. It is surprising that sample #2, which is lattice-matched at the growth temperature, has the highest value of σ, whereas sample #3, which has $\Delta a/a$ = +0.26%, has the smallest σ. Thus, we can conclude that lattice mismatch has no effect on creating the heterointerface fixed charge. That is, the defects induced by lattice mismatch are not electrically active. The energy states created by defects at the heterointerface are either pulled into the conduction or valence band at the heterointerface, instead of residing in the band gap region.

In conclusion, we have measured the interface fixed charge density and conduction band discontinuity of three $In_xGa_{1-x}As/InP$ HJs with lattice mismatches ranging from -0.24% to +0.26%. The measurements show that the interface charge density is independent of both the magnitude and the sign of the lattice mismatch, contrary to assertions made in previous work. We conclude that the fixed interface charges, therefore, must come from the other sources, e.g. from phosphorus vacancies created during wafer translation [12], or impurities incorporated during growth. In fact, we attribute the very low interface charge densities obtained in this work to the use of ultra high purity In in the growth melt. Experiments in our laboratory with slightly less pure In sources (99.99995%) show higher values of σ than those reported here, and a detailed report of those experiments will appear elsewhere. The results described here,

therefore, suggest that perfect lattice match is not a strict requirement for devices utilizing this heterojunction system.

From the device processing point of view, slightly negative lattice mismatched LPE-grown $In_{0.53}Ga_{0.47}As$ might be more suitable for device processing since the surface is smoother than those with perfect or positively mismatched layers. However, for devices requiring thin epitaxial layers, positive lattice mismatch is desired because the growth rate is much slower, and thus the layer thickness is easier to control.

The authors gratefully acknowledge the Army Research Office (M. Stroscio) for partial support of this work.

References

1. H.Yonezu, I. Sakuma, T. Kamejima, M. Ueno, K. Nishda, Y. Nannichi, and I. Hayashi, Appl. Phys. Lett. 24, 18 (1974).
2. P. S. Whitney and C. G. Fonstad, J. Crystal Growth, 83, 219 (1987).
3. M. Ogura, M. Mizuta, and K. Oraka, Japan J. Appl. Phys. 22, 1502 (1983).
4. H. Kroemer, W. Y. Chien, J. S. Harris, and D. D. edwall, Appl. Phys. Lett. 36, 295 (1980).
5. S. M. Sze, *Physics of Semiconductor Devices*, 2nd ed. (Wiley, New York, 1981).
6. G. A. Antypas, Appl. Phys. Lett. 37, 64 (1980).
7. Super high mobility grade high purity In (99.99999+%), Nimic Inc., Cupertino, California.
8. M. A. Pollack, R. E. Nahory, J. C. Dewinter, and A. A. Ballman, Appl. Phys. Lett. 33, 314 (1978).
9. S. R. Forrest, P. H. Schmidt, R. B. Wilson and M. L. Kaplan, J. Vac. Sci. Technol. B4, 37 (1986).
10. S. R. Forrest, M. L. Kaplan and P. H. Schmidt, Ann. Mater. Sci. 17, 189 (1987).
11. D. V. Lang, M. B. Panish, F. Capasso, J. Allan, R. A. Hamm, and A. M. Sergent, Appl. Phys. Lett. 50, 736 (1987).
12. S. R. Forrest and O. K. Kim, J. Appl. Phys. 53, 5738 (1981).
13. K. Kazmierski, P. Philippe, P. Poulain and B. de Cremoux, J. Appl. Phys. 61, 1941 (1987).

Figure Captions

Fig. 1. Apparent free carrier concentration profiles for sample #1, #2, and #3 measured at 83K. The inset shows the energy band diagram of a typical n-N Type 1 Heterojunction.

Fig. 2. Measured conduction band offset as a function of temperature for samples #1, #2 and #3.

Fig. 3. Interface fixed charge density as a function of temperature for the three samples in Fig. 2.

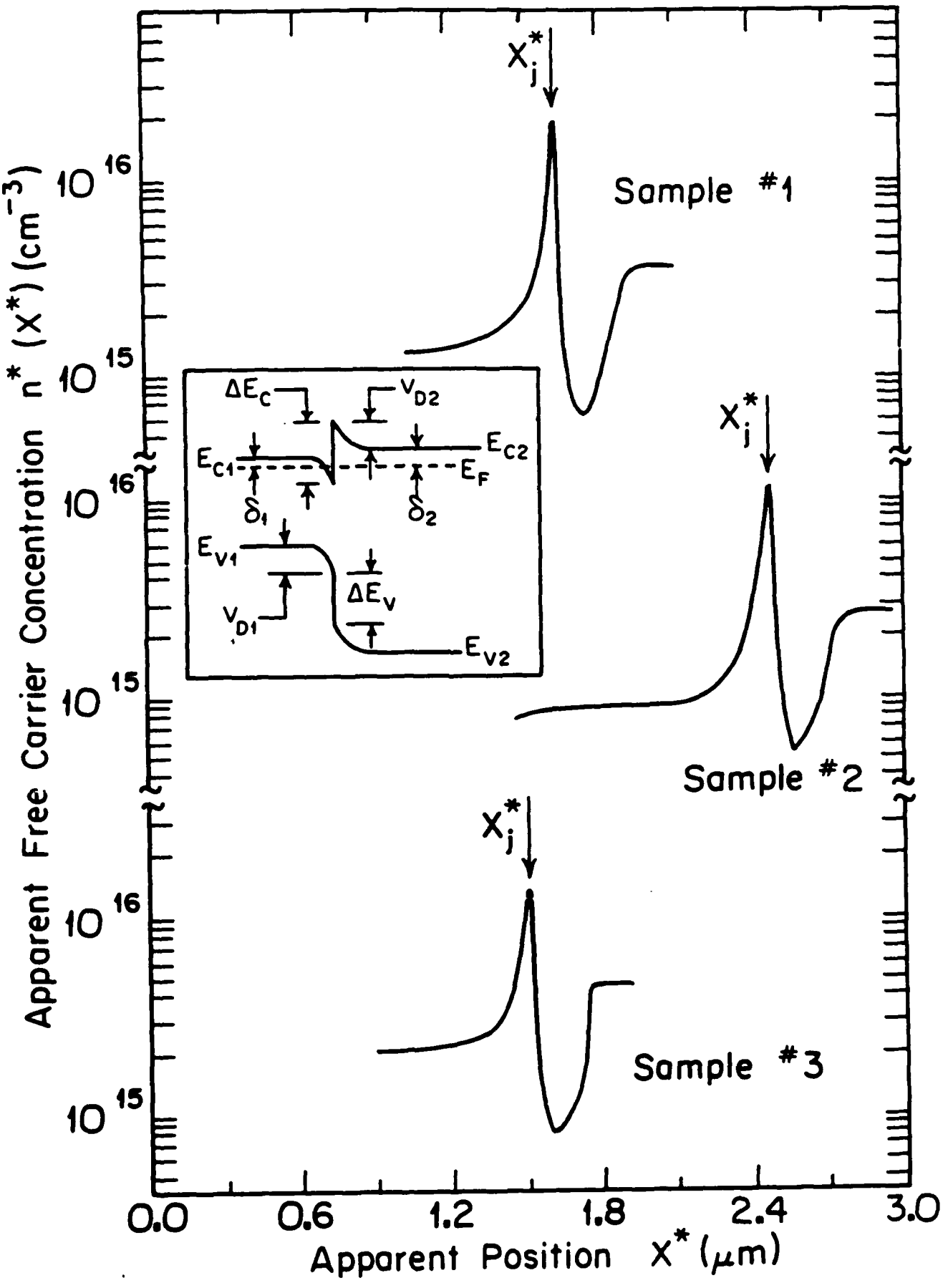
Apparent Free Carrier Concentration $n^*(X^*)$ (cm^{-3})
10^{16}
10^{15}
10^{16}
10^{15}
10^{16}
10^{15}
X_j^*
Sample #1
X_j^*
Sample #2
X_j^*
Sample #3
ΔE_C
V_{D2}
E_{C2}
E_{C1}
E_F
δ_1
δ_2
E_{V1}
ΔE_V
V_{D1}
E_{V2}
0.0
0.6
1.2
1.8
2.4
3.0
Apparent Position X^* (μm)

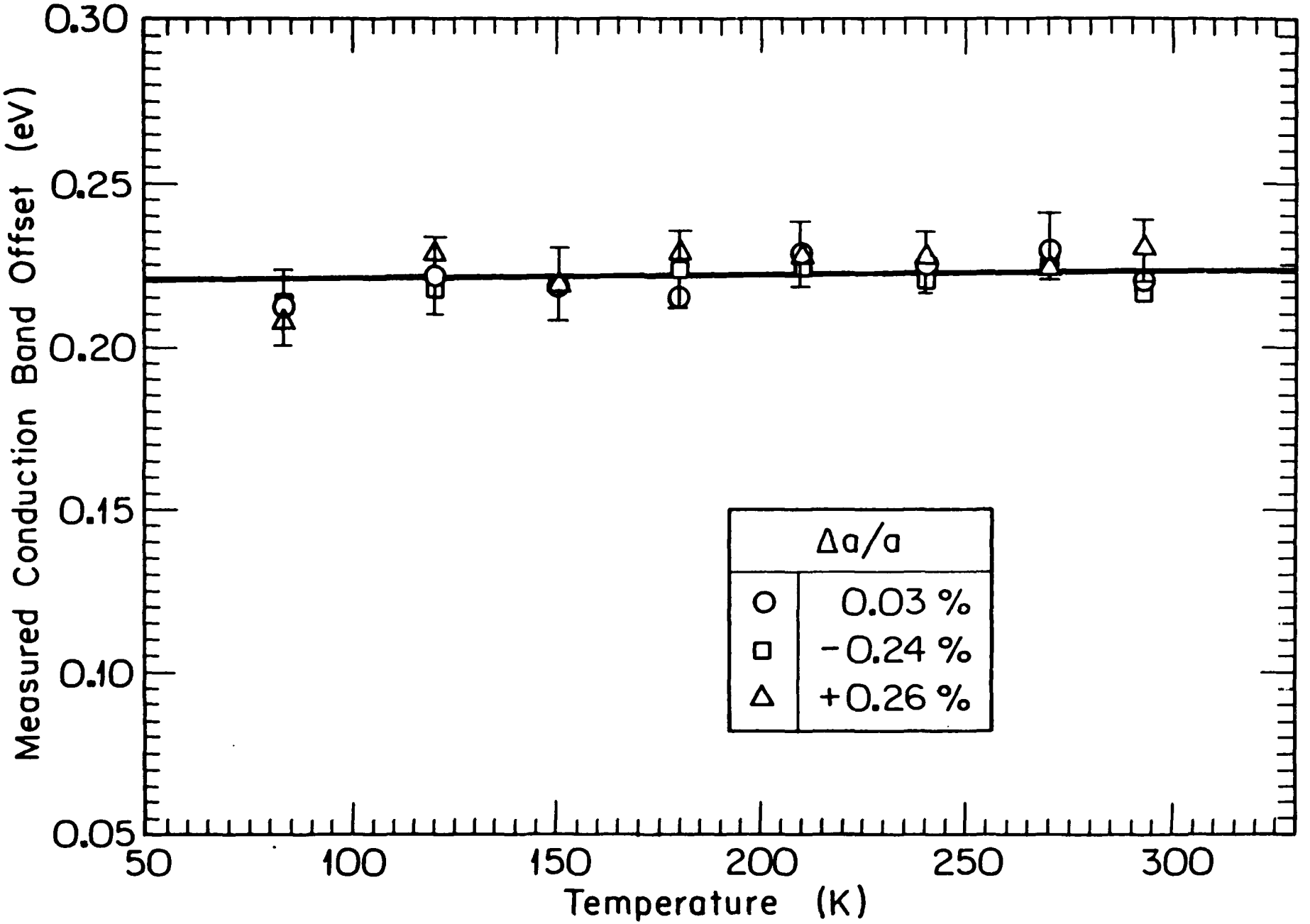
0.30
0.25
0.20
0.15
0.10
0.05
Measured Conduction Band Offset (eV)
50
100
150
200
250
300
Temperature (K)
Δa/a
O 0.03 %
□ -0.24 %
△ +0.26 %

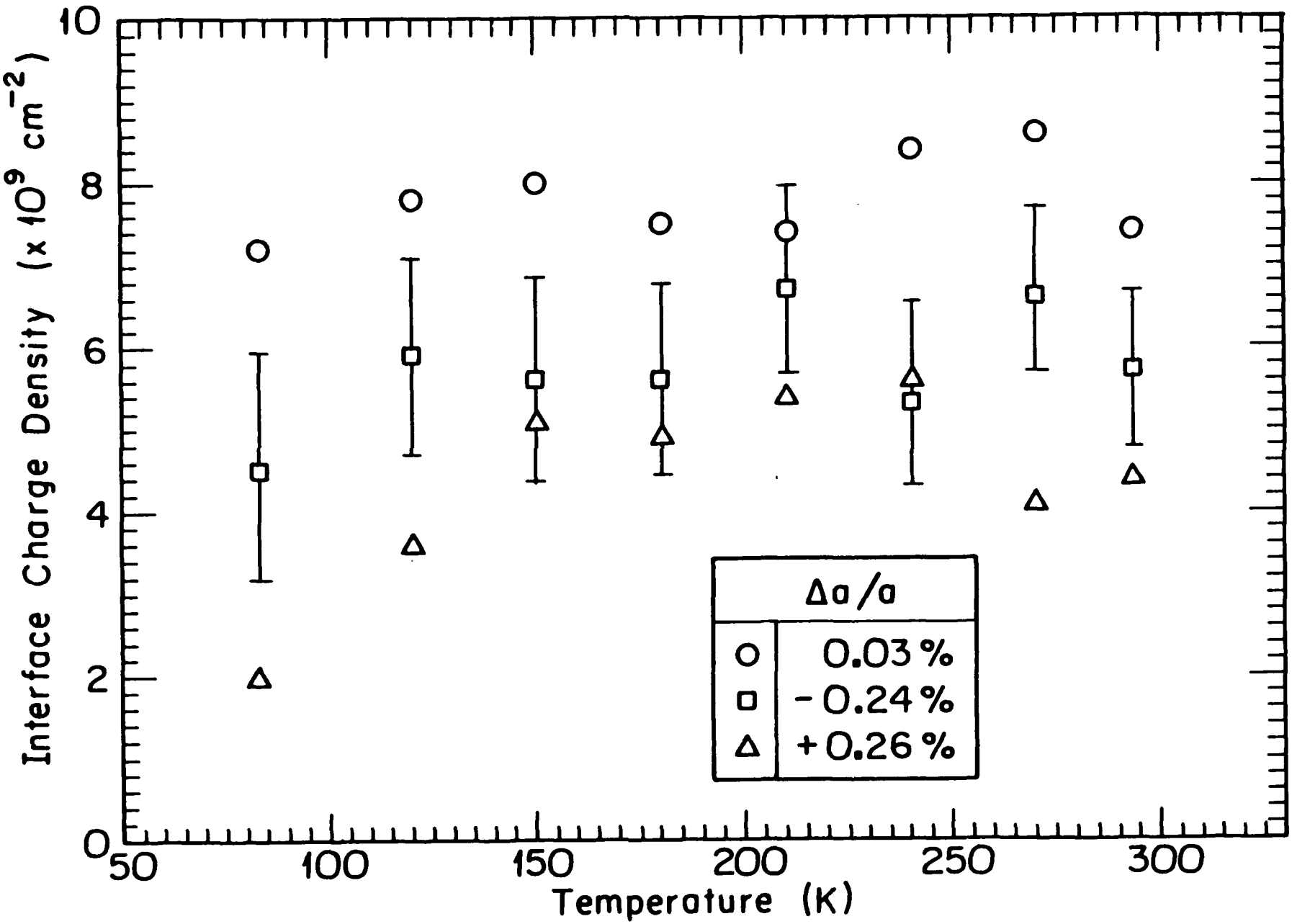
Interface Charge Density (x 10^9 cm^-2)
10
8
6
4
2
0
50
100
150
200
250
300
Temperature (K)
Δa/a
0.03 %
-0.24 %
+0.26 %